Lappeenranta
University of Technology

Tommi Kääriäinen

POLYMER SURFACE MODIFICATION BY ATOMIC LAYER DEPOSITION

Thesis for the degree of Doctor of Science (Technology) to be presented with due permission for public examination and criticism in the Auditorium of the Mikkeli University Consortium, Mikkeli, Finland on the 19th of December, 2011, at noon.

Acta Universitatis
Lappeenrantaensis 461

Supervisor Professor David Cameron
Faculty of Technology
Department of Mechanical Engineering
Advanced Surface Technology Research Laboratory
Lappeenranta University of Technology
Mikkeli, Finland

Reviewers Professor Peter Kelly
Dalton Research Institute
Manchester Metropolitan University
UK

Professor Steven George
Department of Chemistry and Biochemistry
University of Colorado at Boulder
USA

Opponent Professor Steven George
Department of Chemistry and Biochemistry
University of Colorado at Boulder
USA

ISBN 978-952-265-188-4
ISBN 978-952-265-189-1 (PDF)
ISSN 1456-4491
Lappeenranta University of Technology
Digipaino 2011

ABSTRACT

Tommi Kääriäinen

Polymer surface modification by atomic layer deposition

Current industrial atomic layer deposition (ALD) processes are almost wholly confined to glass or silicon substrates. For many industrial applications, deposition on polymer substrates will be necessary. Current deposition processes are also typically carried out at temperatures which are too high for polymers. If deposition temperatures in ALD can be reduced to the level applicable for polymers, it will open new interesting areas and applications for polymeric materials. The properties of polymers can be improved for example by coatings with functional and protective properties.

Although the ALD has shown its capability to operate at low temperatures suitable for polymer substrates, there are other issues related to process efficiency and characteristics of different polymers where new knowledge will assist in developing industrially conceivable ALD processes. Lower deposition temperature in ALD generally means longer process times to facilitate the self limiting film growth mode characteristic to ALD. To improve process efficiency more reactive precursors are introduced into the process. For example in ALD oxide processes these can be more reactive oxidizers, such as ozone and oxygen radicals, to substitute the more conventionally used water. Although replacing water in the low temperature ALD with ozone or plasma generated oxygen radicals will enable the process times to be shortened, they may have unwanted effects both on the film growth and structure, and in some cases can form detrimental process conditions for the polymer substrate.

Plasma assistance is a very promising approach to improve the process efficiency. The actual design and placement of the plasma source will have an effect on film growth characteristics and film structure that may retard the process efficiency development. Due to the fact that the lifetime of the radicals is limited, it requires the placement of the plasma source near to the film growth region. Conversely this subjects the substrate to

exposure by other plasma species and electromagnetic radiation which sets requirements for plasma conditions optimization.

In this thesis ALD has been used to modify, activate and functionalize the polymer surfaces for further improvement of polymer performance subject to application. The issues in ALD on polymers, both in thermal and plasma-assisted ALD will be further discussed.

Lappeenranta, 2011

p. 79

Acta Universitatis Lappeenrantaensis 461

Diss. Lappeenranta University of Technology

ISBN 978-952-265-188-4, ISBN 978-952-265-189-1 (PDF)

ISSN 1456-4491

Keywords: atomic layer deposition, polymers

UDC 541.64:621.794:539.2

PREFACE / ACKNOWLEDGEMENTS

The research work was carried out at Advanced Surface Technology Research Laboratory, LUT Metal Technology (former Department of Mechanical Engineering) at the Lappeenranta University of Technology during the years 2006-2011.

I would like to express my deepest gratitude to my supervisor Prof. David Cameron for his advice and creative scientific discussions during this work. I express my gratitude to the reviewers of my thesis Prof. Dr. Peter Kelly and Prof. Dr. Steven George for contribution and valuable comments.

Markku Heinonen from the Department of Physics and Astronomy at the University of Turku is thanked for the XPS measurements. Dr. Ramanathaswamy Pandian from the Department of Applied Physics, Zernike Institute for Advanced Materials as the University of Groningen in Netherlands is thanked for the TEM analysis. My special thanks go to Dr. Milja Mäkelä, whose encouragement and contagious enthusiasm has been a great support in my work. I am also thankful to everyone at Beneq for their technical support and fruitful discussions during this project.

I am very grateful to all my co-authors for your expertise and fruitful scientific discussions during the studies. I would also like to thank all my colleagues and co-workers in ASTRaL, LUT Savo and MAMK over the past seven years for building up and develop the research environment. It has been a pleasure working with you.

My warmest thanks go to everyone in my family - thank you for sharing the memorable moments in my life. I am deeply grateful of having three wonderful children, Emil, Elsa, and Elias – you have brought such joy and love to my life. Finally, my most loving thanks go to my wife Malla – you are my mentor and the love of my life.

Mikkeli, December 2011

Tommi Kääriäinen

LIST OF PUBLICATIONS

The dissertation will be based on the summary part and the following four original peer-reviewed publications referred in the text by the Roman numerals I-IV.

I **T. O. Kääriäinen** and D. C. Cameron. " Plasma-assisted Atomic Layer Deposition of Al_2O_3 at Room Temperature" Plasma Process. Polym. 2009, 6, S237-S241.

II **T. O. Kääriäinen**, D. C. Cameron and M. Tanttari. "Adhesion of Ti and TiC Coatings on PMMA Subject to Plasma Treatment: Effect of Intermediate Layers of Al_2O_3 and TiO_2 Deposited by Atomic Layer Deposition".Plasma Process. Polym. 2009, 6, 631-641.

III **T.O. Kääriäinen**, P. Maydannik, D.C. Cameron, P. Johansson, K. Lahtinen and J. Kuusipalo. " Atomic Layer Deposition on Polymer Based Flexible Packaging Materials: Growth Characteristics and Diffusion Barrier Properties". Thin Solid Films 519 (2011) 3146-3154.

IV **T.O. Kääriäinen**, S. Lehti, M.-L. Kääriäinen and D.C. Cameron. " Surface modification of Polymers by Plasma-assisted Atomic Layer Deposition". Surface and Coatings Technology 205 (2011) S475-S479.

The original publications are reprinted with the permission of the copyright holders.

AUTHOR'S CONTRIBUTION IN THE PUBLICATIONS

I The author carried out the literature survey, all the experimental work, and wrote the first manuscript of the paper.

II The author carried out the literature survey, organized the study, did most of the experimental work and analyzed the data. The author wrote the first manuscript of the paper.

III The author carried out the literature survey and did the experimental work excluding the WVTR and O_2TR measurements. The author analyzed all the data excluding the WVTR and O_2TR data, which was analyzed together with co-authors. The author wrote the first manuscript of the paper.

IV The author carried out the literature survey and organized the whole study. The author carried out all the thin film deposition work and film characterization excluding XPS measurements. The author analyzed the XPS data for the paper. The optical emission measurements were carried out together with co-authors. The author did not contribute to the data manipulation of the optical emission measurements but analyzed the data presented in the paper. The author wrote the first manuscript of the paper.

OTHER PUBLICATIONS BY THE SAME AUTHOR

Related to the current field of study

Kääriäinen, T. O. Kääriäinen, M-L. Gandhiraman, R. P. Cameron, D. Atomic Layer Deposition of TiO_2 films at low temperatures using tetrakis-dimethyl-amido-titanium and ozone, AVS 7th International Conference on Atomic Layer Deposition, 24-27 June San Diego, CA, 2007.

Kääriäinen, T. O. Cameron, D. C. ALD-deposited nanometer scale metal oxide films as adhesion promoters for sputtered metal and ceramic coatings on PMMA. Annual Technical Conference Proceedings - Society of Vacuum Coaters (2009), 52nd, 678-682.

Kääriäinen, T. Kääriäinen, M-L. Cameron, D. Plasma-assisted atomic layer deposition of oxides at low temperature: growth characteristics and interaction between plasma and polymer substrate, AVS 9th International Conference on Atomic Layer Deposition, 19-22 July, Monterey, CA, 2009.

Kääriäinen, M-L. **Kääriäinen, T. O.** Cameron, D.C. Thin Solid Films 517 (2009) 6666-6670.

Kääriäinen, T.O. Maydannik, P. Cameron, D. C. Johansson, P. Lahtinen, K. Kuusipalo, J. Atomic Layer Deposition of Metal Oxide Films as Diffusion Barriers on Flexible Packaging Materials. Annual Technical Conference Proceedings - Society of Vacuum Coaters (2010), 53rd, 93-97.

Maydannik, P. **Kääriäinen, T. O.** Cameron, D. C. A continuous ALD process for deposition of diffusion barriers on flexible substrates, AVS 10th International Conference on Atomic Layer Deposition, June 20-23, Seoul, Korea, 2010.

Maydannik, P. S. **Kääriäinen, T. O.** Cameron, D. C. A continuous ALD process for deposition on flexible substrates. Annual Technical Conference Proceedings - Society of Vacuum Coaters (2010), 53rd, 138-141.

Johansson, P. Lahtinen, K. Kuusipalo, J. **Kääriäinen, T.** Maydannik, P. Cameron, D. Atomic layer deposition process for barrier applications of flexible packaging, TAPPI/PLACE Conference, 19th-21st April, Albuquerque, 2010.

Lahtinen, K. Maydannik, P. Johansson, P. **Kääriäinen, T.** Cameron, D. C. Kuusipalo, J. Surf. Coat. Technol. 205 (2011) 3916-3922.

Maydannik, P. S. **Kääriäinen, T. O.** Cameron, D.C. Chem. Eng. J. 171 (2011) 345-349.

Other publications

Kääriäinen, M-L. **Kääriäinen, T**. Cameron, D. Nitrogen doped ALD-grown titanium dioxide films, 2007, AVS 7th International Conference on Atomic Layer Deposition San Diego CA 24-27 June 2007.

Kääriäinen, T. Rahamathunnisa, M. Tanttari, M. Cameron, D. C. Properties of magnetron sputtered hard coatings on carbon and glass fibre composites. Annual Technical Conference Proceedings - Society of Vacuum Coaters (2006), 49th, 548-553.

Kääriäinen M-L. **Kääriäinen, T.** Cameron, D. C. TiO_2 thin films and doped TiO_2 nanolaminates, their structure and its effect on their photocatalytic properties. Annual Technical Conference Proceedings - Society of Vacuum Coaters (2007), 50th, 335-339.

Kääriäinen, M-L. **Kääriäinen, T.** Cameron, D. The Synergy between Anatase and Rutile Phase in the Photocatalytically Active Titanium Dioxide Thin Films, AVS 9th International Conference on Atomic Layer Deposition, 19-22 July, Monterey, CA, 2009.

Maydannik, P. **Kääriäinen, T.O.** Cameron, D. C. Soininen, P. Putkonen, M. Continuous Atomic Layer Deposition Process: towards roll-to-roll ALD, AVS 10th International Atomic Layer Deposition (ALD) Conference, June 20-23, Seoul, Korea, 2010.

Jalkanen, P. Kulju, S. Arutyunov, K. Antila, L. Myllyperkiö, P. Ihalainen, T. **Kääriäinen**, **T**. Kääriäinen, M-L. Korppi-Tommola, J. Thin Solid Films 519 (2011) 3835-3839.

TABLE OF CONTENTS

ABSTRACT 3
PREFACE / ACKNOWLEDGEMENTS 5
LIST OF PUBLICATIONS 6
AUTHOR'S CONTRIBUTION IN THE PUBLICATIONS 7
OTHER PUBLICATIONS BY THE SAME AUTHOR 8
TABLE OF CONTENTS 10
NOMENCLATURE 12
1 INTRODUCTION 14
1.1 Research problem and scope of the work 14
1.2 Atomic layer deposition 16
1.3 Atomic layer deposition on polymers 17
1.4 Low temperature ALD process enhancement; Substitutive oxidizing agents for water 24
1.5 General properties of polymers 25
1.5.1 Chemical solubility of polymer and free volume of the polymer surface region 28
1.5.2 Polymers under ultraviolet radiation 29
1.5.3 Polymer surface structure 32
1.5.4 Thermo-mechanical behavior of thin film on flexible polymer substrate 33
2 EXPERIMENTAL METHODS 41
2.1 Thin film deposition and plasma treatments 41
2.2 Substrate materials 42
2.2.1 PMMA 42
2.2.2 PC 42
2.2.3 Low density polyethylene (LDPE) 42
2.2.4 Polypropylene (PP) 43
2.2.5 Polyethylene terephthalate (PET) 43
2.2.6 Polylactide (PLA) 44
2.3 Film and ALD process characterization 45

3 RESULTS AND DISCUSSION 49
3.1 Film growth characteristics 49
3.2 Film composition and film structure 53
3.3 Film performance 57
3.3.1 ALD film adhesion 57
3.3.2 ALD film shielding effect against UV/VUV –radiation and ion bombardment 58
3.3.3 ALD film diffusion barrier properties on polymer extrusion coated flexible packaging materials 60
3.3.4 PA-ALD process characteristics and their effect on polymer substrate and film performance 63
4 CONCLUSIONS 66
REREFENCES 69

NOMENCLATURE

Abbreviations

AFM	Atomic force microscopy
ALD	Atomic layer deposition
ATR-FTIR	Attenuated total reflection fourier transform infrared
CIGS	Copper indium gallium selenide
CTE	Coefficient of thermal expansion
CVD	Chemical vapor deposition
DC	Direct current
DEZ	Diethyl zinc
EDS	Energy dispersive X-ray spectrosopy
F-OLED	Flexible organic light emitting diode
IRE	Internal reflection element
MEMS	Microelectromechanical systems
MLD	Molecular layer deposition
NEMS	Nanoelectromechanical systems
OES	Optical emission spectroscopy
OPV	Organic photovoltaics
PA-ALD	Plasma assisted atomic layer deposition
PCBM	6,6-phenyl-C61-butyric acid methyl ester
PCL	Poly(ε-caprolactone)
PE-ALD	Plasma enhanced atomic layer deposition
PE	Polyethylene
PEDOT:PSS	Poly-3,4-ethylenedioxythiohene-poly-styrenesulphonate
PET	Polyethylene terephthalate
PGA	Polyglycolic acid
P3HT	Poly-3-hexylthiophene-2,5-diyl
PLA	Polylactide
PMMA	Polymethyl(methacrylate)
PPX	Poly(p-xylylene)
PS-DVB	Poly-styrene divenylbenzene
PVC	Polyvinyl cloride
PVK	Poly N-vinylcarbazole
RE-ALD	Radical enhanced atomic layer deposition
RF	Radio frequency
SAED	Selected area electronic diffraction (SAD also used)
SEM	Scanning electron microscopy
SRIM	The stopping and range of ions in matter
TEM	Transmission electron microscopy
TFT	Thin film transistors
TDMAH	Tetrakis(dimethylamido)hafnium
TDMAT	Tetrakis(dimethylamido)titanium

TMA	Trimethylaluminium
TPS	Tris(tert-pentoxy)silanol
TTIP	Titanium tetraisopropoxide
QCM	Quartz crystal microbalance
UV	Ultraviolet
VUV	Vacuum ultraviolet
XPS	X-ray photoelectron spectroscopy
XRD	X-ray diffraction

List of symbols

A	Absorbance
α	Thermal expansion coefficient
α_f	Thermal expansion coefficient of the film
α_s	Thermal expansion coefficient of the substrate
ΔT	Difference between deposition and room temperature
D_{bm}	Dunder's elastic mismatch parameter, bulk modulus
D_{tm}	Dunder's elastic mismatch parameter, tensile modulus
E	Young's modulus
$\overline{E}_f$	The effective modulus of the film
$\overline{E}_s$	The effective modulus of the substrate
ε_{bi}	Built-in strain in the film
ε_f	In-plane strain in the film
ε_s	In-plane strain in the substrate
d_f	Film thickness
d_s	Substrate thickness
I_0	Intensity of incident energy
I	Intensity of transmitted light
λ	Wavelength
M_n	The number average molecular weight
R	Radius
T	Temperature
T_g	Glass-transition temperature
T_m	Melting temperature
T_d	Deposition temperature
v	Poisson ratio
Y	Young's modulus
Y_f	Young's modulus of the film
Y_f^*	Biaxial strain moduli of the film
$Y_f^{'}$	Plain strain moduli of the film
Y_s	Young's modulus of the substrate
Y_s^*	Biaxial strain moduli of the substrate
$Y_s^{'}$	Plain strain moduli of the substrate

1 INTRODUCTION

1.1 Research problem and scope of the work

Up to now, atomic layer deposition (ALD) has only been applied in a large scale to a few commercial products, principally flat panel displays and, to a growing extent, in the semiconductor industry. There are many other industrial sectors to which this process could be applicable. The great potential of ALD has been notified in the applications where there is a need for very high performance diffusion barriers or to cover complex geometrical shapes, such as nanoporous structures for catalysis and filtration purposes, with conformal and ultra thin layers. One group of materials of great interest is polymers because they are often used in these industrial applications.

Polymeric materials have countless applications in our daily life. The applications are varying from common domestic to very sophisticated scientific and technical instruments. The characteristics of polymers that give advantages compared to other materials are lightness, resilience, resistance to corrosion, color fastness, transparency, ease of processing etc. These characteristics of polymer materials can be furthermore enhanced with appropriate surface treatment such as thin film deposition. Thin film coatings on polymers will give new fascinating areas for their usage.

Current ALD processes are often confined to glass or silicon substrates and deposition processes are also typically carried out at temperatures which are too high for polymers. If deposition temperatures in ALD can be reduced to the level applicable for polymers, it will open new interesting opportunities to develop the existing applications or new applications where polymers could be utilized. The properties of polymers can be improved for example by coatings with functional and protective properties.

Plasma assisted atomic layer deposition (PA-ALD) has been considered as a possibility to extend the materials selection for ALD and a way to lower the substrate temperature. Using plasma in ALD can result in increased reaction rates on surfaces, increased fragmentation of the precursor molecules, bombardment-enhancement of the removal of product molecules, or a combination of all of these steps [1-2]. Therefore it has been investigated, more and more, for low temperature applications. In PA-ALD the additional energy for the chemical reactions in the deposition chamber is provided by applying a pulse of plasma energy at an appropriate point during the reaction cycle. Using plasma in polymer processing will also set demands on process development. The process development is a routine step in PA-ALD to optimize the film growth, but in the case of polymers it is necessary also because of polymer related issues, such as the damaging effect of ion-bombardment and electromagnetic radiation from plasma.

In this research the problems of functional and protective oxide ALD films on polymer substrates will be addressed. The study of different precursor combinations will be informative particular in deposition on polymers and will gain understanding in chemical reactions both on the polymer surface and grown film. The behavior of the polymer substrates during the deposition will give the knowledge which enables the application of ALD films to polymeric materials for a wide range of uses in many industrial applications. The main focus of the research will be based on the development of a low temperature ALD processes for protective and functional films, applicable to polymer substrate materials.

1.2 Atomic layer deposition

Atomic Layer Deposition (ALD) is a surface controlled layer-by-layer process for the deposition of thin films with atomic layer accuracy [1]. Each atomic layer formed in the sequential process is a result of saturated surface controlled chemical reactions. Commonly, in the growth of binary compounds such as metal oxides, a reaction cycle consists of two reaction steps. In one step the metal compound precursor is allowed to react with the surface, and in the other step it reacts with the oxygen precursor. Between the steps a purge is applied to remove the excess of precursor and the reaction by-products. The self-controlled growth mode of atomic layer deposition contributes several advantages. The thickness of the films can be controlled in a straightforward manner by controlling the number of reaction cycles, therefore enabling the controlled growth of ultra thin layers. The precursors form stoichiometric films with large area uniformity and conformality even on complex surfaces with deformities. Layer-by-layer growth allows one to change the material abruptly after each step. This gives the possibility of depositing multicomponent films, so called nanolaminates or mixed oxides, for example [1-4].

1.3 Atomic layer deposition on polymers

Atomic layer deposition on polymer substrates is increasingly gaining interest both in research and industry. Combining the properties of organic polymer and inorganic nanometer scale coating to form composite structures, may create unique properties that will expand the application range of polymers. Based on the requirements for future devices [5], research efforts in the field of ALD have revealed that ALD can provide the extremely high performance to meet these requirements. The applications with the most potential for ALD on polymers can be seen in barrier and transparent conducting layers for flexible organic light emitting diodes (F-OLEDs) [6-11], organic photovoltaics (OPVs) [12-17], CIGS photovoltaics (CIGS PVs) [18], thin film transistors (TFT) [19, 20], packaging materials [**III** , 7, 21-23], structures to be exposed to electromagnetic radiation and ion flux [**II,** 24, 25], polymer surface modification to improve wettability, printability, biocompatibility and adhesion properties [**II,** 26-28], and in more fundamentally and characteristically to ALD, encapsulation and formation of complex shapes and nanostructures [29-41].

The literature review of ALD on polymers is presented in Table 1, by means of the film materials, precursors used, deposition temperature and polymer substrates used in the study.

Table 1. Materials deposited on polymers by ALD.

Material	Metal precursor	Counter reactant	Polymer substrate	Deposition temperature [ºC]	Reference
Al_2O_3	TMA	H_2O	PS-DVB	33	[30, 33]
			HDPE particles	77	[31]
			PET	25-100	[6, 42, 43]
		H_2O, O_3, O_2 plasma, CO_2 plasma	PET	75	[44]
			heat-stabilized PEN PEN, PET, PI (Kapton)	100-180	[7, 9, 10 24, 45-47, 125]
			PES (polyethersulfone)	90	[48]
			LDPE, PE, PLA, PEN, PP, PET, PLA	80-100	[21-23, 49]
			PMMA, PEEK, PTFE, ETFE	80-250	[26]
			Cellulose cotton	100	[27]
			nonwoven PP, PP	120	[28]
			LDPE particles	77	[34]
			PS, PP, PMMA, PE, PVC	85	[50]
			PMMA	100-150	[51]
			PEDOT:PSS, P3HT/PCBM	140-150	[17]

Material	Metal precursor	Counter reactant	Polymer substrate	Deposition temperature [ºC]	Reference
		H_2O and O_3	PEDOT:PSS, P3HT/PCBM	140	[15]
			metallized PET	100	[52]
			P3HT, PVP, PMMA	125	[53, 54]
			PVA fibers	45	[37]
			PMMA, PI (Kapton H), PTFE (FEP Teflon)	90	[25]
			FEP Teflon	65-200	[125]
			PP	60-90	[55]
			porphyrin	50-80	[56]
		CO_2 plasma	Cr metallized PI	200	[20]
		Oxygen radicals	PE, PP, PTFE	25-300	[57, 58]
		O_3	PMMA	65	[**II**]
			LDPE, PP, PET, PLA	65	[**III**]
		O_2 plasma	PEN	RT - 100	[8]
		O_2 plasma	PES	90-150	[59]
		O_2 plasma	PVK	RT	[41]
	$AlCl_3$	H_2O	PC	100	[60]
AlO_x	-	-	PET	-	[61]
Al_2O_3/W nano-laminates	TMA, WF_6	H_2O, Si_2H_6	Kapton, PI, PEN	125	[62]

Material	Metal precursor	Counter reactant	Polymer substrate	Deposition temperature [ºC]	Reference
HfO_2	TDMAH	H_2O	PMMA	100-150	[51]
			PEDOT:PSS, P3HT/PCBM	140-150	[17]
Pd	$(Pd^{II}(hfac)_2$	H_2/N_2 plasma	PPX	80	[63]
SiO_2	TPS	TMA	Kapton, heat-stabilized PEN	175	[9]
TiO_2	TTIP	H_2O	HDPE particles	77	[32]
			PC	80-200	[64]
			PVP	70	[65]
			porphyrin	50-80	[56]
		Oxygen radicals	PC, PP, PE	50	[66]
	$TiCl_4$	H_2O	PC	80	[67]
			PMMA, PEEK, PTFE, ETFE	80-250	[26]
			PA particles	40	[29]
			PET	40-120	[42]
			PS spheres	80	[38]
			PMMA	90	[25]
			PC	120	[68]

Material	Metal precursor	Counter reactant	Polymer substrate	Deposition temperature [ºC]	Reference
	TDMAT	O_2 plasma	PI (Kapton)	150-250	[69,70]
		O_2 plasma	PMMA, PP, PC	70	[**IV**]
		O_3	PMMA	65	[**II**]
			LDPE	65	[**III**]
W	WF_6	Si_2H_6	PVC, PS, PMMA, PC, PP	80	[35]
WCN	WF_6	$(C_2H_5)_3B$ and NH_3	SiLK		[71]
ZnO	DEZ	H_2O	ITO-coated PEN	45-80	[13]
			PET	100-210	[12]
			porphyrin	50-80	[56]
			PS	85	[72]
			PP (ALD Al_2O_3 seed layer), cellulose cotton, cotton fiber	115	[73]
		N_2O plasma	Cr metallized PI	200	[20]
		O_2 plasma	Poly-4-vinylphenol (PVP)	150	[74]
ZrO_2	TDMAZ	H_2O	PMMA	100-150	[51]
	ZTB $Zr(O^tBu)_4$	H_2O	PC	80-200	[64]
	ZTB	H_2O with UV assistance	PET	20	[69]

Polymers are challenging materials for processes which are dependent on external thermal or other source of energy to initiate and enhance the chemical reactions for the film growth. In the case of ALD both thermal energy and e.g. plasma can be used. Since ALD on polymers must be performed at low temperatures, due to the thermal fragility of the polymers, the processing conditions shall meet a number of complexities compared to ALD at elevated temperature. In general these can be divided into ALD process dependent, and polymer material dependent factors. The ALD process dependent factors can be scrutinized by using the so-called ALD window in Figure 1, which defines the dependency of the film growth rate on the deposition temperature [1]. Ideal and self-limiting ALD film growth conditions can be found inside the ALD window. At low deposition temperature the increase in film growth rate may result from multilayer adsorption and condensation of precursors, and the decrease in growth rate from slow and incomplete chemical reactions. Depending on the precursor chemistry the self-limiting growth rate inside the ALD window may be temperature dependent. This will usually appear as a decreasing growth rate with increasing deposition temperature due to a decreased density of reactive surface species [1].

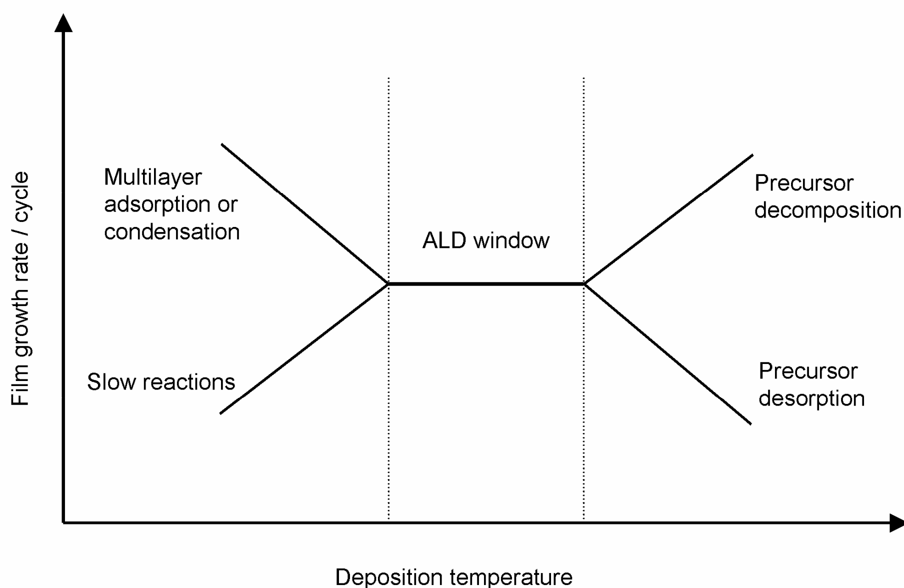

Figure 1. The growth rate vs deposition temperature dependencies in ALD processes that may occur outside the ALD window [1].

A generic model of ALD on polymers for binary compounds suggests that the film nucleation and growth occurs through the following steps: a) Diffusion of one precursor into the near surface region of the polymer; b) Cluster formation of the ALD material through bimolecular reaction between two ALD precursors; c) The cluster growth and coalescence; d) Continuous film growth that prevents the additional precursor diffusion into the polymer, and; e) The linear ALD film growth [50]. Although many studies have proven the possibility of ALD on polymers, the process is complicated due to the inhomogeneous nature of the polymer surface, and the lack of functional groups terminated on it. Due to this the reactions between the surface species and the precursor are limited to the sites on the surface where the exchange reaction or chemisorption can take place.

1.4 Low temperature ALD process enhancement; Substitutive oxidizing agents for water

Low temperature ALD suffers from slow reactions and often longer purge times are required to avoid CVD film growth. The commonly used oxidizer in ALD oxide processes is water. Water is known as a substance difficult to remove and requires relatively long purge times at low deposition temperatures to meet ALD growth mode [5]. More reactive oxidizers such as ozone [75-77] and radicals produced by plasma [2, 8, 41, 42, 44, 57, 58, 63, 66, 78- 81] have been studied to enhance process efficiency and possibly to decrease the deposition temperatures. Plasma activation will also extend the range of materials suitable for ALD and has enabled efficient deposition of e.g. metal ALD films [2, 39, 82, 83]. In plasma assisted atomic layer deposition (PA-ALD), plasma is used to produce radicals by gas dissociation. A very common plasma source in PA-ALD is the radio frequency-generated plasma with inductively [2, 8] or capacitively [83, 84] coupled design. In general the plasma assistance used in ALD can be divided into two modes based on how the plasma interacts with the ALD process, and with the substrate. In the remote mode the plasma source is located remotely from the substrate so that only radicals generated by the plasma are allowed to reach the substrate surface. Based on this the term radical enhanced ALD (RE-ALD) is used to define distinction between RE-ALD and PA-ALD or plasma enhanced ALD (PE-ALD) [58]. In the direct plasma mode, referred also as PA-ALD and PE-ALD, the plasma source is located in the same space or very near at the substrate [**I**, 84]. In the case of PE-ALD, in addition to radicals, the other plasma species and electromagnetic radiation of the plasma may also interact with the substrate. The issues that may arise due to this fact are further discussed in papers **II** and **IV**.

Demands for higher process efficiency can be justified through one of the ALD applications on polymers with the most potential, which are barrier and modification layers on flexible polymer substrates. In these applications industrial production depends on high throughput roll-to-roll production technology. Although the ALD process temperature can be decreased and process efficiency increased by plasma assistance, other issues may arise when treating polymers with plasma. Depending on the plasma

characteristics and polymer photochemistry the resulting film performance and effect on the polymer substrate itself can be detrimental. Both oxygen plasma and ozone used in ALD oxide processes can lead to formation of reaction by-products that are reactive and capable of re-adsorbing on the surface [76, 79, 80]. Readsorption of by-products may lead to decreased growth rate if they are blocking the adsorption sites from the precursor molecules, or cause thickness non-uniformity if readsorption occurs non-uniformly across the substrate [85].

1.5 General properties of polymers

Polymer materials are an integral part of human life and their applications and usage vary widely from domestic items [86] through medical and biomaterials [87], microfabricated devices and MEMS/NEMS structures [88, 89] to fibre-based packaging materials [87]. The applicability of polymer materials is often determined by their physical and chemical properties. Optical properties, transparency being one of the most important, of polymers are important e.g. in applications where a substitute for glass is desired [90]. Transparency can be sacrificed for flexibility e.g. in flexible packaging. Among the thermoplastic materials the material structure, amorphous or semi-crystalline, generally defines the characteristics of the material. For example amorphous polymers, such as poly(methyl methacrylate) (PMMA), polycarbonate (PC), and polystyrene (PS) are the most transparent polymers (around 90 % transparency in visible light region). Usually transparency decreases with increasing crystallinity [91]. Amorphous thermoplastics in general have lower chemical resistance than crystalline thermoplastics due to a more open random structure [86]. In thermal processes, such as in ALD, the defining polymer properties like glass transition temperature (T_g) and the coefficient of thermal expansion (CTE) are of great importance. Although these properties can be generally quantified for each polymer they depend on a number of factors, even within the same polymer type. For example T_g depends on the rate of cooling, the pressure, and the number of average molecular weight (M_n). T_g changes also with degree of crystallinity and the nature of the morphology of the materials, which increase the variance of properties such as density and CTE in polycrystalline polymers [92, 93]. Tg, especially for amorphous polymers, is

useful information since it correlates with CTE, so that usually there is a sudden increase in CTE at T_g. For example, the CTE for PMMA below its T_g ranges from 1.8 to $2.7 \cdot 10^{-4}$ K^{-1} and increases to $5.5 \cdot 10^{-4}$ K^{-1} above the T_g [92, 93]. From the ALD perspective the CTE of the polymer can be seen to be more relevant than Tg, since it defines how much the polymer will change in dimension when subject to a change in temperature. CTE values of polymers are tens of times higher than CTE values of inorganic ceramic materials. At too high and uncontrolled processing temperature this mismatch between CTE's can lead to a build up of unfavorable compressive stress in an inorganic ALD film, which finally causes cracking of the film. Furthermore the cracking of the film will deteriorate the film performance, especially in barrier applications [126]. The values of T_g and CTE of some polymer materials are presented in Table 2. The critical characteristics of polymers concerned in this study are shortly described hereafter, concentrating on glass transition temperature, thermal expansion coefficient and behavior under chemical, mechanical and UV exposure.

Table 2. Some properties of polymers.

Material	CTE,α (µm/m/ºC)	T_g (ºC)	Max. operating temperature (ºC)	Typical structure A – amorphous SC – semi crystalline	Reference
LDPE	126-198 *	-120 -25- -15 *	50	SC	[86, 94*]
PP	122-180 *	-10 -25- -15 *	100	SC	[86, 94*]
PET	114-120 *	68-80 *	110	SC	[86, 94*]
PLA	*$2 \cdot 10^{-2}$ (K^{-1})**	50-60	-	SC	[95, 96*]
PMMA (acrylic)	72-162 *	105, 85-165 *	50	A	[86, 94*]
PC	120-137 *	142-205 *	125	A	[86, 94*]

The physical and chemical properties of thermoplastics depend on morphology i.e., the state of crystallinity [97]. The morphology of thermoplastics can be controlled by controlling the temperature during the processing. Among the polyesters semi-crystalline PET, and biodegradable polylactide (PLA) are good examples. Semi-crystalline PET has good strength, ductility, stiffness, hardness, chemical resistance and possesses low moisture absorption. Amorphous PET is more ductile than crystalline PET, but is not so stiff and hard [86, 98]. The desired structure and consequently the property may be application driven, such as in the polymer extrusion coated fibre-based packaging materials. In packaging applications the state of crystallinity of PET is lowered towards the amorphous state by cooling the polymer melt rapidly from high temperature (300 ºC) to below its glass transition temperature (T_g), for PET that is 70-80 ºC. More amorphous PET is heatsealable, which is a particular characteristic desired in packaging application

[90]. Amorphous PET crystallizes in the solid state when it is heated above the T_g. This can be beneficial for the improvement of barrier properties [99] or detrimental if crystallization takes place at too high and uncontrolled temperature leading to a brittle structure [**III**]. Barrier properties of PLA can also be improved by heat treatment above T_g through morphological change and control of the structure [100]. Polyolefins such as PE and PP similarly change their properties depending on morphological change due to a thermal cycling [101].

It is critical to know how different thermoplastic polymers behave under thermal cycling. In general two polymer dependent factors can be considered as a critical for polymer processing; T_g and CTE. From these T_g is often too high for further processing, since the modification of structure and properties may initiate already at considerably lower temperature than T_g.

1.5.1 Chemical solubility of polymer and free volume of the polymer surface region

Since in ALD the film deposition will take place from the chemical vapor phase, the chemical solubility and free volume of the polymer surface region are important characteristics. The film nucleation on polymer substrates during the first ALD cycles has been suggested to differ depending on the chemical solubility and free volume of the particular polymer. In the case that the polymer has a large free volume it has high diffusion rate of precursor molecules into the polymer surface region. If the polymer has high chemical solubility it largely retains these precursor molecules. Within the polymers PP, PMMA and PE have been found to have a high diffusion rate of TMA, whereas the diffusion rate is small for PVC. At the same time PMMA and PP have low chemical solubility and PVC and PE have high chemical solubility for TMA [50]. Polyesters such as PET, PEN and PLA and polyolefins such as PE and PP can change their morphology during the thermal cycling. This also affects solubility. Solubility together with diffusivity defines the polymer permeability [98]. ALD film nucleation and growth on PP has been observed to be temperature dependent. Jur et.al. suggested that the penetration

of precursor and reactants into the polymer leading to subsurface generation on PP is due to a increase in free volume and diffusivity of the polymer with the increase of growth temperature [55].

1.5.2 Polymers under ultraviolet radiation

Polymer characteristics under ultraviolet (UV) radiation become important in this study for two reasons. Since plasma is used as a part of the ALD process the polymers may be exposed to deteriorating plasma UV radiation. Another interest is related to protection of the polymer from degrading UV radiation, where the ALD films have been demonstrated to provide a good barrier [**II**, 24]. Polymer degradation under plasma UV radiation is based on the dissociation of covalent bonds caused by photon energy. These photochemical changes can affect the physical, chemical and mechanical properties of the polymer and therefore are of great importance. The consequence of photodegradation can be e.g. polymer surface damage leading to film delamination. This will be further discussed in paper **II**.

UV radiation is based on emission from transitions between electronic states of a molecule [96]. Therefore the emission spectrum is depending on the gas species present in the plasma. In chemical processes, such as in PA-ALD, molecular spectra can be very complex due to a number of different gases. In addition to mono- and diatomic gases, such as argon, nitrogen and oxygen typically used in ALD processes, the plasma species can originate from a variety of reactants and reaction products such as organometallic species, hydrocarbons, other carbonous molecules, water and hydroxyl. Atomic and molecular transition probabilities are well documented in the literature for optical emission analysis of measured spectra [103-105].

Dissociation energies for common covalent bonds in polymers lie on the energy range of 3 – 4.3 eV, corresponding approximately to 413 – 310 nm in radiation wavelength. Molecular bond dissociation energies e.g. for CH_3, CH and CH_3O-H are 110.4 kcal/mol, 80.9 kcal/mol and 104.6 kcal/mol corresponding to 4.8 eV, 3.5 eV and 4.5 eV

respectively [106]. Photodegradation of the polymer is possible when the UV radiation is absorbed by the polymer and pathways for photoexcited singlet (S) and triplet (T) species exists to transfer the absorbed photon energy to polymer bond dissociation. Based on the absorption coefficient of the polymer, they have different cut-off wavelengths for UV radiation. For example cut-off wavelengths for PMMA, PC, PET, PP and PE are 240 nm, 280 nm, 310 nm, < 180 nm and < 180 nm respectively. Cut-off wavelength for these polymers has been considered to be the level of 1 absorbance of 10 µm thick polymer film [107]. Absorbance is a measure of absorbed radiation and is defined as [108]:

$$A = \log_{10}\left(\frac{I_0}{I}\right) \qquad (1)$$

Where,

I_0 is the intensity of incident energy
I is the intensity of transmitted light

In practice the cut-off wavelength alters within the polymer depending on e.g. the morphology of the polymer and impurities and additives present. Fundamentally the photochemical reactions in the polymers leading to photodegradation are well studied with the intention of developing their stability under environmental conditions (solar UV radiation). Photodegradation behavior of the polymers generally has been classified to categories such as photodegradation with and without significant chain scission, and photoinitiated oxidation with and without significant chain scission. The photodegradation can be initiated by different species in the polymer, originating from the polymer chain, but also from processing and oxidation. For example the photodegradation in polymethacrylates may be initiated by –C=O groups through so called Norrish I reactions, or direct photolysis of ester or methyl side groups, or photolysis of -O-O- groups from processing or from oxidation. In thermoplastic polyolefins, such as in PE and PP, the initiation process is reportedly still controversial. The potential initiation species for polyolefins can be the -O-O-, OOH, -C=O and C=C

groups from processing or from oxidation, pigments and metal catalyst residues, and charge transfer complexes with O_2 [107, 109].

The role of plasma and vacuum ultraviolet (VUV) radiation in polymer processing has been intensively studied among the vacuum coaters and those using plasma for polymer treatment [110-120]. In plasma treatment the desired effect can be e.g. a sterilized or functionalized polymer surface to improve compatibility or adhesion to another substance. In vacuum plasma processing the plasma can have beneficial, neutral or detrimental effects on the polymer surface. Plasma pretreatment can improve the coating adhesion through the modification of the surface layer of PMMA by ion bombardment, but also deteriorate the adhesion due to the detrimental effect of VUV radiation on polymer surface structure [111]. Polyolefins, that have tendency to photo-oxidation and oxidative degradation may undergo optical deterioration during the plasma treatment, but at the same time improve the coating adhesion [121]. Depending on the polymer absorption coefficient and plasma emission characteristics, the bond breakage in the polymer may result in unwanted effects. In the case of PMMA, both beneficial and detrimental effects have been reported. In PMMA the structural change may happen through the side-chain scission or cross-linking caused by photon energy and plasma ions or electrons [111, 114, 116, 121]. In the VUV wavelength region (λ < 200 nm) the absorption of the electromagnetic radiation is also characteristic of each polymer. PE absorbs below 170 nm due to the $\sigma \rightarrow \sigma^*$ transitions in C-C and C-H bonds. At higher wavelengths the absorption is due to double bonds or oxidation products. PMMA absorbs around 210 nm due to the transitions in carbonyl (C=O) group, and at 150 nm due to the transitions in its elementary unit. The absorptions in PMMA at higher energy are typical for the hydrocarbon backbone [118].

Concerning the electromagnetic radiation of plasma, the energy required for polymer bond dissociation lies in the optical frequency range, i.e., from ultraviolet (UV) to near infrared (IR) region (100 nm to 1000 nm). The plasma emission can be measured by using optical emission spectroscopy (OES) to determine the species present in the

plasma. OES has also been used in PA-ALD processes to monitor the generated radicals and reaction products, only referring to a few here [65, 79, 80, 122, **IV**].

1.5.3 Polymer surface structure

Polymer surface modification, where molecules are introduced from the gas phase with the intention of adsorption on the surface, is challenging because of the inhomogeneous nature of the polymer surface. The adsorption process is influenced by the chemical and physical properties of the polymer surface such as the appearance of functional groups, charge degree (oxidation, ionization), polarity, surface morphology (roughness, degree of crystallinity) and surface contamination [123, 124]. The orientation of the polymer chain and the concentration of chain ends in the surface plane will also change the surface structure influencing the adsorption of desired molecules [124]. Some of these above mentioned surface characteristics are beneficial, some disadvantageous for surface modification by atomic layer deposition.

Polymers are mostly required to maintain their structure and morphology in their end application under a diversity of temperature and environmental conditions. The same requirements can be set on polymers during vacuum deposition processing. Since in this study ALD has been applied to polymer substrates, the deposition has been carried out in a low deposition temperature range (< 150 ºC). Plasma has been utilized to enhance the low temperature ALD process by substituting for the water as an oxidizer. Within the polymers the appropriate processing temperature is also characteristic to each polymer. The same polymer may exhibit different properties such as thermo-mechanical resistance, surface properties (free surface volume), chemical solubility, etc. depending on the manufacturing and process conditions such as casting, extrusion and vacuum processing. Processing temperature should not reach the level where the polymer changes its mechanical performance. This is especially important in those applications where the inorganic thin nanometer scale film is intended to provide extreme barrier performance combined with polymer substrate. For this reason, knowledge of the elastic and inelastic behavior of the flexible polymer substrate is important.

1.5.4 Thermo-mechanical behavior of thin film on flexible polymer substrate

Barrier films on polymer substrates are one the applications seen to have the most potential for ALD films. The barrier properties and performance of thin ALD films have been studied for flexible electronics [6-11, 78] and food packaging [21-23, 100, 101] applications. In both of these applications the polymer substrate is typically flexible foil material, which will be exposed to mechanical stress and thermal load under processing conditions. Even though ALD has shown its capability in low temperature processing, it is of great importance to understand the thermo-mechanical behavior of the substrate-thin film structure, especially in barrier applications. In general the lower the processing temperature will be, the less mismatch in thermo-mechanical behavior between the polymer substrate and thin inorganic film will occur.

Stresses present in thin films can be divided into two general categories; 1) intrinsic stresses, and 2) extrinsic stresses. Mechanical theory of thin films on flexible substrates can be scrutinized by using Figure 2 describing dimension and strain change (mechanical strain is defined as a relative change in dimensions) in this system at room and elevated temperatures [125].

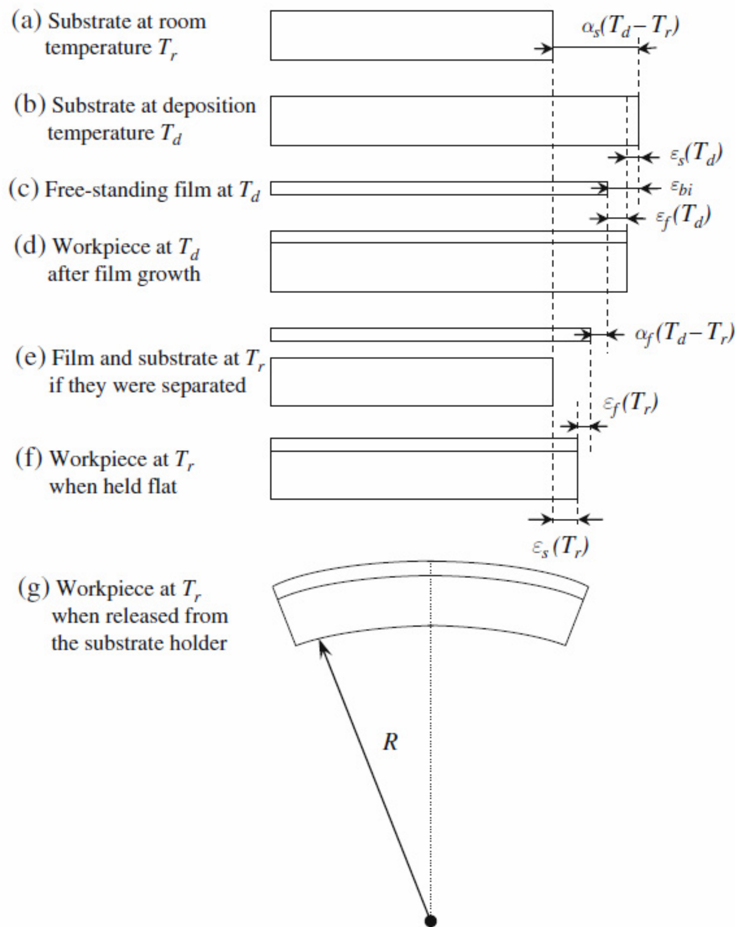

Figure 2. Length and width of film-on-foil structure at room and film growth temperatures [125].

When a substrate (s) with the thickness of d_s is coated with a film (f) with the thickness of d_f, the in-plane strain (ε_s) in the substrate of the flattened work piece with respect to the uncoated substrate at temperature T can be defined as [125]:

$$\varepsilon_s(T) = \frac{\lfloor (T_d - T)(\alpha_s - \alpha_f) + \varepsilon_{bi} \rfloor}{1 + \frac{Y_s^* d_s}{Y_f^* d_f}} \quad (2)$$

Where,

α_s and α_f are the coefficients of thermal expansion (CTE) of the substrate and the film respectively

ε_{bi} is the built-in strain in the film

Y_s^* and Y_f^* are the biaxial strain moduli of the substrate and the film respectively defined as

$$Y^* = \frac{Y}{1-\nu} \quad (3)$$

Where,

Y is the Young's modulus

ν is the Poisson ratio

Similarly the in-plane strain in the film of the flattened workpiece with respect to the free-standing film at the temperature T can be defined as:

$$\varepsilon_f(T) = -\frac{\lfloor (T_d - T)(\alpha_s - \alpha_f) + \varepsilon_{bi} \rfloor}{1 + \frac{Y_f^* d_f}{Y_s^* d_s}} \quad (4)$$

Applications where thin films are used generally require accurate overlay of the film on the substrate on which the device is to be fabricated. This is especially important in the

case of integrated circuits where misalignment between source/drain and gate electrodes can cause inferior device performance [125]. Strain/stress behavior of the film on the flexible substrate is of great importance also in those cases where thin inorganic films perform as diffusion barriers. Uncontrolled stress in the film will lead to the fracture of the film and consequently degraded diffusion barrier performance.

Accurate overlay alignment of the film would require ε_s (at room temperature after deposition) to become close to zero. ε_s can be minimized by minimizing the numerator $(T_d\text{-}T)(\alpha_s - \alpha_f) + \varepsilon_{bi}$ and maximizing denominator $1+\frac{Y_s^* d_s}{Y_f^* d_f}$ in equation 1. In practice in the case of flexible polymer substrates this can be made by 1) choosing the CTE of the polymer close to that of device layer, 2) lowering the deposition temperature, and 3) compensating the CTE mismatch with the strain built into the film. CTE of the polymer is usually larger than the CTE of the inorganic material and this option is quite difficult to implement in practice. Lowering the deposition temperature and compensation of the CTE mismatch caused by built in strain in the film are both related to deposition process optimization. In ALD, lower deposition temperatures require longer deposition times due to the need for longer purge times between the precursor pulses. Lowering the deposition temperature in ALD will also lead to a higher amount of impurities in the film, which may not be beneficial in the final application. A low deposition temperature in ALD, enabling deposition on polymer substrates, will mostly lead to an amorphous film structure. This can sometimes be beneficial for the film behavior during processing and in the final application.

In barrier applications where flexible polymer substrates are used, an amorphous structure of the thin film may find benefits over crystalline films through lack of grain boundaries [47]. The inorganic film thickness, though, has been found to be of primary importance since the critical strain leading to steady state channel crack propagation decreases with increasing film thickness. Miller's et al. results show that the film thickness has a significant role in the mechanical performance of thin films on compliant substrates, especially in applications where the substrate will be bent in its end

application or shall withstand a certain amount of curvature during the processing as in roll-to-roll deposition [47]. The failure modes such as film delamination, channel cracking, spalling of the film/substrate, and film buckling combined with delamination are related to elastic mismatch between the film and substrate. This elastic mismatch between two isotropic materials (substrate s and film f) can be scrutinized by using the so-called Dunder's elastic mismatch parameters, which define the mismatch in the plane tensile modulus across the interface (D_{tm}) and the mismatch in the in-plane bulk modulus (D_{bm}) [47].

$$D_{tm} = \frac{(\overline{E}_f - \overline{E}_s)}{(\overline{E}_f + \overline{E}_s)} \tag{5}$$

$$D_{bm} = \frac{1}{2}\frac{E_f(1+\nu_s)(1-2\nu_s) - E_s(1+\nu_f)(1-2\nu_f)}{E_f(1+\nu_s)(1-\nu_s) + E_s(1+\nu_f)(1-\nu_f)} \tag{6}$$

The effective modulus of the substrate or film in the case of in-plane strain can be expressed by equation 7.

$$\overline{E}_i = \frac{E_i}{(1-\nu_i^2)} \tag{7}$$

In the equations E and v are Young's modulus (Pa) and Poisson's ratio (unitless) respectively. Subscripts f and s are indicating the film and the substrate respectively. As can be seen from equation 5 the value of D_{tm} comes close to 1 when film material is much stiffer than substrate material and comes close to -1 when film material is compliant with

the substrate material. In the case where an inorganic film is deposited on polymer substrates the D_{tm} parameter indicates values close to 1 varying by some extent with the polymer used and the inorganic material characteristics. Mechanical robustness of ALD Al_2O_3 and molecular layer deposited (MLD) aluminum alkoxide has been studied by Miller and Jen [47, 126]. In Miller et.al's work the ALD and MLD films were studied as ~~a~~ monolayers on PEN substrates and also as multilayer structures forming nanolaminate films of aluminum oxide and aluminum alkoxide. They found experimentally that the critical strain of single layer ALD Al_2O_3 leading to crack propagation is increasing with decreasing film thickness. This was also supported theoretically. A 5 nm thick Al_2O_3 layer had a critical strain of 5 %, which was found to be significantly higher than the critical strain for conventional thin film materials on the micrometer scale. This strain is equivalent to 0.64 mm critical bending radius on a 75 µm thick PEN substrate. However, the critical strain of a 25 nm thick Al_2O_3 layer had a value of 1.56 %, which already is at the same level as conventional thin film materials. Dependency of critical tensile strain on ALD film thickness has also been reported by Jen et.al. Ultrathin Al_2O_3 films deposited on heat-stabilized PEN showed clearly higher critical strains than thicker films. The critical tensile strains for 5 nm and 80 nm Al_2O_3 films were reported to be 2.4 % and 0.52 % respectively. In the same study, Teflon FEP substrates were used to study the critical compressive strains of Al_2O_3 ALD films due to a large thermal expansion coefficient of Teflon FEP and consequently larger contraction of the substrate than ALD Al_2O_3 films during the cooling down. Similarly to tensile strain, the critical compressive strain was found to be higher for thinner ALD films [126].

The substrate-film curvature caused by elastic mismatch strain may have a different origin such as thermal expansion effects, epitaxial mismatch, phase transformation, chemical reaction, moisture absorption or other physical effect [127]. Regardless of the reason for the strain, it is important for many applications to identify the critical limit for the substrate/film curvature where the film remains in the elastic deformation region and avoid mechanical failure in the device. The radius of curvature can be defined by the Stoney formula (8) [125, 127, 128].

$$R = \frac{d_s}{6 \frac{Y_f^* d_f}{Y_s^* d_s} \cdot \varepsilon} \tag{8}$$

In equation 8 ε is the mismatch strain, which arises from the thermal mismatch strain caused by the difference between the thermal expansion coefficient of the substrate $\alpha_{s,}$ and that of the film $\alpha_{f,}$ and the built-in strain ε_{bi} in the film. ε can be written as,

$$\varepsilon = (\alpha_f - \alpha_s) \cdot \Delta T + \varepsilon_{bi} \tag{9}$$

where ΔT is the difference between the deposition and the room temperature. Equation 8 applies only when $Y_f d_f << Y_s d_s$, when the substrate dominates and the film complies with it. In the case where a stiff film has been deposited on a compliant substrate the products of Young's modulus and thickness may become close to equal, $Y_f d_f \approx Y_s d_s$, and it leads to much more complicated mechanical situation than with resistant substrates [125, 127]. Now the radius of curvature is given by,

$$R = \frac{d_s}{6 \frac{Y_f^* d_f}{Y_s^* d_s} \cdot \varepsilon} \cdot \left[\frac{\left[\left(1 - \frac{Y_f^* d_f^2}{Y_s^* d_s^2} \right)^2 + 4 \frac{Y_f^* d_f}{Y_s^* d_s} \left(1 + \frac{d_f}{d_s} \right)^2 \right] \left[\left(1 - \nu_s^2 \right) + \left(\frac{Y_f' d_f}{Y_s' d_s} \right)^2 \left(1 - \nu_f^2 \right) \right]}{\left(1 + \frac{d_f}{d_s} \right) \left(1 + \frac{Y_f' d_f}{Y_s' d_s} \right) \left[\left(1 - \nu_s^2 \right) \left(1 + \nu_f \right) + \frac{Y_f' d_f}{Y_s' d_s} \left(1 - \nu_f^2 \right) \left(1 + \nu_s \right) \right]} + \right.$$

$$\left. + \frac{3 \left(\frac{Y_f' d_f}{Y_s' d_s} \right)^2 \left(1 + \frac{d_f}{d_s} \right)^2 \left[\left(1 - \nu_s^2 \right) + \left(1 - \nu_f^2 \right) \right] + 2 \frac{Y_f' d_f}{Y_s' d_s} \left(1 - \nu_s \nu_f \right) \left(1 + \frac{Y_f' d_f}{Y_s' d_s} \right) \left(1 + \frac{Y_f' d_f^3}{Y_s' d_s^3} \right)}{\left(1 + \frac{d_f}{d_s} \right) \left(1 + \frac{Y_f' d_f}{Y_s' d_s} \right) \left[\left(1 - \nu_s^2 \right) \left(1 + \nu_f \right) + \frac{Y_f' d_f}{Y_s' d_s} \left(1 - \nu_f^2 \right) \left(1 + \nu_s \right) \right]} \right] \tag{10}$$

In equation (10) $Y_f^{'} = \frac{Y_f}{1-\nu_f^2}$ and $Y_s^{'} = \frac{Y_s}{1-\nu_s^2}$ represent the plain strain moduli of the film and the substrate, respectively.

2 EXPERIMENTAL METHODS

2.1 Thin film deposition and plasma treatments

The ALD films were grown in a flow-type hot-wall Beneq TFS-500 ALD tool, that was equipped with a plasma reactor (**I, IV**) or conventional thermal energy reactor (**II,III**). The film depositions were mainly carried out at temperature below 65 ºC to be suitable for the polymer substrate used in this study. The effect of higher deposition temperature of 150 ºC on PET substrates and the combined performance of ALD layers on PET was scrutinized in the study presented in paper **III**. The pressure during the deposition was around $2 \cdot 10^{-2}$ Pa. Two different ALD film materials, Al_2O_3 and TiO_2 were deposited by using trimethylaluminium (TMA) and tetrakis(dimethylamido)titanium (TDMAT) as metal precursors and both O_3 and O_2 plasma as oxidizers. The films were deposited on Silicon (100), sodalime glass and number of polymer substrates presented hereafter.

Magnetron sputtering of Ti and TiC films was carried out in a Sloan SL1800 magnetron sputtering deposition system. These films were deposited on PMMA and ALD coated PMMA substrates to study the performance of the ALD oxide film as an intermediate adhesion layer on polymer substrates and as a shield against ion bombardment and plasma UV radiation [**II**]. In this study two different plasmas were studied. A pulsed DC plasma exposure was carried out in the Sloan SL1800 magnetron sputtering system and the RF plasma treatments with argon in the plasma reactor attached to the Beneq TFS-500 ALD system, described more detailed in [**I**].

2.2 Substrate materials

2.2.1 PMMA

Polymethylmethacrylate (PMMA) has wide range of applications. It is used e.g. in optoelectronic and optical applications due to its high optical clarity [110, 111, 121, 129-131], in medical applications such as in microfluidic devices and in tissue engineering due to its biocompatibility [132-135], and in microelectromechanical systems (MEMS) [86]. Commercial PMMA (PLEXIGLAS® XT) with average molecular weight of 150000 – 160000 g·mol^{-1} was used in this study.

2.2.2 PC

Polycarbonate (PC) is a widely used engineering plastic with high toughness. It is used e.g. in compact discs and as a food packaging material [86]. Polycarbonate is transparent and therefore finds its usage in optical applications [110, 131]. Commercial PC plate with thickness of 2 mm was used in this study.

2.2.3 Low density polyethylene (LDPE)

LDPE is very widely used polymer and one of its main applications is in packaging film. LDPE is very tough and flexible, that makes it especially suitable for flexible packaging applications [86]. In this study the LDPE was used as an extrusion coated barrier film on paper to form a typical fiber based flexible packaging material. In extrusion coating processes the melt temperatures are much higher than the melting temperatures of coating polymers. For LDPE, the melt temperature is approximately 200 ºC over the melting temperature. The polymer melt is then cooled down rapidly on a chill roll when laminated with the web material. The morphology of extrusion coated LDPE is semicrystalline with the level of crystallinity typically around 50 % [90]. Crystallinity of the LDPE coating, however, depends on processing conditions and the crystallinity of the

polymer pellet. The crystallinity of the polymer coating may be lower than the crystallinity of its pellet due to a rapid cooling in the process and consequently a short time for the polymer to crystallize [136].

2.2.4 Polypropylene (PP)

Polypropylene is a multipurpose thermoplastic and it has been used in various formats. Polypropylene is available in fibre form and it is a widely used polymer in nonwoven products. Other usage can be found from different types of consumer and engineering products and it is also used in packaging applications. As a packaging and cover material it finds use in applications where temperature and grease resistance is required [86]. Isotactic polypropylene is a semicrystalline material. The crystallinity depends on the rate of melt quenching and annealing [137]. Similarily to LDPE, the crystallinity of extrusion coated PP may decrease in the extrusion coating process [136].

2.2.5 Polyethylene terephthalate (PET)

Polyethylene terephthalate (PET) belongs to the group of polyesters. PET is a product of esterification of ethylene glycol with a dibasic acid [90]. Depending on the thermal cycling during its processing PET can be found both in an amorphous and a semicrystalline form. Similarily to polyolefins, the state of crystallinity determines the properties of PET. Semicrystalline PET together with polyethylene naphthalate (PEN) are the two main polymeric transparent film material used in the development of flexible electronic applications [138]. Commercial PET films are available in a heat stabilized form, which can undergo higher temperatures with higher thermal stability [138, 139]. In extrusion coating, PET can be processed as an amorphous or as a semicrystalline material depending on the required end properties. Amorphous PET is clear and heat-sealable, an important characteristic in packaging applications. Amorphous PET will crystallize under thermal cycling. Increased crystallinity will reduce the permeability of e.g. oxygen [90].

2.2.6 Polylactide (PLA)

Biodegradable polymers are an interesting group of materials because of their biocompatibility and biodegradability and consequent wide range of applications from medicine and surgery to packaging [90, 95]. Synthetic biodegradable polymers, such as polylactides (PLA), have been studied in extrusion coating to meet the requirement of sustainable development and polymer waste management [90]. Copolymers of PLA with polyglycolic acid (PGA) and poly(ε-caprolactone) (PCL) have been studied in medical applications, such as in implant materials [90, 95]. The percentage of the L-unit in PLA (repeating unit of polymer) is commonly used to indicate its optical purity. PLA with high optical purity is a semicrystalline material. Optical purity decreases with decreasing crystallinity and PLA with less than 87,5 % optical purity is amorphous. PLA is a strong but brittle polymer with 4 % elongation at break [95].

2.3 Film and ALD process characterization

The films and their performance were characterized by many different methods. The ALD film thickness and refractive index were measured from silicon substrates with a spectroscopic ellipsometer M-2000FI from J. A. Woollam. The sputtered Ti and TiC film thickness was measured with a stylus profiler Veeco DEKTAK 6M.

The structure of the deposited ALD films and polymer substrates was studied with ATR-FTIR (Attenuated total reflection Fourier transform infrared) spectroscopy method using a Nicolet 4700 FT-IR spectrometer equipped with a Smart Orbit ATR accessory. In ATR-FTIR spectroscopy contrary to FTIR where the IR beam travels through the sample, the substrate is placed in close optical contact with an internal reflection element (IRE) that is transparent to the IR wavelengths concerned. This measurement set up is surface sensitive and is well suited for thin film characterization [111]. In ATR-FTIR the IR radiation is used to initiate the molecular vibrations in the material. When the vibrational or rotational motion of the molecule has been initiated, its dipole moment can change. The molecule will absorb the infrared radiation if there is a net change in the dipole moment. If the infrared radiation and molecular vibration oscillates at the same frequency, a net transfer of energy occurs that will be seen as a change in amplitude of the molecular vibration. Molecules will vibrate at particular frequencies which then can be identified [140].

Raman spectroscopy and IR spectroscopy can be seen as complementary techniques to each other. Some molecular bonds are infrared active, whereas some others are Raman active. Similarly to IR spectroscopy the Raman spectroscopy can be used to identify the type of quantized vibrational changes in molecules. Whereas IR absorption requires a change in molecule dipole moment, in Raman scattering a change must occur in the polarization of the molecule. When an electric field is applied to a molecule it can distort the distribution of electrons causing temporary polarization and induce a change in dipole moment. In Raman spectroscopy a sample will be irradiated with a powerful laser source with variable wavelengths. When photons interact with the molecules of a sample they

can induce transitions between energy states of the molecules. The photons are scattered by the molecular system, characteristic to the material, and the scattered radiation will be depicted with a spectrometer. When the scattered radiation has the same wavelength as the irradiated radiation, the emitted radiation is elastic and is called Rayleigh scattering. In Rayleigh scattering no energy will be lost. Raman scattering occurs when the incident and emitted radiation have different wavelengths. If the energy changes in the molecule due to a photon interaction the energy of the scattered photon will also change in respect to the incident photon energy. This energy change will produce so-called Stokes and anti-Stokes scattering depending on whether the energy of the scattered radiation is less or greater than the incident photon energy. The Stokes and anti-Stokes scattering is frequency-shifted from the Rayleigh scattering corresponding to the energy change [140]. In this study, a Horiba Jobin Yvon HR 800 UV Raman spectrometer was used to scrutinize the structure and structural transitions with increasing deposition temperature of TiO_2 films. The laser source used was a He-Cd laser with 325.04 nm wavelength.

The structure and the crystallinity of TiO_2 films grown from TDMAT and ozone were verified by X-ray diffractometry (XRD) with a Philips X'Pert system using CuKα radiation at wavelength of 1.54 Å. The glancing angle used for the incident beam was 1º and scanning was performed over the 2θ ranging between 20 to 60º.

The films chemical analysis, both qualitative and quantitative, were performed by energy dispersive X-ray spectroscopy (EDS) (EDAX Sapphire Si(Li) detecting unit), attached to scanning electron microscopy (SEM) and X-ray photoelectron spectroscopy (XPS). In EDS the energy of the X-rays emitted when the material is bombarded with electrons is collected by energy dispersive spectrometer. The X-rays are formed in a process where the emitted electron from the inner orbital of the atom is replaced by the electron from the outer orbital of the same atom. The energy of the emitted X-rays is characteristic to each element depending on the difference between the orbitals of the atom [140]. In XPS the source of radiation is X-ray photons. When material is bombarded with photons of sufficient energy the energy will be transferred to the electrons of the atoms and thus can be ejected. The specific kinetic energy and intensity of the ejected photoelectrons can be

measured by an electron spectrometer. When the energy of the X-ray photons is known (typically used sources are MgKα with photon energy of 1253.6 eV and AlKα with 1486.6 eV) the binding energy of an electron, characteristic to the atom and orbital from which the electron was emitted, can be determined. The advantage of XPS is that additionally to atomic composition of material it can provide information about the structure and oxidation state of the compounds [140]. This characteristic was used to study the structure of PA-ALD TiO_2 films presented in paper **IV**. In this study the XPS measurements were performed by using PHI 5400 XPS system with MgKα radiation (1253,6 eV) at $1,33 \cdot 10^{-6}$ Pa pressure in the measurement chamber.

The surface morphology of the substrates, films and fracture interfaces was studied from scanning electron microscopy (SEM) images taken with a field emission gun (FEG) SEM Hitachi S-4800, and by tapping mode atomic force microscopy (AFM) using a CP-II scanning probe microscope from Veeco Instruments. In SEM the surface of the sample is scanned with an electron beam resulting in a number of emitted signals, from which the backscattered and secondary electrons are used to visualize the object. In AFM the force-sensing cantilever with tip is scanned over the sample surface. The force between the flexible cantilever and the sample surface causes deflections of the cantilever, which can be detected optically. In tapping mode AFM the cantilever is oscillated at a frequency of a few hundred kilohertz and the tip will be in contact to sample surface only periodically at the bottom of each oscillation cycle. The changes in frequency when the position of the tip changes in respect to sample surface will then be used to image the surface topography. Contrary to contact mode AFM, by tapping mode it is possible examine highly sensitive materials such as biological samples and soft polymers [140].

Transmission electron microscopy (TEM) was used to examine further the structural changes taking place in TiO_2 films with increasing deposition temperature. The TEM system used was a JEOL 2010 F microscope with accelerating voltage of 200 kV. TiO_2 films produced using TDMAT and ozone at 55 and 180 ºC deposition temperatures were deposited directly on an electron-transparent Si/SiO_2 membrane window. The method was used both for surface imaging and for selected area electron diffraction (SAED, or

SAD). In TEM a thin sample is irradiated with a high-energy electron beam. The electron intensity distribution behind the sample is then imaged with the specific lens system [141].

The film adhesion was measured by a simple peel-off tape test and by the stud pull-off method using the PAT adhesion tester according to the ASTM D 4541-02 standard. The ALD film performance as a barrier against water (WVTR) and oxygen vapor (O_2TR) was studied by using the cup-method following the SCAN P22:68 and Mocon Ox-Tran Model 2/21 following the standard ASTM D 3985 respectively.

Optical emission spectroscopy (OES) was used to study the plasma characteristics during the plasma pulse of the ALD cycle. Two different OES systems were used. The time-resolved emission of particular spectral lines was collected with an IFU AOS-4 system and the full emission spectra between the wavelengths of 180 nm to 880 nm were collected with a Plasus Emicon system.

3 RESULTS AND DISCUSSION

The main results are summarized in this Chapter. More detailed experimental work, results and discussion are presented in the original publications (**I-IV**).

3.1 Film growth characteristics

Plasma-assistance in ALD has been shown to provide a tool to develop efficient ALD processes at low temperatures suitable for thermally fragile polymer substrates. A new design of plasma source was used to study the growth characteristics of Al_2O_3 by using TMA and O_2 plasma at room temperature [**I**]. The film growth rate was found to follow a different trend when the substrate distance from the plasma source was changed (Figure 3). The lower film growth rate with the longer plasma source distance and short oxygen plasma pulse length is believed to be caused by reduced oxygen radical concentration at the substrate surface leading to unsaturated film growth. This shows that the distance of plasma source from the substrate is a critical factor in respect of film growth and process efficiency. The efficient radical production and flux for the ALD surface reactions becomes more dominant in the spatial ALD processes, where the conventional time sequencing of precursor pulses and purges is dependent on substrate speed [52, 140]. In general, insufficient radical flux may lead to unsaturated film growth [57, 58, 66] and in the case of spatial ALD to a compromise between film growth rate and web speed [52, 142].

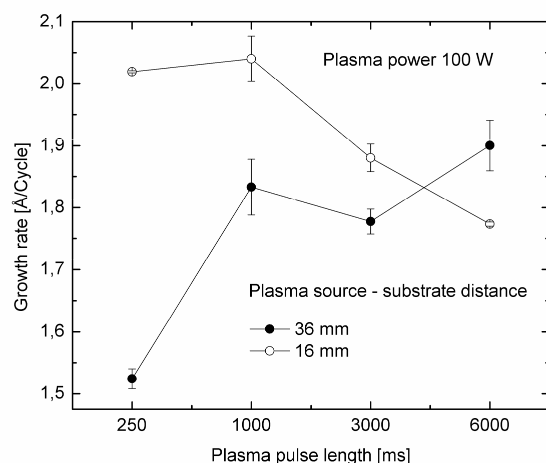

Figure 3. The film growth rate of Al_2O_3 films as a function of oxygen plasma pulse length and the plasma source distance from the substrate.

In addition to the difference in oxygen radical concentration available to ALD reactions between two different plasma source distances, the difference in film growth rate was attributed to a difference in reaction mechanism. The higher growth rate with shorter plasma source distance and with short oxygen plasma pulse length may lead to a concurrent reaction path with H_2O possibly produced in this type of oxygen plasma process [77].

The growth rate of PA-ALD TiO_2 increases with an increase of oxygen pulse length and saturates at the level of around 0,1 nm/cycle after 3 seconds pulse length as shown in Figure 4. An earlier study with ozone as the counter reactant revealed that the growth rate is temperature dependent at deposition temperature below 100 ºC as shown in Figure 5 [143]. The growth rate above 100 ºC saturates at the level of around 0,044 nm/cycle, that agrees well with the earlier studies where water [144], H_2O_2 [145] and oxygen plasma [146] have been used as a counter reactant to TDMAT. In the case where the film below 100 ºC (at 55 and 70 ºC) is grown in the self-limiting manner, one can expect that the

density of the reactive surface species is higher at these lower temperatures. When temperature has been increased the growth rate decreases due to the decreased density of reactive surface species [1]. If the film growth is out of the self-limiting region the increase in growth rate can be explained through multilayer adsorption and the condensation of precursors as described in Figure 1 [1]. However, the film growth rate of PA-ALD TiO_2 using TDMAT and O_2 plasma in the low deposition temperature region is clearly higher (Figure 4) than the growth rate of the film grown from TDMAT and ozone (Figure 5).

One characteristic related to process efficiency shown in Figure 4 compared to previous studies [144, 145] is the several times longer oxygen plasma pulse required to saturated film growth compared to water and H_2O_2. The issue of low radical concentration was discussed earlier together with Al_2O_3 PA-ALD and should be considered here also as a possible debilitating factor for process efficiency. On the other hand at low temperature, especially, water requires relatively long purge time.

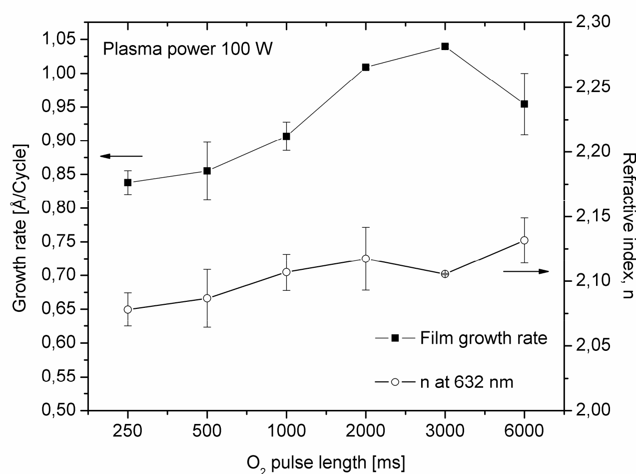

Figure 4. Growth rate and refractive index of PA-ALD TiO_2 films as a function of O_2 pulse length. Nitrogen was used as a carrier gas.

The change of process parameters by means of carrier gas and plasma power used in PA-ALD TiO_2 process revealed some divergences. At low plasma power level (25 W) and with nitrogen carrier gas the growth rate remained at a considerably lower level than with higher plasma power and with argon carrier gas (Figure 1 in paper **IV**).

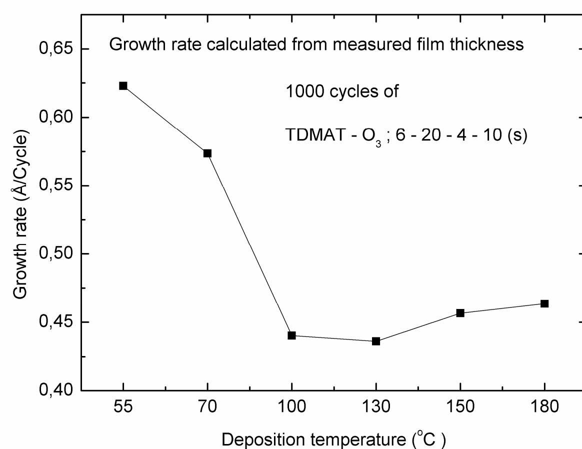

Figure 5. Growth rate of ALD TiO_2 films as a function of deposition temperature. Precursors used were TDMAT and ozone.

3.2 Film composition and film structure

The PA-ALD Al_2O_3 film chemical composition was determined and scrutinized by EDS and ATR-FTIR [**I**]. The films had an aluminum content similar to previous studies [57], were oxygen rich and had carbon as an impurity. Due to the insensitivity of the EDS method to light elements, the elemental compositions are not quantitatively precise, but will show relative changes between the films grown under different conditions. In general the carbon and carbonaceous groups content decreased with increasing oxygen plasma pulse length with both plasma source positions. Longer oxygen plasma pulse length with both plasma source distances led to a quite similar film composition. Nitrogen incorporation was detected from the films in the case of short plasma source distance and when longer oxygen plasma pulse and higher plasma power was used for longer plasma source distance. It was also noticed that the plasma power has an effect both on film growth characteristics and film chemical composition. Lower plasma power with this particular plasma source design resulted in lower growth rate but more a stoichiometric O/Al ratio than with higher plasma power.

The PA-ALD TiO_2 chemical composition measured by XPS revealed no significant difference was found in Ti, O, N, and C concentration between the films deposited with different plasma power, different carrier gas, and varied oxygen plasma pulse length (Table 1 in **IV**). Similarly to Al_2O_3 films TiO_2 films have carbon contamination in the film. All the films regardless of deposition conditions have relatively high nitrogen incorporation in the film thought to originate from the TDMAT precursor. Further examination of chemical bonding in the films from the Ti 2p, O 1s, N 1s and C 1s peaks of the XPS spectra revealed that the Ti in the films is mostly in TiO_2 format, but is also somewhat dependent on plasma power and the carrier gas used in the process. This can be seen most clearly in the film grown with 25 W plasma power and nitrogen carrier gas, which has highest concentration of reduced oxidation states (Ti_2O_3, Ti^{3+}) within the films studied. The same deposition conditions led also to the lowest growth rate, shown in Figure 4 in the previous Chapter.

XRD analysis of TiO_2 films grown from TDMAT and ozone indicated that the film structure is amorphous regardless of deposition temperature in the range 55 to 180 ºC. Raman spectroscopy, though, showed itself to be an applicable method to study the film structure and the transitions occurring in the film structure with increasing deposition temperature. Raman spectra of these films shown in Figure 6 agree well with those in previous studies for anatase [148-155] and reveal that Raman active optical modes develop in the films with increasing deposition temperature. Anatase TiO_2 belongs to the space group D_{4h}^{19} ($I4_1$/amd) and its primitive unit cell is tetragonal [147]. Based on factor group analysis there are six Raman active modes E_g (v6), E_g(v5), B_{1g} (v4), (A_{1g}+B_{1g}) (v2+v3) (duplicate), and E_g(v1) [148-153] . In bulk anatase (e.g. in powder format) these Raman active modes have Raman shifts at 143, 196, 396, 515, 637 cm^{-1} respectively [153]. Similar peak positions of these Raman active vibrational modes have been reported also for magnetron sputtered TiO_2 [148, 149] and sol-gel type TiO_2 films [151]. Bands can shift to higher position in wave number, broaden asymmetrically and decrease in intensity with the decrease in particle size [153, 154]. Shifting of wave number to higher position has also been suggested to be due to a heating and plasma effect of the laser [150]. The peak positions in Figure 6 are 156.3, 206.6, 400.3, 522.7, and 632.7 cm^{-1} attributed to belong to Raman active modes of anatase E_g (v6), E_g(v5), B_{1g} (v4), (A_{1g}+B_{1g}) (v2+v3) (duplicate), and E_g(v1) respectively. All the wave numbers, except Eg(v1) at 632.7 cm^{-1}, are shifted to higher positions from those to reported bulk anatase. As reported in earlier studies [150, 153, 154] this is attributed to a heating and plasma effect of the UV laser used in the measurements, and also to the fine grain size existing in the mainly amorphous film matrix. The other two crystal structures of TiO_2, brookite and rutile have also been studied by Raman spectroscopy. Brookite may show 36 Raman active modes, which are $9A_{1g}$, $9B_{1g}$, $9B_{2g}$ and $9B_{3g}$, where as Rutile has four Raman active modes A_{1g}, B_{1g}, B_{2g} and E_g [154]. Three natural crystal structures of TiO_2 (anatase, brookite and rutile) can be distinguished by Raman spectroscopy and their Raman shifts can be found from literature [152, 153, 155-157].

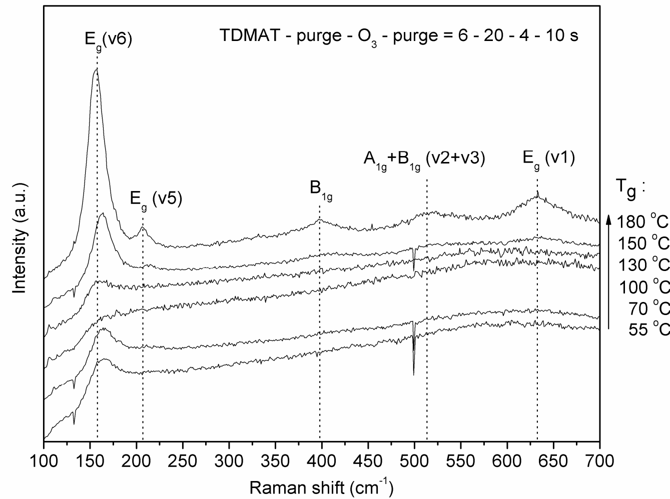

Figure 6. Raman spectra of ALD TiO_2 films deposited at temperature range of 55 to 180 ºC. The measurement was done on the film deposited on sodalime glass by using UV (254 nm) laser.

Transition in film structure studied by Raman spectroscopy can be further scrutinized and confirmed by transmission electron microscopy (TEM). TEM images and inserted selected area electronic diffraction (SAED) patterns of TiO_2 films grown at 55 and 180 ºC using TDMAT and ozone in Figure 7 reveal the transition of film structure with increasing deposition temperature. The TiO_2 film grown at 55 ºC shows an amorphous structure in the TEM image, and the diffraction rings in SAED insets, typically observed in crystalline films [158-164] can not be seen. Furthermore a similar diffuse ring is observable in SAED of dark-field TEM image (lower SAED inset in Figure 7a), earlier reported to be indicative of the amorphous state of material [165]. The TEM image of TiO_2 grown at 180 ºC shown in Figure 7b indicates the transition of the film from amorphous (7a) to fine-grained structure (dark spotty network) embedded in an amorphous matrix. The size of the crystallites, attributed to anatase, measured from the Figure 7b, is approximately 10 nm. The inset SAED pattern in Figure 7b clearly shows diffraction spots along the diffraction rings indicating the development of crystalline structure [158-160, 162]. The fine grained structure shown in Figure 7 agrees well with

Raman spectroscopy analysis, where the shifting of peak positions to higher wave numbers was partly attributed to a small particle size.

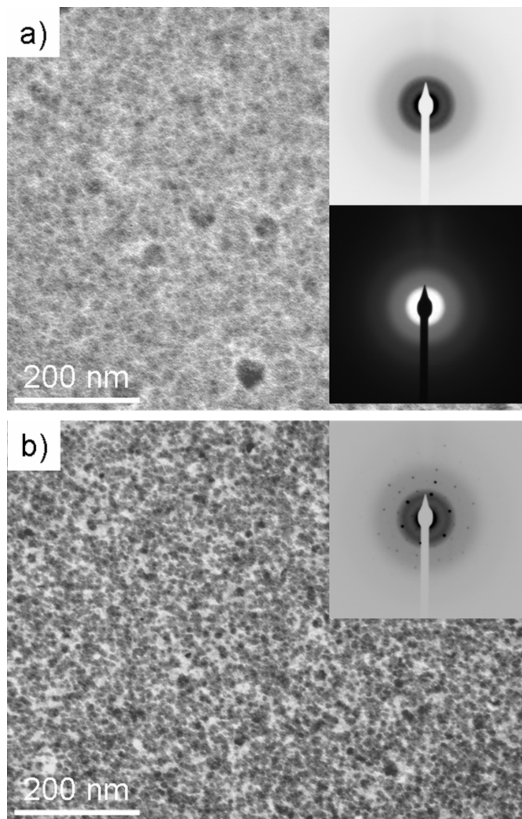

Figure 7. TEM images with SAED insets of ALD TiO_2 films grown from TDMAT and ozone at deposition temperature of a) 55 ºC and b) 180 ºC.

3.3 Film performance

3.3.1 ALD film adhesion

ALD has shown its ability to deposit functional and extremely well-adhered films on a number of polymeric substrates. In certain cases the film adhesion, though, can be degraded due to deposition process characteristics [**II**, **IV**, 111, 113, 114, 117-120]. In this study, the ALD oxide film adhesion was studied on PMMA substrates. It is known that the photodegradation of PMMA is happening through the direct photolysis of ester or methyl side groups that will lead to side chain scission [96, 107]. This will then greatly weaken the bonded surface region of PMMA and can cause poor film adhesion. PMMA, as susceptible to radiation damage, makes plasma deposition processes especially challenging given the existence of plasma UV radiation and ion bombardment e.g. in the case of magnetron sputtering. ALD oxide films were studied as intermediate adhesion layers and plasma UV shielding layers prior to magnetron sputtered Ti and TiC [**II**]. The cross-cut image of such a duplex film on PMMA substrate is shown in Figure 8.

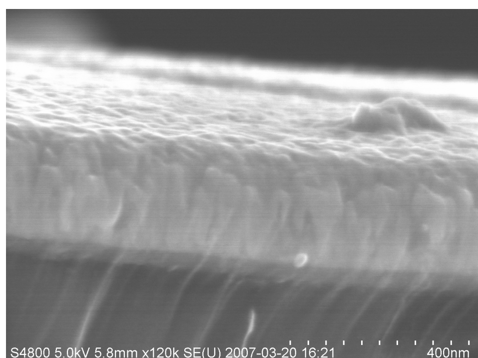

Figure 8. The cross-cut SEM image of ALD Al_2O_3 and magnetron sputtered Ti films on PMMA.

Adequate film adhesion of magnetron sputtered Ti or TiC was achieved only with an intermediate ALD layer between the PMMA substrate and magnetron sputtered film. Film adhesion increases with increasing ALD film thickness and around 30 nm ALD film thickness was required to achieve an adhesion strength higher than the cohesive strength of PMMA itself. This can be seen as a clear removal of polymer from the polymer bulk in a pull-off adhesion test (Figure 9a). In contrast to high film adhesion case in Figure 8a, the figure 9b represents the situation without ALD intermediate layer. The low adhesion strength measured by pull-off test visualizes as a removed weakly bonded polymer netlike structure together with deposited film, caused by the mechanism described above.

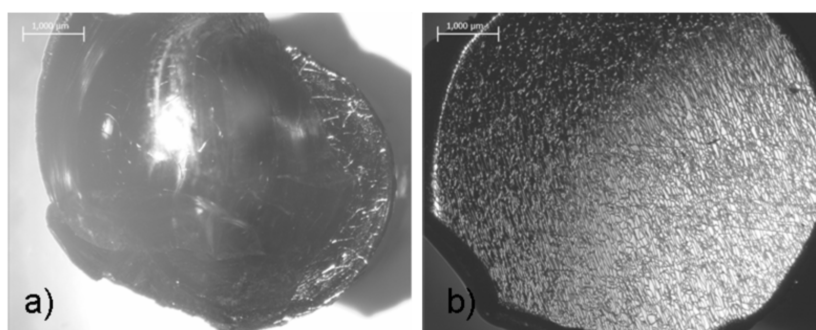

Figure 9. Fracture interface viewed from the metal stud removed from the PMMA substrate by pull-off test procedure: a) PMMA with around 30 nm ALD Al_2O_3 and sputtered Ti; b) PMMA with sputtered Ti.

3.3.2 ALD film shielding effect against UV/VUV –radiation and ion bombardment

ALD films can be used to protect polymers from atomic oxygen erosion, ion bombardment and VUV-induced degradation [**II**, 25]. Initially, the magnetron sputtering of Ti and TiC films and the adhesion evaluation proved that this concept of polymer protection is possible. Further investigations to study the effect of ion bombardment and plasma UV radiation on PMMA substrate were carried out by using two different plasma sources. A pulsed DC plasma source was used to provide a source of both ion

bombardment and plasma UV radiation, whereas an RF plasma source with relatively low self-bias voltage was used as a source for the plasma UV radiation. In fact, the same RF plasma source was used in the PA-ALD studies [**I, IV**]. Furthermore the RF plasma treatment on PMMA substrates was carried out behind a quartz window, with an absorbance edge of 170 nm, to see if the UV radiation above this wavelength affects PMMA and thin film adhesion deposited on PMMA. Initially both plasma treatments showed degradation of the PMMA surface. The outcome is poor ALD film adhesion after plasma treatments. The shielding effect of an ALD oxide layer against plasma exposure was found to depend on both plasma type and the composition and thickness of the ALD layer. The damaging effect of plasma exposure created by the pulsed DC was able to be avoided with 33 nm Al_2O_3, whereas with TiO_2 only 20 nm was required. More effective shielding by TiO_2 is attributed to the higher absorption coefficient of TiO_2 than Al_2O_3 and consequently better shielding of UV radiation [**II**]. Less than 10 nm ALD film thickness for Al_2O_3 on PMMA, when exposed to pulsed DC plasma, showed CH_2 formation in ATR-FTIR attributed to a PMMA side chain scission. The formation of CH_2 could be detected with the same thickness of TiO_2, which further indicates the better UV resistance of the TiO_2 film. The better shielding effect of ALD TiO_2 film than the Al_2O_3 has also been reported by Minton et.al. [25]. In their study the PMMA degradation under UV exposure was measured as a mass-loss by QCM. They found that Al_2O_3 with thickness of 15,2 nm will significantly prevent the mass-loss of PMMA under VUV radiation. Due to a low absorption coefficient and consequently low absorption capability of Al_2O_3 in the VUV region, the phenomena was suggested to be caused by the physical barrier effect of Al_2O_3 to avoid the escape of photodegraded gaseous products rather than shielding the PMMA from VUV radiation. Particular plasma conditions have a significant role in polymer surface modification both directly and through side effects when plasma is used as a part of the deposition process. According to film adhesion results both Al_2O_3 and TiO_2 showed shielding effects against VUV radiation. The shielding effect is, however, dependent on the particular plasma conditions and consequently the radiation wavelengths created. The RF plasma conditions showed themselves to be more detrimental to coating adhesion than the pulsed DC plasma suggesting that RF plasma had more intense radiation in the VUV region. ATR-FTIR results revealed that the

modification depth is greater for pulsed DC plasma than for the RF plasma. This can be explained through higher intensity of DC plasma in the UV/VUV region or existence of the particular wavelengths in each of the plasmas. One hypothesis can be drawn based on the pressure difference and consequently difference in molecules present in these different plasmas. The operating pressure for the RF plasma was around 100 Pa while for the DC-plasma it was 3 Pa. Higher pressure allows higher concentration of molecules from air and water contamination present in the plasma that can build up intensive emission in the VUV region. However RF plasma creates radiation that causes greater degradation of the PMMA side chains than DC plasma.

The effect of ion bombardment on PMMA degradation can not be disregarded, especially in the case of magnetron sputtering, but also in the case of pulsed DC plasma treatment, where the average self-bias voltage is set around -350 V. A distinction between the effect of UV radiation and ion bombardment on the polymer substrate is relevant when tailoring the barrier structure. SRIM Monte Carlo ion implantation simulation for Ar ions with ion energy of 300 eV gives no significant difference in the penetration depth between Al_2O_3 and TiO_2. According to simulation the maximum implantation depth for both Al_2O_3 and TiO_2 is around 6 nm. Thus ion bombardment cannot account for the differences between the effect of TiO_2 and Al_2O_3 films of low thickness and therefore the structural changes in PMMA are attributed to be due to the plasma VUV radiation.

3.3.3 ALD film diffusion barrier properties on polymer extrusion coated flexible packaging materials

ALD films have shown their potential as diffusion barriers on flexible polymer substrates. Here the ALD Al_2O_3 and TiO_2 films and their performance have been studied as moisture and oxygen barriers on polymer extrusion coated flexible packaging materials [**III**]. Initially LDPE coated paper material was used to investigate the diffusion barrier properties as a function of polymer coating thickness and ALD film thickness. For this purpose the reciprocal of the measured WVTRs were plotted, named as the "diffusion resistance" of the material (a combination of paper, extrusion coated polymer

and ALD film) (Figure 1 in paper **III**). Increase in diffusion resistance will designate the decrease in WVTR. The study revealed that below an ALD film thickness of 15 nm the diffusion resistance is only slightly increased and therefore the polymer coating is dominating the gas diffusion. After an ALD film thickness of between 20 and 30 nm the additional diffusion resistance was found to be almost proportional to the additional ALD film thickness for all polymer coating weights and therefore above this ALD film thickness the gas diffusion is dominated by the ALD film.

ALD Al_2O_3 deposited on LDPE reached its maximum WVTR value for thicknesses of around 100 nm. One explanation can be the susceptibility of inorganic ALD films to exterior effects caused by thermal misfit between the polymer and ALD film. The handling of the sample pieces after ALD was done carefully but the degradation of the film due to a lack of mechanical robustness of ALD films with this thickness cannot be disregarded. The study of mechanical robustness by means of defect detection with the accuracy required for ALD films [45], though, was beyond the scope of this study.

Oxygen permeation shows different behavior from that of water permeation within the different polymer coating weights and ALD film thicknesses. The threshold value found in the case of WVTR can not be observed for oxygen (Figure 2 in paper **III**). O_2TR results also reveal that the polymer coating weight does not have a major effect, if any, on barrier performance after initial ALD film growth. This result provides an option to reduce the polymer coating weight in barrier structures. Similarly to WVTR, the O_2TR is not further decreased after the ALD film thickness has reached the level of 100 nm and one possible reason can be the defect formation in the ALD film.

Different polymers applied on flexible packaging material by extrusion coating have initially different performance as a moisture barrier (Table 1 in paper **III**). These polymers also behave differently in the barrier system where ALD film has been applied. The comparison of relative WVTR and O_2TR between LDPE, PP, PET and PLA with over 100 nm ALD Al_2O_3 denotes that the highest relative decrease in transmission values can be achieved on PET (Figure 3 in paper **III**). This can be explained through the lowest

initial O_2TR for PET. Presumably PET has lower level of surface defects that makes it favorable substrate for ALD. The highest decrease in WVTR for PET with ALD supports this hypothesis as well. Furthermore the AFM topography (in Figures 5b and 6c in paper **III**) shows the lowest surface roughness for PET. In the earlier study it has been suggested that the oxygen diffusion through the inorganic film is mainly dominated by defects and micron-scale pinholes [139]. Some evidence for this can be seen from the WVTR and O_2TR results where the ALD film was deposited on PET at 150 ºC (table 3 in paper **III**). The barrier against water vapor has not been completely damaged since the WVTR with ALD film is still lower than initial WVTR of bare PET, but barrier against oxygen, that is reportedly dominated by defects and micron-scale pinholes, has been dramatically deteriorated. This suggests the defect formation has occurred not only in the ALD film but PET as well due to a high deposition temperature. The difference between the coefficient of thermal expansion of polymer and inorganic film will lead in an uncontrolled situation to increase in strain and consequently cracking of the film under thermal cycling. This is critical in barrier applications since it has a direct effect on product performance.

Even if the strain in the polymer can be controlled other structural changes may take place during the deposition at elevated temperature. The surface morphologies studied by AFM show that the polymers behave differently under thermal cycling even at low temperature. LDPE seems to remain its surface structure at deposition temperature of 65 ºC, whereas PET and PP undergo structural changes at the surface. Both PET and PP form round shaped granules during deposition, which can be attributed to crystallization of the polymer. However, according to WVTR and O_2TR results, the crystallization of the polymer does not seemingly affect barrier performance. One factor suggested is still the relatively thick ALD layer deposited on the polymer. The effect of polymer crystallization may become more relevant in the case of ultrathin ALD layers (few nm), because the amorphous and crystalline sites of the polymer may give significantly different templates to ALD film nucleation and consequently initial film growth.

3.3.4 PA-ALD process characteristics and their effect on polymer substrate and film performance

Plasma conditions have particular interest in the case of PA-ALD. Plasma conditions in PA-ALD have been shown to affect film growth characteristics, film structure, and also polymer surface structure. The effect of plasma exposure can be beneficial or detrimental depending on the particular objective desired for the polymer surface modification.

One motive in using PA-ALD is to lower the deposition temperature allowing deposition on polymers. The mixture of plasma and carrier gases used in PA-ALD process and the reaction products created, such as hydrocarbons, can form a complex plasma situation and an intense source of VUV radiation [114]. Primarily in the case of thin film deposition by PA-ALD, the deposition itself is the desired modification of the polymer surface and the effect of plasma alone is mostly undesired. PMMA provides a good template to study the effect of plasma in respect of detrimental surface modification resulting in poor film adhesion [**IV**].

TiO_2 deposited on PMMA, PC and PP substrates by PA-ALD demonstrated the importance of understanding the plasma characteristics in PA-ALD on polymers [**IV**]. Satisfactory film adhesion measured by the peel off tape test was observed only in certain conditions depending on the RF plasma power and carrier and plasma gases used. The plasma emission spectra for two different processing conditions studied with plasma power of 50 W are shown in Figure 10. The plasma power of 50 W was the upper limit where the film adhesion was still satisfactory when nitrogen was used as the carrier gas. The same plasma power with argon carrier gas caused complete film delamination. Radiation power density (irradiance) increases with increasing plasma power. This is also shown as having a detrimental effect on PMMA, with nitrogen plasma above 50 W RF plasma power.

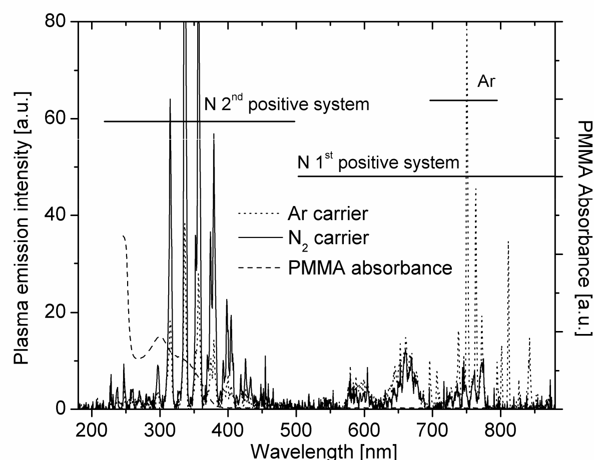

Figure 10. Plasma emission spectra from argon and nitrogen carrier gas plasma with 50 W plasma power during the plasma exposure step of the PA-ALD cycle (Figure 2 in paper IV).

The argon emission spectrum in Figure 10 gives the evidence for the argument in the previous Chapter where the more detrimental effect of RF plasma was attributed to the presence of contaminant molecules in the plasma. This is shown in Figure 10 as a clear nitrogen emission from the 2nd positive system for the argon plasma as well. That is attributed to originating from the background gas, mainly air remaining in the chamber. However this particular emission at this wavelength region can not be the source of photodegradation leading to poor film adhesion since the film deposited with nitrogen carrier gas showed satisfactory film adhesion. The dissociation energies of covalent bonds in polymers generally are within the range of about 3.0 – 4.3 eV corresponding approximately to 413 – 310 nm in radiation wavelength. The intensity of the nitrogen 2nd positive system emission shown in Figure 10, however, is not enough to cause the film delamination by side chain scission of PMMA within the 3 seconds plasma pulse over the 500 ALD cycles. Furthermore absorption of electromagnetic radiation is required before the photodegradation can take place [107]. The cut-off wavelength for PMMA film sits around 240 nm [107], which agrees well with measured absorbance of 2 mm PMMA plate shown in Figure 10 where the absorbance starts to increase around 250 nm. Thus it

can be concluded that the detrimental VUV radiation in the case of argon carrier gas lies below 200 nm. Time-resolved OES spectroscopy measurements of different plasma species revealed that the possible source of intensive VUV radiation exists through reaction products of PA-ALD process shown in Figure 8, where the optical emission of the chosen plasma species are compared between the processes where nitrogen and argon where used as carrier gases. The plasma emission monitoring and characterization in the VUV region below 200 nm, which was beyond the scope of this study, would provide valuable information from the plasma emission itself, but also about further chemical gas phase reactions taking place during the plasma pulse step. One example of such a reaction is hypothesized from the intensive OH-cation production with nitrogen carrier gas plasma, which may indicate the water molecule breakage [105]. More detailed plasma characterization and VUV emission monitoring are given as a future study prospect.

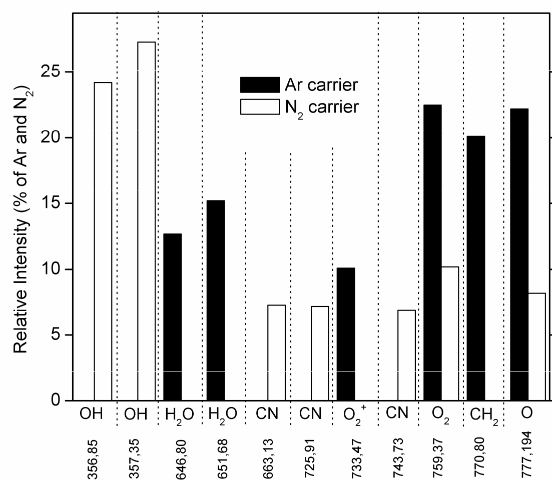

Figure 11. Average optical emission of selected plasma species in argon and nitrogen carrier gas plasmas during the plasma pulse step. (Figure 3b in paper IV).

4 CONCLUSIONS

Surface modification of polymers in industrial applications is often required to improve the performance to the desired level or to provide a way to create new value-adding properties. One surface modification method that has great potential to meet these demands is ALD. The results of this work show that ALD can be used to modify the polymer surface for further processing, to create certain characteristics on the polymer surface, and also to improve the performance e.g. in barrier applications.

Polymer material processing is limited by the temperature characteristic of each polymer and also by the electromagnetic radiation that can initiate the photodegradation process in the polymer surface and bulk. These limiting factors can be challenging for ALD especially in industrial applications where roll-to-roll production technology is required and fast product throughput is expected.

Water is the typical oxidizer used in ALD oxide processes. Water, though, has certain drawbacks at low deposition temperatures. Water requires long purge times that may complicate or even prevent the implementation of ALD in current industrial applications of polymers. Therefore it is crucial that more active precursors and, consequently, the enhancement of low temperature ALD process efficiency will be studied. More active oxidizers studied in this work were ozone and oxygen radicals produced by plasma activation. The film growth rate with ozone was found to be lower than with oxygen radicals. One possible explanation is that films grown in this study were achieved still at unsaturated mode even when a relatively long ozone pulse was used. This hypothesis suggests even longer ozone pulse or higher ozone generation is needed to reach saturated film growth. Plasma is an efficient way to generate oxygen radicals for low temperature ALD oxide processes. Plasma activation though will bring issues if the plasma conditions are not controlled with regard to the UV/VUV radiation produced by the plasma. Uncontrolled conditions will lead to photodegradation of the polymer, which can result in insufficient film adhesion.

The limited lifetime of oxygen radicals will put demands on plasma source development. In this study it was shown that the shorter distance between the plasma source and the substrate allows saturated film growth with shorter oxygen plasma pulse length. This supports the idea that for efficient production of radicals the plasma source should be located near at the substrate. On the other hand the close location of the plasma source from the substrate sets more demands on ALD process development and control, because of the existence of plasma UV radiation and possible ion bombardment. Both of these may have an effect on the polymer substrate and on ALD process chemistry and consequently on the film grown.

ALD oxide layers can be used as a shield against UV/VUV radiation and at the same time as an intermediate adhesion layer for the films produced by plasma processes, such as magnetron sputtering as used in this study. TiO_2 films performed better than Al_2O_3, which was attributed to the better absorbance of TiO_2 for UV/VUV radiation. The film performance as studied by means of film adhesion is promising for applications where metallization and hard coatings on plastics are desired.

ALD has been shown to provide extremely good gas barrier layers on polymer substrates and this has been put forward as one of the most promising industrial applications for ALD on polymers. In this study the ALD was applied on polymer extrusion coated flexible packaging materials. The results showed that ALD Al_2O_3 film can provide a sufficient level of barrier performance suitable for tropical packaging use. This particular application as well as many other industrial polymer based application, where barrier improvement is pursued, utilizes roll-to-roll production technology. This determines also the future research and development needs for ALD.

Spatial and roll-to-roll ALD development is necessary to open up the implementation of ALD in many of the industrial applications studied for low temperature ALD films thus far. High throughput processing requires even more efficient ALD processes. Polymers are thermally fragile and susceptible to electromagnetic radiation and due to that the understanding of ALD and PA-ALD process characteristics and their effects on polymers

during the deposition are of great importance. Suggested future work to clarify the findings and develop the ideas given in this work could be done under the following topics:

- Low temperature ALD process development (below 100 ºC) in spatial and roll-to-roll ALD.
- Detailed plasma characterization and photo emission monitoring at UV/VUV region by OES and other plasma characterization methods.
- PA-ALD process development and characterization subject to absorption of electromagnetic radiation of polymers. Here e.g. different gas combinations can be scrutinized to optimize the radical generation and filter out the detrimental electromagnetic radiation.
- Development of plasma sources used in PA-ALD for efficient radical production, also suitable for spatial ALD usage.
- Detailed studies on inorganic ALD film and compliant polymer substrate performance specific to the application. This may included e.g. thermo-mechanical resistance of combined ALD and polymer structure, and barrier performance development through multilayer structures.

REREFENCES

1. Ritala, M., Leskelä, M., in Handbook of Thin Film Materials, (Ed. H.S. Nalwa), Academic Press, San Diego, CA 2002, Vol. 1, p. 103-159.

2. Rossnagel, S. M., Sherman, A. Turner, F. J. Vac. Sci. Technol. B 18(4) 2000.

3. Suntola, T., Anstson, J. 1977 U.S. Patent 4,058,430.

4. Suntola, T., Simpson, M. (Eds.). Atomic Layer Epitaxy. Blackie and Son Ltd., London, 1990.

5. Lewis, J., Materials Today, Vol.9, 2004.

6. Groner, M. D., George, S. M., McLean, R. S., Carcia, P. F., Appl. Phys. Lett. 88, 051907 (2006).

7. Groner, M. D., Fabreguette, F. H., Elam, J. W., George, S. M., Chem. Mater. 16 (2004) 639.

8. Langereis, E., Creatore, M., Heil, S. B. S., Van de Sanden, M. C. M., Kessels, W. M. M., Appl. Phys. Lett. 89, 081915 (2006).

9. Dameron, A. A., Davidson, S. D., Burton, B. B., Carcia, P. F., Mclean, R. S., George, S. M., J. Phys. Chem. C 2008, 112, 4573-4580.

10. Carcia, P. F., Mclean, R. S., Groner, M. D., Dameron, A. A., George, S. M., J. Appl. Phys. 106 (2009) 023533.

11. Meyer, J., Görrn, P., Bertram, F., Hamwi, S., Winkler, T., Johannes, H-H., Weimann, T., Hinze, P., Riedl, T., Adv. Mater. 2009, 21, 1845-1849.

12. Ott, A. W., Chang, R. P. H., Mater. Chem. Phys. 1999, 58, 132-138.

13. Wang, J-C., Weng, W-T., Tsai, M-Y., Lee, M-K., Horng, S-F., Perng, T-P., Kei, C-C., Yu, C-C., Meng, H-F. J., Mater. Chem. 2010, 20, 826-866.

14. Guerrero, A. R., Ramirez, J. C., Polymer Bulletin 33, 541-548 (1994).

15. Sarkar, S., Culp. J. H., Whyland, J. T., Garvan, M., Misra, V., Org. Electron. 11 (2010) 1896-1900.

16. Potscavage, W. J., Yoo, S., Domercq, B., Kippelen, B., Appl. Phys. Lett. 90 (2007) 253511.

17. Chang, C-Y., Chou, C-T., Lee, Y-J., Chen, M-J., Tsai, F-Y., Org. Electron. 10 (2009) 1300-1306.

18. Carcia, P. F., Mclean, R. S., Reilly, M. H., Appl. Phys. Lett. 97 (2010) 221901.

19. Lim, S. J., Kwon, S-J., Kim, H., Park, J-S., Appl Phys. Lett. 91 (2007) 183517.

20. Zhao, D., Mourey, D. A., Jackson, T. N., IEEE Electronic Device Letters, Vol. 31, NO. 4, April 2010.

21. Hirvikorpi, T., Vähä-Nissi, M., Mustonen, T., Iiskola, E., Karppinen, M., Thin Solid films 518 (2010) 2654-2658.

22. Hirvikorpi, T., Vähä-Nissi, M., Harlin, A., Karppinen, M., Thin Solid Films 518 (2010) 5463-5466.

23. Hirvikorpi, T., Vähä-Nissi, M., Harlin, A., Marles, J., Miikkulainen, V., Karppinen, M., Appl. Surf. Sci. 257 (2010) 736-740.

24. Cooper, R., Upadhyaya, H. P., Minton, T. K., Berman, M. R., Du, X., George, S. M. Thin solid films 516 (2008) 4036-4039.

25. Minton, T. K., Wu, B., Zhang, J., Lindholm, N. F., Abdulagatov, A. I., O'Patchen, J., George, S. M., Groner, M. D., ACS Appl. Mater. Interfaces, 2010, 2(9), 2515-2520.

26. Kemell, M., Färm, E., Ritala, M., Leskelä, M., European Polym. J. 44 (2008) 3564-3570.

27. Hyde, G. K., Park, K. J., Stewart, S. M., Hinestroza, J. P., Parsons, G. N., Langmuir 2007, 23, 9844-9849.

28. Hyde, K. G., Scarel, G., Spagnola, J. C., Peng, Q., Lee, K., Gong, B., Roberts, K. G., Roth, K. M., Hanson, C. A., Devine, C. K., Stewart, S. M., Hojo, D., Na, J-S., Jur, J. S., Parsons, G. N., Langmuir 2010, 26(4), 2550-2558.

29. Nevalainen, K., Suihkonen, R., Eteläaho, P., Vuorinen, J., Järvelä, P., Isomäki, N., Hintze, C., Leskelä, M., J. Vac. Sci. Technol. A 27(4), Jul/Aug 2009.

30. Liang, X., George, S. M., Weimer, A. W., Li, N-H., Blackson, J. H., Harris, J. D., Chem. Mater. 2007, 19, 5388-5394.

31. Liang, X., King, D. M., Groner, M. D., Blackson, J. H., Harris, J. D., George, S. M., Weimer, A. W., J. Membrane Sci. 322 (2008) 105-112.

32. Liang, X., King, D. M., Li, P., Weimer, A. W., J. Am. Ceram. Soc. 92 (3) 649-654 (2009).

33. Liang, X., Lynn, A. D., King, D. M., Bryant, S. J., Weimer, A. W., ACS Appl. Mater. Interfaces (2009), 1, 1988-1995.

34. Ferguson, J. D., Weimer, A.W., George, S. M., Chem. Mater. 16 (2004) 5602.

35. Wilson, C. A., McCormick, J. A., Cavanagh, A. S., Goldstein, D. N., Weimer, A. W., George, S. M., Thin Solid Films 516 (2008) 18.

36. George, S. M., Chem. Rev. 110 (2010) 111-131.

37. Peng, Q., Sun, Z-Y., Spagnola, J. C., Hyde, K., Spontak, R. J., Parsons, G. N., Nano. Lett. 2007, 7, 719-722.

38. Wang, X. D., Graugnard, E., King, J. S., Zhong, L., Summers, C. J., Nano Lett. 2004, 4, 2223-2226.

39. Leskelä, M., Ritala, M., Thin Solid Films 2002, 409, 138-146.

40. Leskelä, M., Kemell, M., Kukli, K., Pore, V., Santala, E., Ritala, M., Lu, J., Mater. Sci. Eng. C. 27 (2007) 1504-1508.

41. Kim, W-S., Moon, D-Y., Kang, B-W., Park, J-W., J. Korean Phys, Soc. 55 (2009) 55-58.

42. Dickey, E. R. and Barrow, W. A., 52th Annual Technical Conference Proceedings of the Society of Vacuum Coaters 0737-5921 (2009), p. 700.

43. Carcia, P. F., Mclean, R. S., Hedegus, S., Solar Energy Materials and Solar Cells 94 (2010) 2375-2378.

44. Dickey, E. R. and Barrow, W. A., 53rd Annual Technical Conference Proceedings of the Society of Vacuum Coaters 505/856-7188 (2010), p. 558.

45. Zhang, Y., Zhang, Y-Z., Miller, D. C., Bertrand, J. A., Jen, S-H., Yang, R., Dunn, M. L., George, S. M., Lee, Y. C., Thin Solid Films 517 (2009) 6794-6797.

46. Carcia, P. F., Mclean, R. S., Reilly, M. H., Groner, M. D., George, S. M., Appl. Phys. Lett. 89 (2006) 031915.

47. Miller, D.C., Foster, R. R., Zhang, Y., Jen, S-H., Bertrand, J. A., Lu, Z., Seghete, D., O'Patchen, J. L., Yang, R., Lee, Y-C., George, S. M., Dunn, M. L., J. Appl. Phys. 105 (2009) 093527.

48. Park, S. H. K., Oh, J., Hwang, C. S., Lee, J. I., Yang, Y. S., Chu, H. Y., Electrochem. Solid-State Lett. 8, (2005), H21.

49. Lahtinen, K., Maydannik, P., Johansson, P., Kääriäinen, T., Cameron, D. C., Kuusipalo, J., Surf. Coat. Technol. 205 (2011) 3916-3922.

50. Wilson, C.A., Grubbs, R. K., George, S. M., Chem. Mater. 2005, 17, 5625-5634.

51. Biercuk, M. J., Monsma, D. J., Marcus, C. M., Becker, J. S., Gordon, R. G., Appl. Phys. Lett. 83, 2405 (2003).

52. Maydannik, P. S., Kääriäinen, T. O., Cameron, D. C., Chem. Eng. J. 2011.

53. Ferrari, S., Perissinotti, F., Peron, E., Fumagalli, L., Natali, D., Sampietro, M., Org. Electron. 2007, 8, 407.

54. Fumagalli, L., Binda, M., Lopez, I. S., Natali, D., Sampietro, M., Ferrari, S., Lamagna, L., Fanciulli, M., Org. Electron. 2009, 10, 692.

55. Jur, J. S., Spagnola, J. C., Lee, K., Gong, B., Peng, Q., Parsons, G. N., Langmuir 2010, 26(11), 8239-8244.

56. Zhang, L. B., Patil, A. J., Li, L., Schierhorn, A., Mann, S., Gosele, U., Knez, M., Angew. Chem. Int. Ed. 2009, 48, 4982-4985.

57. Niskanen, A., Arstila, K., Ritala, M., Leskelä, M., J. Electrochem. Soc. 2005, 152:F90-3.

58. Niskanen, A., Radical Enhanced Atomic Layer Deposition of Metals and Oxides. Academic dissertation. University of Helsinki, Helsinki, 2006.

59. Yun, S. J., Lim, J. W., Lee, J-H., Electrochem. Solid State Lett. 2004, 7(1), C13-C15.

60. Latella, B. A., Triani, G., Evans, P. J., Scripta Materialia 56 (2007) 493-496.

61. Louch, S., Edge, S., Hodgson, M., Luxmore, K., 52nd Annual Technical Conference Proceedings of the Society of Vacuum Coaters 505/856-7188 (2009), p.760.

62. Fabreguette, F. H., George, S. M., Thin Solid Films 515 (2007) 7177-7180.

63. Ten Eyck, G. A., Pimanpang, S., Juneja, J. S., Bakhru, H., Lu, T-M., Wang, G-C., Chem. Vap. Deposition 2007, 13, 307-311.

64. Shin, H., Jeong, D-K., Lee, J., Sung, M. M., Kim, J., Adv. Mater. 2004, 16, No. 14, July 19.

65. Kim, G. M., Lee, S. M., Michler, G. H., Roggendorf, H., Gösele, U., Knez, M., Chem. Mater. 2008, 20, 3085-3091.

66. Niskanen, A., Arstila, K., Leskelä, M., Ritala, M., Chem. Vap. Depos. 2007, 13, 152-157.

67. Triani, G., Campbell, J. A., Evans, P. J., Davis, J., Latella, B. A., Burford, R. P., Thin Solid Films 518 (2010) 3182-3189.

68. Triani, G., Evans, P. J., Attard, D. J., Prince, K. E., Bartlett, J., Tan, S., Burford, R. P., J. Mater. Chem. 16 (2006) 1355-1359.

69. Lee, B. H., Cho, S., Hwang, J. K., Kim, S. H., Sung, M. M., Thin Solid Films 518 (2010) 6432-6436.

70. Lee, C-S., Kim, J., Son, J. Y., Choi, W., Kim, H., Appl. Catal. B: Environmental 91 (2009) 628-633.

71. Hoyas, A. M., Schumacher, J., Shamiryan, D., Waeterloos, J., Besling, W., Celis, J. P., Maex, K., J. Appl. Phys. 95, 381 (2004).

72. Scharrer, M., Wu, X., Yamilov, A., Cao, H., Chang, R. P. H., Appl. Phys. Lett. 86 (2005) 151113.

73. Jur, J. S., Sweet III, W. J., Oldham, C. J., Parsons, G. N., Adv. Funct. Mater. 2011, 21, 1993-2002.

74. Choi, W-S. J., Korean Phys. Soc. 54 (2009) 678-681.

75. Kim, J. B., Kwon, D. R., Chakrabarti, K., Lee, C., Oh, K. Y., Lee, J. H., J. Appl. Phys. 92, 11, (2002) 6739.

76. Rose, M., Niinistö, J., Endler, I., Bartha, J. W., Kücher, P., Ritala, M., ACS Appl. Mater. Interfaces 2 (2010) 347-350.

77. Elliott, S. D., Scarel, G., Wiemer, C., Fanciulli, M., Pavia, G., Chem. Mater. 2006, 18, 3764-3773.

78. Langereis, E., Keijmel, J., van de Sanden, M.C. M., Kessels, W. M. M., Appl. Phys. Lett. 2008, 92, 231904.

79. Heil, S. B. S., Kudlacek, P., Langereis, E., Engeln, R., van de Sanden, M. C. M., Kessels, W. M. M., Appl. Phys. Lett. 89 (2006) 131505.

80. Heil, S. B. S., van Hemmen, J. L., van de Sanden, M. C. M., Kessels, W. M. M., J. Appl. Phys. 103 (2008) 103302.

81. Musschoot, J., Xie, Q., Deduytsche, D., Van den Berghe, S., Van Meirhaeghe, R. L., Detavernier, C., Microelectr. Eng. 86 (2009) 72-77.

82. Jeong, C-W., Lee, B-I., Joo, S-K., Mater. Sci. Eng. C 16 (2001) 59-64.

83. Lee, Y. J., Kang, S-W., J. Vac. Sci. Technol. A 2002, 20(6) 1983-1988.

84. Choi, S-W., Jang, C-M., Kim, D-Y., Ha, J-S., Park, H-S., Koh, W., Lee, C-S., J. Korean Phys. Soc. 2003, 41, S975-S979.

85. Ritala, M., Niinistö, J., Chapter 4 in: Chemical vapour deposition: precursors, processes and applications; Jones, A. C. Hitchman, M. L. (Eds.) Royal Society of Chemistry Cambridge, U.K., 2009; pp 158-206.

86. Crawford, R. J., Plastics Engineering, third ed., Butterworth-Heinemann, Burlington, 1998.

87. Suggs, L. J., Moore, S. A., Mikos, A. G., Chapter 55 in: Mark, J. E (ed.) Physical Properties of Polymers Handbook, second ed. Springer, New York, USA 2007.

88. Doraiswami, R., Chapter 11 in: Hesketh, P.J (ed.) BioNanoFluidic MEMS. Springer. New York, USA 2008.

89. Wang, J., Cui, T., Microsystem Technologies 11 (2005) 452-455.

90. Kuusipalo, J. (Ed.), Papermaking Science and Technology, second ed, Paper and Paperboard Converting, Vol 12, Helsinki, Finnish Paper Engineers' Association, Finland 2008.

91. Ram, A., Chapter 4 in: Fundamentals in Polymer Engineering, Springer – Verlag, 1997.

92. Plazek, D. J., Ngai, K. L., Chapter 12 in: Mark, J. E (ed.) Physical Properties of Polymers Handbook, second ed. Springer, New York, USA 2007.

93. Orwoll, R. A., Chapter 7 in: Mark, J. E (ed.) Physical Properties of Polymers Handbook, second ed. Springer, New York, USA 2007.

94. Ashby, M. F., Materials Selection in Mechanical Design, third ed. Butterworth-Heinemann, Burlington, USA 2005.

95. Huang, S. J., Chapter 9 in: Bastioli, C (ed.). Handbook of Biodegradable Polymers, Rapre Technologies Ltd., Shawbury, UK 2005.

96. Santonja-Blasco, L., Moriana, R., Badia, J. D., Ribes-Greus, A., Polym. Degradation and Stability 95 (2010) 2185-2191.

97. Patki, R., Mezghani, K., Phillips, P. J., Chapter 39 in: Physical Properties of Polymers Handbook, second ed. Springer, New York, USA 2007.

98. McKeen, L.W., The Effect of Temperature and Other Factors on Plastics and Elastomers, second ed. William Andrew Inc. Norwich, NY, USA 2007.

99. Natu, A. A., Lofgren, E. A., Jabarin, S. A., Polymer Engineering and Science 45, 2005, 400-409.

100. Lahtinen, K., Kotkamo, S., Koskinen, T., Auvinen, S., Kuusipalo, J., Packag. Technol. Sci. 22 (2009) 451-460.

101. Lahtinen, K., Nättinen, K., Vartiainen, J., Polym. Plast. Tech. Eng. 48 (2009) 561-569.

102. Lieberman, M. A., Lichtenberg, A. J., Principles of plasma discharges and materials processing, John Wiley & Sons, New York, USA 1994.

103. Pearse, R. W. B and Gaydon, A. G., The Identification of Molecular Spectra, fourth ed. Chapman and Hall, London, 1976.

104. Herzberg, G., The spectra and structures of simple free radicals, Dover, New York, USA 1971.

105. Fuhr, J. R., Wiese, W. L., Podobedova, L. I. and Kelleher, D. E., Section 10 in: Haynes, W. M. (ed.) Handbook of Chemistry and Physics, 91st ed. Internet Version 2011.

106. Blanksby, S. J., Ellison, G. B., Acc. Chem. Res. 2003, 36, 255-263.

107. Andrady, A.L., Chapter 51 in: Mark, J. E (ed.) Physical Properties of Polymers Handbook, second ed. Springer, New York, USA 2007.

108. Hollas, J. M., Modern spectroscopy, fourth ed., John Wiley & Sons, Chichester, England, 2004.

109. Rånby, B., Rabek, J. F., Photodegradation, photo-oxidation and photostabilization of polymers: principles and applications. Wiley, London 1975.

110. Schulz, U., Appl. Optics, 45, 7, 2006.

111. Schulz, U., Munzert, P., Kaiser, N., Surf. Coat. Technol. 2001, 142-144, 507.

112. Gröning, P., Kuttel, O. M., Collaud-Coen, M., Dietler, G., Schlapbach, L., Appl. Surf. Sci. 2006, 253, 8185.

113. Guo, Y. B., Hong, F. C.-N., Diamon Relat. Mater. 2003, 12, 946.

114. Wertheimer, M. R., Fozza, A. C., Holländer, A., Nucl. Instrum. Methods Phys. Res. B. 1999, 151, 65.

115. Kaczamarek, H., Chaberska, H., Appl. Surf. Sci. 2006, 252, 8185.

116. Coen, M. C., Lehmann, R., Groening, P., Schlapbach, L., Appl. Surf. Sci. 207 (2003) 276-286.

117. Fozza, C., Roch, J., Kelmberg-Sapieha, J. E., Kruse, A., Holländer, A., Wertheimer, M. R., Nucl. Intrum. Methods Phys. Res. B. 1997, 131, 205.

118. Fozza, C., Klemberg-Sapieha, J. E., Wertheimer, M. R., Plasmas Polym. 1999, 4, 186.

119. Klemberg-Sapieha, J. E., Martinu, L., Yamasaki, N. L. S., Lantman, C. W., Thin Solid Films 2005, 476, 101.

120. Holländer, A., Wilken, R., Behnisch, J., Surf. Coat. Technol. 1999, 116-119, 788.

121. Munzert, P., Schulz, U., Kaiser, N., Surf. Coat. Technol. 174-175 (2003) 1048-1052.

122. Mackus, A. J. M., Heil, S. B. S., Langereis, E., Knoops, H. C. M., Van de Sanden, M. C. M., Kessels, W. M. M., J. Vac. Sci. Technol. A 28, 77 (2010).

123. Bellmann, C., Chapter 12 in: Stamm, M (ed.) Polymer Surfaces and Interfaces, Characterization, Modification, and Applications. Springer-Verlag. Berlin, Germany 2008.

124. Sperling, L. H., Chapter 12 in: Introduction to Physical Polymer Science. John Wiley&Sons. New Jersey, USA 2006.

125. Gleskova, H., Cheng, I-Chun, Wagner, S., Suo, Z., Chapter 2 in: Wong, S.W., Salleo, A. (eds.) Electronic Materials: Science and Technology, Flexible Electronics, Materials and Applications. Springer, NY, USA 2009.

126. Jen, S-H., Bertrand, J. A., George, S. M., J. Appl. Phys. 109, 084305 (2011).

127. Gleskova, H., Cheng, I-C., Wagner, S., Sturn, J. C., Suo, Z., Solar Energy 80 (2006) 687-693.

128. Suo, Z., Ma, E. Y., Gleskova, H., Wagner S., Appl. Phys. Lett. 74 (1999) 8.

129. Elim, H. I., Ji, W., Yuwono, A. H., Xue, J. M., Wang, J., Appl. Phys. Lett. 82, 16, 2003.

130. Nugen, S. R., Asiello, P. J., Connelly, J. T., Baeumner, A., J. Biosensors and Bioelectronics 24 (2009) 2428-2433.

131. Tennico, Y. H., Koesdjojo, M. T., Kondo, S., Madrell, D. T., Remcho, V. T., Sens. Actuators B 2010, 2, 143.

132. Koerner, T., Brown, L., Xie, R., Oleschuk, R. D., Sens. Actuators B 2005, 107, 632.

133. Cheng, J.-Y., Wei, C.-W., Hsu, K.-H., Young, T.-H., Sens. Actuators B 2004, 99, 186.

134. Henry, C., Tutt, T. J., Galloway, M., Davidson, Y. Y., McWhorter, C. S., Soper, S. A., McCarley, R. L., Anal. Chem. 2000, 72, 5331.

135. Varma, H. K., Sreenivasan, K., Yokogawa, Y., Hosumi, A., Biomaterials 2003, 24, 297.

136. Borealis. Low Density Polyethylenes for Extrusion Coating –Booklet, 2002.

137. Maier, C., Calafut, T., Polypropylene – Definite User's Guide and Databook. William Andrew Publishing/Plastic Design Library, Norwich, USA, 1998.

138. Zardetto, V., Brown, T. M., Reale, A., Di Carlo, A., J. Polym. Phys. B. 2011.

139. Erlat, A. G., Henry, B. M., Grovenor, C. R. M., Briggs, A. G. D., Chater, R. J., Tsukahara, Y., J. Phys. Chem. B 108 (2004) 883.

140. Skoog, D. A., Holler, F. J., Nieman, T. A., Principles of Instrumental Analysis, fifth ed. Harcourt Brace College Publishers, USA, 1998.

141. Reimer, L., Kohl, H., Transmission Electron Microscopy, fifth ed. Springer, 2008.

142. Maydannik, P. S., Kääriäinen, T. O., Cameron, D. C., 53rd Annual Technical Conference Proceedings of the Society of Vacuum Coaters 505/856-7188 (2010), p. 138.

143. Kääriäinen, T. O., Kääriäinen, M-L., Gandhiraman, R. P., Cameron, D. C., ALD 2007, 7th Int. Conf. At. Layer Deposition, San Diego, California, USA, 24-27 June 2007.

144. Lim, G. T., Kim, D-H., Thin Solid Films 498 (2006) 254-258.

145. Pheamhom, R., Sunwoo, C., Kim, D-H., J. Vac. Sci. Technol. A 24(4), 2006.

146. Park, J-J., Lee, W-J., Lee, G-H., Kim, I-S., Shin, B-C., Yoon, S-G., Integrated Ferroelectrics, 68 (2004) 129-137.

147. Ashcroft, N. W., Mermin, N. D., Solid State Physics. Thomson Learning, Inc., USA, 1976.

148. Karunagaran, B., Kim, K., Mangalaraj, D., Yi, J., Velumani, S., Solar Energy Mater. and Solar Cells 88 (2005) 199-208.

149. Karunagaran, B., Rajendra Kumar, R. T., Senthil Kumar, V., Mangalaraj, D., Narayandass, S. K., Mohan Rao, G., Mater. Sci. Semcond. Proc. 6 (2003) 547-550.

150. Wang, Z. Saxena, S. K. Solid State Communications 118 (2001) 75-78.

151. Xu, W-X., Zhu, S., Fu, X-C., Chen, Q. Appl. Surf. Sci. 148 (1999) 253-262.

152. Gajovic, A., Stubicar, M., Ivanda, M., Furic, K. J., Mol. Struct. 563-564 (2001) 315-320.

153. Kelly, S., Pollak, F. H., Tomkiewicz, M., J. Phys. Chem. B 1997, 101, 2730-2734.

154. Bersani, D., Lottici, P. P., Ding, X-Z., Appl. Phys. Lett. 72 (1) 1998.

155. Parker, J. C., Siegel, R. W., Appl. Phys. Lett. 57 (9) 1990.

156. Moret, M. P., Zallen, R., Vijay, D. P., Desu, S. B., Thin Solid Films 366 (2000) 8-10.

157. Tompsett, G. A., Bowmaker, G. A., Cooney, R. P., Metson, J. B., Rodgers, K. A., Seakins, J. M., J. Raman Spectrosc. 26 (1995) 57-62.

158. Mitchell, D. R. G., Triani, G., Attard, D. J., Finnie, K. S., Evans, P. J., Barbe, C. J., Bartlett, J. R., Smart Mater. Struct. 15 (2006) S57-S64.

159. Fattakhova-Rohlfing, D., Wark, M., Brezesinski, T., Smarsly, B. M., Rathousky, J., Adv. Funct. Mater. 2007, 17, 123-132.

160. Langlet, M., Kim, A., Audier, M., Herrmann, J. M., J. Sol-Gel Sci. Technol. 25 (2002) 223-234.

161. Martinez-Ferrero, E., Sakatani, Y., Boissiere, C., Grosso, D., Fuertes, A., Fraxedas, J., Sanchez, C., Adv. Funct. Mater. 2007, 17, 3348-3354.

162. Soto, K. F., Carrasco, A., Powell, T. G., Garza, K. M., Murr, L. E., J. Nanoparticles Res. 7 (2005) 145-169.

163. Wang, J-y., Yu, J-x., Liu, Z-h., He, Z-k., Cai, R-x., Semicond. Sci. Technol. 20 (2005) L36-L39.

164. Chen, Y., Stathatos, E., Dionysiou, D. D., Surf. Coat. Technol. 202 (2008) 1944-1950.

165. Jiang, W. H., Pinkerton, F. E., Atzmon, M., Scripta Mater. 48 (2003) 1195-1200.

Paper I

Plasma-assisted Atomic Layer Deposition of Al_2O_3 at Room Temperature

Tommi O. Kääriäinen, David C. Cameron

Plasma Processes and Polymers, 2009, 6, S237-S241

Reprinted with permission from John Wiley and Sons.

Plasma-Assisted Atomic Layer Deposition of Al_2O_3 at Room Temperature

Tommi O. Kääriäinen,* David C. Cameron

A new design of plasma source has been used for the plasma-assisted atomic layer deposition (PA-ALD) of Al_2O_3 films at room temperature. In this PA-ALD reactor the plasma is generated by capacitive coupling directly in the deposition chamber adjacent to the substrate but can be separated from it by a grid to reduce the ion bombardment while maintaining the flow of radicals directly to the substrate surface. During the ALD cycle a mixture of nitrogen and argon was introduced into the reactor to act as a purge gas between precursor pulses and to facilitate the generation of a plasma during the plasma cycle. Sequential exposures of TMA and excited O_2 precursors were used to deposit Al_2O_3 films on Si(100) substrates. A plasma discharge was activated during the oxygen gas pulse to form radicals in the reactor space. The experiments showed that the growth rate of the film increased with increasing plasma power and with increasing O_2 pulse length before saturating at higher power and longer O_2 pulse length. The growth rate saturated at the level of 1.78 $\text{Å}\cdot\text{cycle}^{-1}$. EDS analysis showed that the films were oxygen rich and had carbon as an impurity. This can be explained by the presence of bonds between hydrocarbons from the unreacted TMA precursor and excess oxygen in the film. ATR-FTIR spectroscopy measurements indicated a change in growth mechanism when the distance between the location of the radical generation and the substrate was varied. A similar effect was observed with the use of different plasma power levels.

Introduction

Atomic layer deposition (ALD) is a CVD type thin film deposition method where sequential exposures of gas phase reactants are used for the deposition of thin films with atomic layer accuracy. Each atomic layer formed in the sequential process is a result of saturated surface controlled chemical reactions. Commonly, in the growth of binary compounds such as metal oxides, a reaction cycle consists of two reaction steps. In one step the metal compound precursor is allowed to react with the surface, and in the other step the chemisorbed metal precursor reacts with the oxygen precursor. Between the steps a purge is applied to remove the excess of precursor and the reaction by-products. The self-controlled growth mode of ALD contributes several advantages. The thickness of the films can be controlled in a straightforward manner by controlling the number of reaction cycles, therefore enabling the controlled growth of ultra-thin layers. The precursors form stoichiometric films with large area uniformity and conformality even on complex surfaces with deformities.[1]

In plasma-assisted ALD (PA-ALD), additional energy for the chemical reactions in the chamber is provided by applying plasma energy at an appropriate point during the reaction cycle. Plasmas are used for gas dissociation to produce desired radicals. A very common plasma source used in PA-ALD is radio frequency-generated plasma, both inductively[2,3] and capacitively[4,5] coupled being used. Other plasma sources, such as microwave plasma[6] has also been investigated. In general, the use of plasma activation

T. O. Kääriäinen, D. C. Cameron
Advanced Surface Technology Research Laboratory, Department of Mechanical Engineering, Lappeenranta University of Technology, 50100 Mikkeli, Finland
E-mail: tommi.kaariainen@lut.fi

© 2009 WILEY-VCH Verlag GmbH & Co. KGaA, Weinheim

WILEY InterScience DISCOVER SOMETHING GREAT
DOI: 10.1002/ppap.200930605

will extend the range of materials suitable for ALD.[7] Using plasma in ALD can result in increased reaction rates on surfaces, increased fragmentation of the precursor molecules, bombardment-enhancement of the removal of product molecules, or combination of all of these steps. Furthermore the addition of non-thermal energy to the process can result in lower substrate temperatures than for conventional CVD.[2] Low deposition temperatures that are compatible with thermally fragile polymeric materials have been in the focus of researchers in a field of ALD for some time.[8] Among the oxides, Al_2O_3 has been extensively studied[9] and has low temperature applications, e.g., in gas and moisture permeation barriers.[3,10] Recent studies have shown that PA-ALD at temperatures close to room temperature enables short deposition cycles while still attaining high quality oxide films.[3,6] As in the case of the trimethyl aluminium (TMA) and H_2O ALD process, the mechanism of the TMA and O_2 plasma process is not very well understood. Research has recently focused on the film growth and reaction mechanism in ALD Al_2O_3 processes where O_3 and O_2 plasma are used as oxidizing agent. It has been established that in Al_2O_3 ALD where TMA and O_2 plasma is used the process follows mainly the combustion-like reaction driven by O radicals but there is also the possibility for the existence of a concurrent reaction path with H_2O generated by the plasma.[11–14]

In this paper, we report the details of low temperature PA-ALD of amorphous Al_2O_3 by using a new design of plasma source. In this ALD reactor the capacitively coupled plasma source is situated inside the deposition chamber and it can be separated from the substrate by using a metal grid to reduce ion bombardment while maintaining the flow of radicals to the substrate surface.

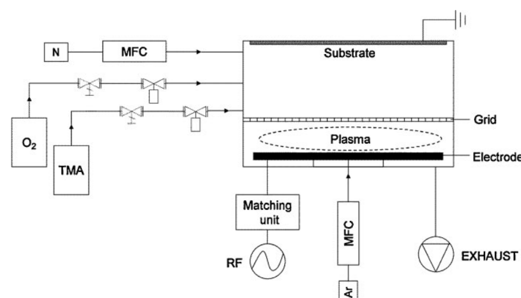

Figure 1. Schematic of PA-ALD reactor.

Experimental Part

Film Deposition

Al_2O_3 films were grown using $Al(CH_3)_3$ (98%, Strem Chemicals) and O_2 (99 999%, AGA) plasma on Si (100) substrates (Si-Mat) in a Beneq TFS-500 ALD tool equipped with a plasma reactor. The reactor is a cylindrical shaped with diameter of 200 mm. The TMA precursor was kept at 20 °C during the deposition. Depositions were done without additional heating of the reactor. In a stable situation, the temperature inside the reactor was around 30 °C. The schematic of the reactor is shown in Figure 1. In the reactor, plasma was generated by capacitive coupling with a 13.56 MHz rf plasma source. The position of electrode and grid between the electrode and substrate can be modified. During the ALD cycle a mixture of nitrogen and argon was continuously introduced into the reactor to act as a purge gas between precursor pulses and to facilitate the generation of plasma during the plasma cycle. Nitrogen gas (99. 999%, AGA) was introduced normally through the precursor channel also to carry the precursors to the reactor. Argon (99. 999%, AGA) was introduced to the reactor through the plasma electrode to improve the plasma generation and also to ensure a pressure difference between the reactor and Ar flow channel. One deposition cycle consisted of a 250 ms TMA pulse, 5 s N_2/Ar mixture purge, varied length of plasma pulse and 5 s N_2/Ar mixture purge. In the N2/Ar mixture the flow rates of N_2 and Ar were 500 and 50 sccm, respectively. During the plasma pulse, O_2 gas (99. 999%, AGA) was introduced through the precursor channel to the reactor to produce oxygen radicals for reactions on the substrate surface. The O_2 pulse length was varied from 250 ms to 6 s to study the effect of the O_2 dose on the film growth and the film properties. In each deposition the plasma was ignited 250 ms before the O_2 pulse and turned off 250 ms after the O_2 pulse to ensure the stable plasma condition during the O_2 pulse. The plasma electrode and grid plate distance was varied with respect to substrate surface. The gap between the electrode and grid was fixed at 12 mm while the position of electrode/grid assembly was varied between 36 and 16 mm distance from the substrate surface. In order to study, the effect of plasma power to the film growth and the film properties, the plasma power was varied from 25 to 200 W. The vacuum level in the reaction chamber during the deposition remained constant during the ALD cycle at 2 mbar.

Film Analysis

The film thickness and consequently the film growth rate was measured by using a spectroscopic ellipsometer M-2000FI from J. A. Woollam Co. Inc. Measurements were made at five different spots to record the film uniformity over the whole deposition area. The structure of the deposited film was studied with ATR-FTIR spectroscopy using a Nicolet 4700 FT-IR spectrometer equipped with a Smart Orbit ATR accessory. The internal reflection element (IRE) used was a diamond crystal. Chemical analysis of the film was collected using an EDAX X-ray spectrometer attached to the FEG-SEM Hitachi S-4800.

Results and Discussion

Film Growth

The film growth rate and refractive index at a wavelength of 633 nm of the Al_2O_3 films as a function of the oxygen pulse

Plasma Process. Polym. **2009**, *6*, S237–S241
© 2009 WILEY-VCH Verlag GmbH & Co. KGaA, Weinheim
DOI: 10.1002/ppap.200930605

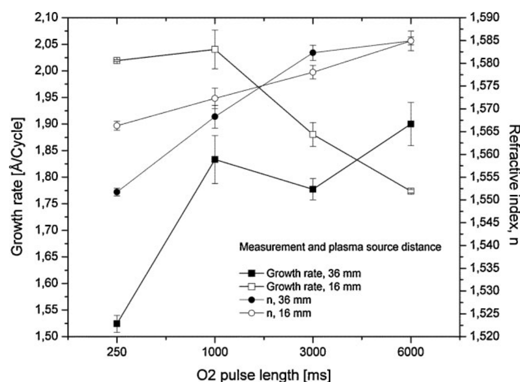

Figure 2. The film growth rate and the refractive index at 633 nm of Al_2O_3 films as a function of O_2 pulse length and the plasma source position. Measurements have been determined for the films grown at room temperature with 100 W plasma power for 1000 ALD cycles by ex situ spectroscopic ellipsometry.

length and plasma source position with a plasma power of 100 W are shown in Figure 2. It can be seen that the growth rate follows a different trend when the position of the substrate is changed with respect to plasma source. It is believed that the longer distance between the grid and the substrate reduces the concentration of O radicals present for the reactions on the substrate surface because of their limited lifetime and results in unsaturated growth at shorter plasma pulses. The growth rate saturates at longer O_2 pulses as the dose of O radicals available for the reaction is increased. The carbon content and absorbance of the carbonaceous groups in the film decreases with increasing O_2 pulse length as shown in Table 1 and in Figure 3, respectively. This is attributed to the more effective removal of hydrocarbon ligands from the substrate surface during the plasma pulse, as suggested by an earlier study.[14] When the grid–substrate distance is reduced, more O radicals are already provided for the surface reactions with shorter O_2 pulse length. It has been previously shown that in the reaction between TMA and O_2 plasma the reaction products include CO, CO_2, H_2O, and CH_4.[12–14] It has been reported that the CH_4 is a reaction product during the O_2 plasma pulse formed in a concurrent reaction with H_2O produced in the combustion-like reaction of the $-CH_3$ surface group.[14] This is true during the early stage of O_2 plasma pulse. The higher growth rate at shorter O_2 pulse lengths may be explained both with higher concentration of compounds formed by hydrocarbons and O radicals on the surface but also through the concurrent reaction path described above. It is believed that this concurrent reaction path, where H_2O is produced by the plasma, has a more dominant role in the reaction at shorter pulse length compared with longer pulse length leading to additional growth of Al_2O_3 during the following TMA half-cycle by a chemical vapor deposition path. This is supported by previous results where this concurrent reaction pathway plays a significant role only during the time when there are still CH_3 groups present at the surface.[14] With shorter pulse length the concentration of hydrocarbons is higher for this

Table 1. Properties of Al_2O_3 films deposited at room temperature using a) 1000 cycles TMA and varied O_2 pulse length during the plasma ignition (plasma power = 100 W) and b) 1000 cycles of TMA and 1 s O_2 pulse length with different plasma power.

Plasma source distance[a)]	**O_2 pulse length**	**Composition [at. %]$_{EDS}$**				
a)		**O/Al ratio**	**Al**	**O**	**C**	**N**
36 mm	250 ms	3.6	17.4	61.9	20.7	0
	1 s	2.9	22.3	64.9	12.9	0
	3 s	2.7	25.3	67.67	7.1	0
	6 s	2.6	26.0	68.6	5.1	0.2
16 mm	250 ms	3.1	21.0	64.5	13.6	0.9
	1 s	2.9	22.6	66.1	10.0	1.3
	3 s	2.8	23.8	66.3	8.2	1.7
	6 s	2.5	26.0	64.1	8.9	1.0
b)	**Plasma power [W]**					
36 mm	25	2.5	26.1	64.5	9.4	0
	100	2.9	22.3	64.82	12.9	0
	200	2.7	24.1	66.0	8.3	1.6

a)Plasma source distance is the distance between the grid and the substrate.

© 2009 WILEY-VCH Verlag GmbH & Co. KGaA, Weinheim

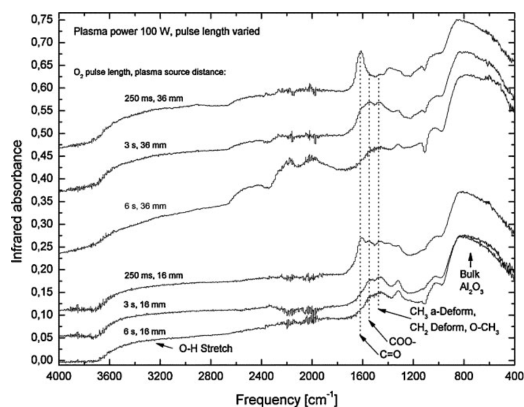

Figure 3. ATR-FTIR difference spectra of Al_2O_3 films on Si(100) wafer after 1 000 ALD cycles of TMA and O_2 plasma as a function of O_2 pulse length and plasma source position. The signal from the substrate has been subtracted from the spectra. The films were grown at room temperature and the spectra were recorded after deposition using as deposited films.

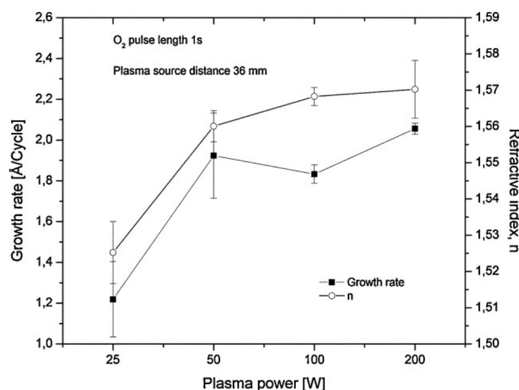

Figure 4. The film growth rate and the refractive index at 633 nm of Al_2O_3 films as a function of rf plasma power. Measurements have been determined for the films grown at room temperature for 1 000 ALD cycles by ex situ spectroscopic ellipsometry.

reaction. ATR-FTIR spectra shown in Figure 3 support these insights as well. The features at frequencies of 1 620, 1 550, and 1 473 cm^{-1} are attributed to C=O, COO−, and the asymmetric deformation of CH_3, respectively.[15] The feature at 1 473 cm^{-1} may belong to $O-CH_3$ as well. The distinction between these two groups cannot be confirmed in this study. The absorbance of these groups decreases with increasing O_2 pulse length revealing a decrease in the concentration of hydrocarbons and other carbonaceous groups in the film. The same phenomena can be observed with longer distance between the plasma source and the substrate. A longer O_2 pulse length in both plasma field positions leads to the same growth rate and growth fits into the same ALD window. Figure 3 also reveals the existence of the bulk Al_2O_3 vibrational mode at 400–1 000 cm^{-1} which agrees well with previous studies.[16]

Plasma power was varied at 36 mm plasma source distance from the substrate in order to study its effect on film growth and film properties. Figure 4 shows the film growth rate and refractive index of the films deposited with different plasma power. The O_2 pulse length used was 1 s. The growth rate increases with increasing plasma power. It was also noticed that deposition at plasma powers of 50 and 25 W resulted in non-uniform growth over the substrate area and that deposition was not consistent from run to run. With this specific reactor configuration, stable plasma conditions for ALD require a certain minimum plasma power which according to this study lies around 100 W. One notable result is that deposition with plasma power of 200 W leads to nitrogen incorporation in the film as shown by energy dispersive X-ray spectroscopy (EDS) measurement. This is also seen with longer plasma pulses, particularly for closer grid–substrate separation. This arises since nitrogen was used in both the carrier and purging gas. This could be simply avoided by replacing the Ar/N_2 mixture carrier gas with an inert gas such as argon. For longer plasma pulse cycles there is some increase in reactor temperature. During the deposition of 1 000 cycles with 1 s plasma pulse with 200 W power the reactor wall reached a temperature ~46 °C due to the heating effect of the plasma. The same phenomenon was observed with depositions where plasma power was fixed at 100 W while plasma pulse length and plasma source distance were changed. Reactor wall temperature increased from starting level of 31 to around 55 °C with 6 s plasma pulse.

Film Properties

Ellipsometry measurements indicated that refractive indices of Al_2O_3 films grown using 1 000 cycles of TMA and O_2 plasma increases slightly with increasing plasma pulse length and plasma power as shown in Figure 2 and 4. The lowest refractive index of 1.525 at the wavelength of 632 nm was measured from 25 W plasma power deposited film and the highest 1.585 from the films where 6 s O_2 pulse was used. The refractive index of these films is slightly higher than has been reported earlier for $TMA + H_2O$ process at low temperatures.[17] However, the refractive index for these amorphous Al_2O_3 films remain clearly lower than for the crystalline hexagonal Al_2O_3 ($n = 1.7673$ at 589 nm).[18]

Energy dispersive X-ray spectroscopy (EDS) analysis for the films deposited on Si (100) substrates reveals that films are oxygen rich and have also carbon as an impurity. The compositions calculated according to the ZAF method taking into account the background are shown in Table 1.

© 2009 WILEY-VCH Verlag GmbH & Co. KGaA, Weinheim
DOI: 10.1002/ppap.200930605

Because of the insensitivity of EDS to light elements, the elemental compositions shown here should not be taken as definitive but as showing relative changes which occur under different conditions. The compositions change according to the process parameters used. The decrease in carbon content as a function of plasma pulse length was discussed in the previous chapter. It is noticeable that even for a short 250 ms O_2 pulse, the carbon content is lower with a shorter plasma source distance than for longer O_2 pulses at larger distance. Comparison between the IR absorbance of the films deposited in shorter and longer plasma separation distance using a 250 ms O_2 pulse in Figure 3 reveals that the feature at 1 620 cm^{-1} attributed to C=O bond is reduced for the film deposited with shorter plasma field distance. Consequently fewer carbon containing groups are present in the film. It is also evident that using nitrogen both as a carrier and purging gas leads to nitrogen doping of the film. Although EDS is not an ideal technique for measuring low nitrogen concentrations, emission peaks from the N atoms can clearly be seen above the background in some cases. The exact levels of N will be subject to some uncertainty but it is clear that there is some N in certain films. This is not observable with 36 mm distance of plasma source from the substrate for oxygen plasma pulses shorter than 6 s. The reason for this may be a less complete reaction between TMA and O radicals since radical concentration on the substrate surface is believed to be lower with 36 mm plasma source distance or the lifetime of the excited nitrogen species may be shorter. The O/AL ratio of the films measured by EDS decreased with increasing O_2 pulse length for both plasma source positions. The low O/AL ratio of the film deposited with 25 W plasma power is notable. One reason for this may be that plasma conditions are drastically different at this power level compared to higher power level, indicated by the substantially smaller in magnitude self-bias on the powered electrode at 25 W. The radical mixture in the plasma may be significantly different with a consequently different effect on film growth such as less complete fragmentation of the TMA molecules on the surface. This is a topic for future investigations.

Conclusion

A new design of capacitively coupled plasma reactor was used for PA ALD of Al_2O_3 by using TMA and O_2 plasma as a reactants at room temperature. We have shown that the reaction mechanism leading to the film growth is dependent on the distance between the plasma source and the substrate surface consistent with the effects of radical lifetime on the concentration at the substrate. The film growth rate, which is dependent on the distance between the plasma source and the substrate surface, the O_2 plasma pulse length, and plasma power, achieved the level of 2 Å·$cycle^{-1}$. A shorter distance between the plasma source and the substrate allowed saturated growth with shorter O_2 pulse lengths. The films are oxygen rich and the carbon content of the film decreased with increasing O_2 pulse length consistent with a more complete precursor reaction. There was significant nitrogen concentration in the film in particular at higher powers and longer pulse times. The exact nature of the reactions which occur to produce this nitrogen content have still to be clarified.

Acknowledgements: Acknowledgement is made of support by *ESR* from Itä-Suomen Lääninhallitus under project S10148.

Received: September 26, 2008; Accepted: March 16, 2009; DOI: 10.1002/ppap.200930605

Keywords: aluminum oxide; ATR-FTIR; plasma enhanced chemical vapor deposition; radicals

[1] M. Ritala, M. Leskelä, in: *Handbook of Thin Film Materials*, H. S. Nalwa, Ed., Vol. 1, Academic Press, San Diego, CA 2002, pp. 103–159.
[2] S. M. Rossnagel, A. Sherman, F. Turner, *J. Vac. Sci. Technol., B* **2000**, *18*(4), 2016.
[3] E. Langereis, M. Creatore, S. B. S. Heil, M. C. M. Van de Sanden, W. M. M. Kessels, *Appl. Phys. Lett.* **2006**, *89*, 081915.
[4] Y. J. Lee, S.-W. Kang, *J. Vac. Sci. Technol., A* **2002**, *20*(6), 1983.
[5] S. W. Choi, C. M. Jang, D. Y. Kim, J. S. Ha, H. S. Park, W. Koh, C. S. Lee, *J. Korean Phys. Soc.* **2003**, *41*, S975–S979.
[6] A. Niskanen, K. Arstila, M. Ritala, M. Leskelä, *J. Electrochem. Soc.* **2005**, *152*, F90–F93.
[7] M. Leskelä, M. Ritala, *Thin Solid Films* **2002**, *409*, 138–146.
[8] C. A. Wilson, R. K. Grubbs, S. M. George, *Chem. Mater.* **2005**, *17*, 5625–5634.
[9] R. L. Puurunen, *J. Appl. Phys.* **2005**, *97*(12), 121301.
[10] M. D. Groner, S. M. George, R. S. McLean, P. F. Carcia, *Appl. Phys. Lett.* **2006**, *88*, 051907.
[11] S. D. Elliott, G. Scarel, C. Wiemer, M. Fanciulli, G. Pavia, *Chem. Mater.* **2006**, *18*, 3764–3773.
[12] S. B. S. Heil, P. Kudlacek, E. Langereis, R. Engeln, M. C. M. Van de Sanden, W. M. M. Kessels, *Appl. Phys. Lett.* **2006**, *89*, 131505.
[13] S. B. S. Heil, J. L. van Hemmen, M. C. M. van de Sanden, W. M. M. Kessels, *J. Appl. Phys.* **2008**, *103*, 103302.
[14] E. Langereis, J. Keijmel, M. C. M. van de Sanden, W. M. M. Kessels, *Appl. Phys. Lett.* **2008**, *92*, 231904.
[15] Brezinski. Darlene, R Ed., "An Infrared Spectroscopy Atlas for the Coating Industry", Federation of Societies for Coatings, Technology., 4th edition, Vol. I, Blue Bell, Pennsylvania 1991.
[16] J. D. Ferguson, A. W. Weimer, S. M. George, *Chem. Mater.* **2004**, *16*, 5602–5609.
[17] M. D. Groner, F. H. Fabreguette, J. W. Elam, S. M. George, *Chem. Mater.* **2004**, *16*, 639–645.
[18] "Index of Refraction of Inorganic Crystals", in: *CRC Handbook of Chemistry and Physics*, D. R. Lide, Ed., 89th edition, CRC Press/Taylor and Francis, Boca Raton, FL 2009.

© 2009 WILEY-VCH Verlag GmbH & Co. KGaA, Weinheim

Paper II

Adhesion of Ti and TiC Coatings on PMMA Subject to Plasma Treatment: Effect of Intermediate Layers of Al_2O_3 and TiO_2 Deposited by Atomic Layer Deposition

Tommi O. Kääriäinen, David C. Cameron, Mari Tanttari
Plasma Processes and Polymers, 2009, 6, 631-641

Reprinted with permission from John Wiley and Sons.

Adhesion of Ti and TiC Coatings on PMMA Subject to Plasma Treatment: Effect of Intermediate Layers of Al_2O_3 and TiO_2 Deposited by Atomic Layer Deposition

Tommi O. Kääriäinen,* David C. Cameron, Mari Tanttari

Magnetron sputtered metal and metal compound films generally show very poor adhesion to PMMA; this limits the use of the polymer for components which are wear or scratch resistant or have a decorative finish. We have shown that adhesion could be significantly improved by a duplex process where a nanometer-scale thickness adhesion layer of TiO_2 or Al_2O_3 was deposited by low temperature atomic layer deposition (ALD) prior to magnetron sputtering. The metal precursors used for TiO_2 and Al_2O_3 were TDMAT and TMA, respectively, and ozone was used as a source of oxygen in both processes. This process was followed by deposition of the metal/metal carbide layer using pulsed DC reactive magnetron sputtering. With the presence of the ALD adhesion layer, the pull-off adhesion strength increased with its thickness until a point where the failure mechanism was due to cohesive disruption of the substrate material itself. It has been shown that the ALD deposited layers protect the PMMA against plasma damage during the sputtering process by blocking both direct ion damage and disruption of the polymer structure by ultra-violet radiation.

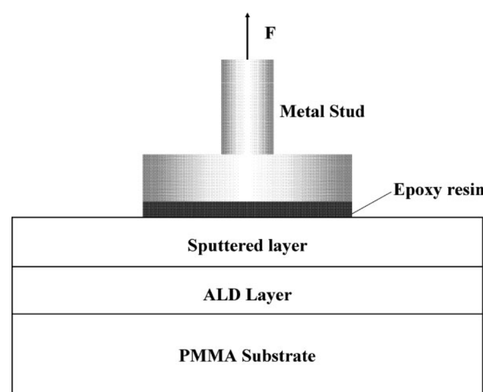

Introduction

Poly (methyl methacrylate) (PMMA) is a widely used polymer due to its low cost, good optical characteristics and biocompatibility. It is one of most important optical polymer materials used in precision optics today.[1] Applications for PMMA also include microfluidic devices,[2–4] composite implant materials for tissue engineering,[5] microfabricated devices for chemical analysis[6] and MEMS.[7] In many applications, the functionalization of the polymer surface is desired to improve its properties, such as mechanical durability, wettability, printability, adhesion to other substances and biocompatibility.[8,9] Applications for polymers can be expanded with thin film coatings deposited by sputtering or other methods. Deficient adhesion of these thin film coatings on PMMA is a well-known problem; this is due to the combination of

T. O. Kääriäinen, D. C. Cameron
Department of Mechanical Engineering, Advanced Surface Technology Research Laboratory, Lappeenranta University of Technology, Prikaatinkatu 3 E, FI-50100 Mikkeli, Finland
E-mail: tommi.kaariainen@lut.fi
M. Tanttari
Sandvik Mining and Construction Oy, Pihtisulunkatu 9, P.O. Box 100, FI-33311 Tampere, Finland

© 2009 WILEY-VCH Verlag GmbH & Co. KGaA, Weinheim
WILEY InterScience DISCOVER SOMETHING GREAT
DOI: 10.1002/ppap.200900038

the low surface energy of PMMA and the effects of deposition, for example stress in the deposited film.[9] Many methods have been studied to modify the PMMA surface chemistry and structure to enhance film adhesion. Among these methods are surface activation by different plasma glow discharges,[9–11] ultra-violet (UV) and vacuum ultra-violet (VUV) radiation,[12] and deposition of intermediate adhesion layers.[11] In general, depending on treatment used, there are several reactions that take place on the polymer surface during the surface modification including oxidation, crosslinking, degradation and isomerisation.[13]

Plasma treatment can be used to modify the polymer surface region without affecting the bulk properties of the polymer. The polymer surface is affected by plasma UV and VUV radiation through the photo-chemically induced chain scission. According to Coen et al., the structural modification through microwave (2.45 GHz) plasma exposure occurs below the surface typically within thickness of a few tens of nm.[14] The penetration depth of UV/VUV radiation into the polymer and the etch rate of different polymers depends on their chemical structure, consequently the absorption coefficient of the polymer,[15] and also on the plasma conditions used defining the emission of UV/VUV radiation.[12] According the Shultz et al.,[9] the modified layer thickness of PMMA after DC glow discharge was at least 150 nm. Although only the near surface region is affected during the plasma treatment or processing, it might also have some deleterious effects on the bulk polymer properties. The limited coating adhesion on PMMA has been reported to be due to cohesive failure in the subsurface region of PMMA close to the film-polymer surface.[16] Furthermore, thermal or ion bombardment induced film stress combined with the low surface energy of PMMA has been suggested to cause the poor adhesion.[11] Groening et al. have shown that chemical modification of the PMMA surface is due to the ions from the argon plasma and leads to the scission of the whole side chain of PMMA.[10] This happens by degradation of the ester group in a two-step process. After this process, the chemical state of the main chain of PMMA will be similar to polypropylene. Additionally, Shultz et al. suggested that the coating adhesion of plasma-treated PMMA is more determined by the modification of the subsurface region, rather than a change of surface energy. They reported that DC plasma treatment improved the coating adhesion, but microwave plasma treatment which didn't improve the adhesion only deposited oxygen groups at the surface.[9] The nature of PMMA as susceptible to radiation damage makes the adhesion improvement of thin films difficult. This is especially true with plasma processes (magnetron sputtering, for example) where ion bombardment and VUV radiation take place due to the existence of the plasma. The effect of VUV radiation ($\lambda < 200$ nm) on the properties of the polymer-film interface and polymer subsurface has been widely studied and its complexity has been observed.[12,15,17,18]

Atomic layer deposition (ALD) is a thin film deposition method where sequential exposures of gas phase reactants are used for the deposition of thin films with atomic layer accuracy. Each atomic layer formed in the sequential process is a result of saturated surface controlled chemical reactions. Commonly, in the growth of binary compounds such as metal oxides, a reaction cycle consists of two reaction steps. In one step, the metal compound precursor is allowed to react with the surface, and in the other step it reacts with the oxygen precursor. Between the steps a purge is applied to remove the excess of precursor and the reaction by-products. The self-controlled growth mode of atomic layer deposition presents several advantages. The thickness of the films can be controlled in a straightforward manner by controlling the number of reaction cycles, therefore enabling the controlled growth of ultra thin layers. The precursors form stoichiometric films with large area uniformity and conformality even on complex surfaces with deformities.[19] Due to the nature of polymeric substrates, ALD on polymers has several requirements. One of the main limitations is the thermal fragility of polymers which requires deposition to be restricted to low temperatures. For commercial PMMA used in this study, the maximum temperature given for continuous usage is 70 °C. Higher temperature may lead to thermal degradation of the polymer. As a chemical gas phase method, ALD has advantages for materials such as PMMA which are susceptible to radiation damage that is caused when plasma processes are used. PMMA has a flat surface with sporadically occurring dendritic features.[20] Nucleation and initial growth of Al_2O_3 ALD film on PMMA has been suggested to be affected by the large porosity of PMMA and its low chemical solubility for the trimethyl-aluminium (TMA) reactant.[21] The ALD film grows conformally all over the surface, including inside pores and other features. However, a certain minimum thickness is needed to obtain a uniform film on the surface due to the nucleation behavior of the film and the dendritic features possessed by the PMMA surface.

In this paper, we aim both to demonstrate that ALD coatings can make a significant improvement to the adhesion of sputtered metal and ceramic coatings on PMMA and to clarify the mechanisms whereby exposure of PMMA surfaces to a plasma can alter the coating adhesion. This has been done by (i) exposing the PMMA to RF and DC plasmas and measuring the change in chemical bonding at the surface, (ii) measuring the effect of various thickness of ALD-deposited TiO_2 and Al_2O_3 interlayers on the surface changes in the PMMA and the adhesion of the metal/ceramic coatings, and (iii) exploring the relationship between the various bombarding species (UV photons,

© 2009 WILEY-VCH Verlag GmbH & Co. KGaA, Weinheim
DOI: 10.1002/ppap.200900038

VUV photons and ions) on the surface and subsurface structure of the PMMA.

Experimental Part

The Film Deposition

ALD Deposition

Amorphous Al_2O_3 and TiO_2 were deposited on commercial poly(methylmethacrylate) (PMMA) plates (PLEXIGLAS® XT, $\overline{M}_w = 150\,000$–$160\,000\ g \cdot mol^{-1}$) at temperatures between 60 and 65 °C by atomic layer deposition (ALD) using a Beneq TFS-500 ALD tool with a 200 mm^2 reaction chamber basal area. The pressure in the reaction chamber during the deposition was approximately 2 mbar. Nitrogen (99.999%, AGA) was used as the precursor carrier gas, as well as for purging between the precursor pulses. The PMMA substrate material was pre-cleaned in 5% NaOH solution for ten minutes and in de-ionized water for 20 min in an ultrasonic bath at room temperature. Samples were then baked in the oven at 50 °C for several hours to remove the absorbed water. TiO_2 films were grown from tetrakis(dimethylamido)titanium (TDMAT) (Sigma-Aldrich, 99,999%) and O_3 and Al_2O_3 films from trimethylaluminum (TMA) (STREM Chemicals, 98%) and ozone (O_3). TDMAT has been used earlier for TiO_2 ALD process development with H_2O,[22,23] O_3,[23,24] H_2O_2[25] and O_2 plasma[26] as a counter reactant. TMA used together with H_2O form a very common ALD process for Al_2O_3.[27] The TMA and O_3 process has been studied quite extensively,[28] and it has also been used previously in ALD for deposition on polymer substrates.[24] In this study, O_3 was generated from O_2 (99.999%, AGA) in an ozone generator (Wedeco Ozomatic 4 HC) and injected into the reactor at a nominal ozone concentration of around $90\ g \cdot m^{-3}$ as informed by the generator manufacturer. One deposition cycle consisted of a metal precursor pulse, N_2 purge, ozone pulse and N_2 purge. For depositing TiO_2, TDMAT was vaporized from the source at a temperature of 23 °C. One deposition cycle consisted of a 10 s TDMAT pulse, 40 s purge, 4 s ozone pulse and 10 s purge. The deposition started with 30 s water pulse and 90 s purge to increase the number of OH groups on the PMMA surface. Neither the changes due to the 30 s water exposure nor 120 s ozone exposure could be detected from PMMA surface by FTIR-ATR method. Due to the low vapor pressure of TDMAT at 23 °C, a relatively long pulse time for TDMAT was needed to allow it to saturate the substrate surface. The overall number of cycles used were 120, 320 and 820 leading to film thicknesses around 7 nm, 20 nm and 50 nm respectively measured by spectroscopic ellipsometry. TMA was vaporized from the source at a temperature of 20 °C. The pulse and purge times during one deposition cycle were 0.5 s TMA pulse, 3 s purge, 3 s ozone pulse and 5 s purge. The overall number of cycles deposited for the Al_2O_3 films were 70, 170 and 420 leading to film thicknesses around 7, 19 and 33 nm respectively.

Sputter Deposition

In order to study the behavior of ALD Al_2O_3 and TiO_2 films as intermediate adhesion layers for the magnetron sputtered metal and metal compound films, Ti and TiC were first sputtered on uncoated and ALD coated PMMA substrates. The deposition was carried out in a Sloan SL1800 magnetron sputtering deposition system. One single rectangular titanium target was used. The sputtering gases were Ar and CH_4, the latter as a reactive gas for TiC films. The stoichiometry of TiC was controlled using optical emission monitor (OEM) feedback from the titanium emission line at 501 nm. The OEM setting was 80% of the maximum titanium emission. Asymmetric pulsed DC power was applied to the titanium target at a frequency of 250 kHz and a pulse off time of 1 600 ns using an Advanced Energy Pinnacle Plus power supply. The target was operated in the controlled current mode, fixed at 2 A. The average target power was $\approx 3\ W \cdot cm^{-2}$. The background pressures in the chamber was 7×10^{-5} mbar and the sputtering pressure during titanium and titanium carbide deposition were around 3×10^{-3} mbar and 9.5×10^{-3} mbar, respectively. The thickness of the deposited films was approximately 350 nm. Ti with thickness of around 50 nm was deposited as an adhesion layer prior to the TiC. The temperature of the substrate during deposition was monitored by means of temperature-sensitive tapes attached to substrate surface and it was maintained below 50 °C during the deposition.

Plasma Treatments

To investigate further the effects of plasma processing on the PMMA structure and magnetron sputtered film adhesion, different plasma treatments were applied to the plain PMMA and ALD coated PMMA substrates. After these treatments, the Ti layer was sputtered on the selected surface to evaluate the effect of treatment on coating adhesion. A pulsed DC plasma with frequency of 250 kHz was created in the Sloan SL1800 magnetron sputtering system, where the substrate holder was biased to produce a plasma glow discharge. The plasma gas used was argon at an operating pressure of 3×10^{-2} mbar. A bias voltage of 350 V applied to the substrate gave a plasma power of 140 W. The RF plasma treatments with Ar were carried out in a plasma reactor attached to the Beneq TFS-500 ALD system. The plasma power used was 300 W at a frequency of 13.56 MHz. The substrate was placed on the grounded electrode. The operating pressure during the Ar RF-plasma treatment was around 1 mbar. Process time in all plasma treatments was 10 min.

Film and Polymer Surface Characterization

ALD film thickness was measured on silicon (100) and soda lime glass substrates by using spectroscopic ellipsometry (J.A.Woollam Co., Inc. M-2000FI). Sputtered film thicknesses were measured with a stylus profiler (Veeco, DEKTAK 6M). The ALD film structure and the structural changes in PMMA after plasma treatment were studied with ATR-FTIR spectroscopy using a Nicolet 4700 FT-IR spectrometer equipped with a Smart Orbit ATR accessory. The internal reflection element (IRE) used was a diamond crystal. The ATR-FTIR method was also applied for evaluating the fracture interface after the film adhesion test.

Film Adhesion Measurements

The adhesion testing for combined ALD and magnetron sputtered coating on PMMA substrate was carried out by the stud pull-off

© 2009 WILEY-VCH Verlag GmbH & Co. KGaA, Weinheim

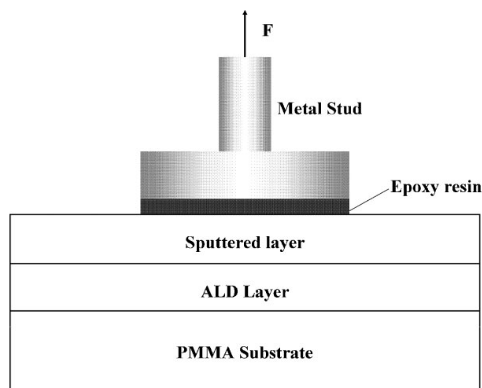

Figure 1. Pull-off test arrangement for thin film adhesion measurement.

method using the PAT adhesion tester of DFD® INSTRUMENTS according to the ASTM D 4541-02 standard. The circular stud used had an area of 12.6 mm^2. Surface contaminants were removed from the stud by a three step cleaning procedure in detergent solution, isopropyl alcohol and acetone in an ultrasonic bath. The stud was attached to the titanium and titanium carbide surface with a thermally curable epoxy adhesive (Locktite 9466 A&B Hysol), which was cured at 40 °C for 5 h. The mechanical tensile strength of the coating was measured by determining the force needed to break the bond between the coating and substrate. An illustration of the pull-off test method is shown in Figure 1. The tape adhesion test (Scotch 810) was used as a prerequisite for the pull-off test method and as an adhesion test for the plasma treated PMMA samples. The tape test was used only as a peel off test where no cross-cuts were applied on the film prior to tape removal. The fracture interface was analyzed by using an optical stereomicroscope Leica MZ 16.

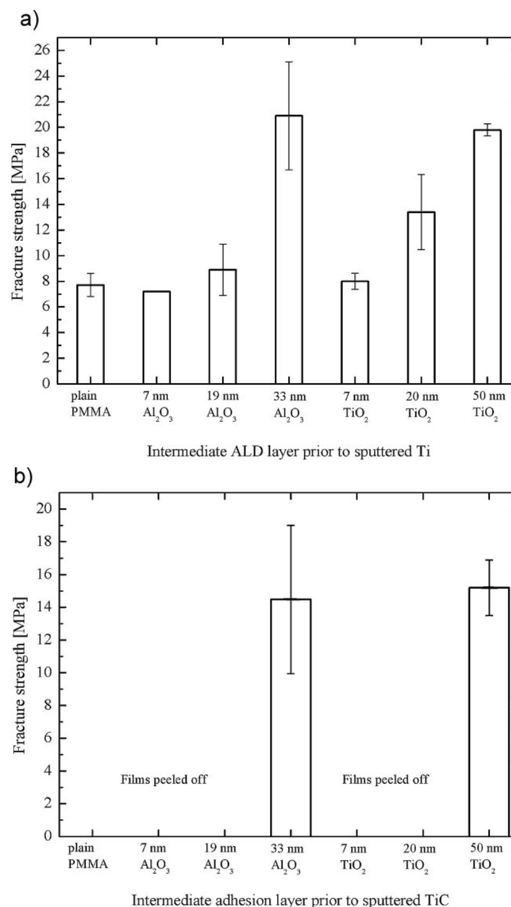

Figure 2. Adhesion strength of sputtered a) Ti and b) TiC films on plain PMMA and on PMMA with intermediate ALD layer.

Results and Discussion

Film Adhesion

The adhesion of the sputtered Ti and TiC was significantly improved with the intermediate ALD oxide layer as shown in Figure 2. The reported value is an average of five single measurements. The error bars show the standard deviation. Poor or no adhesion was observed with the samples with no intermediate layer. It can be seen that the adhesion strength increases with ALD film thickness. With 33 nm Al_2O_3 and 50 nm TiO2 ALD intermediate film, adhesion increased to the point where the failure mechanism was due to cohesive disruption of the substrate material itself. The maximium measured adhesion value of ≈20 MPa was limited by the cohesive strength of the PMMA. The bond strength between film and substrate exceeded this level. This was observed visually with the procedure following the ASTM D 4541-02 standard. It is important to remark that even though the test results in the pull off test are given quantitatively, the overall adhesion strength evaluation requires visual examination. The fracture strength recorded is always a combination of the adhesion of the various layers in the system described in Figure 1. Microscopic examination together with ATR-FTIR analysis of the fracture interface provides a reasonably accurate evaluation tool for studying the adhesion mechanism on PMMA. In Figure 3, the metal stud and PMMA sample surface are viewed after the pull-off test. The various images show the different failure conditions, depending on the coating and the pretreatment used prior to deposition. Visual inspection revealed that in all of the cases shown in Figure 3, the metal film had been completely removed from the PMMA surface by the metal stud. Figure 3a and Figure 3b illustrate the

Plasma Process. Polym. **2009**, *6*, 631–641
© 2009 WILEY-VCH Verlag GmbH & Co. KGaA, Weinheim
DOI: 10.1002/ppap.200900038

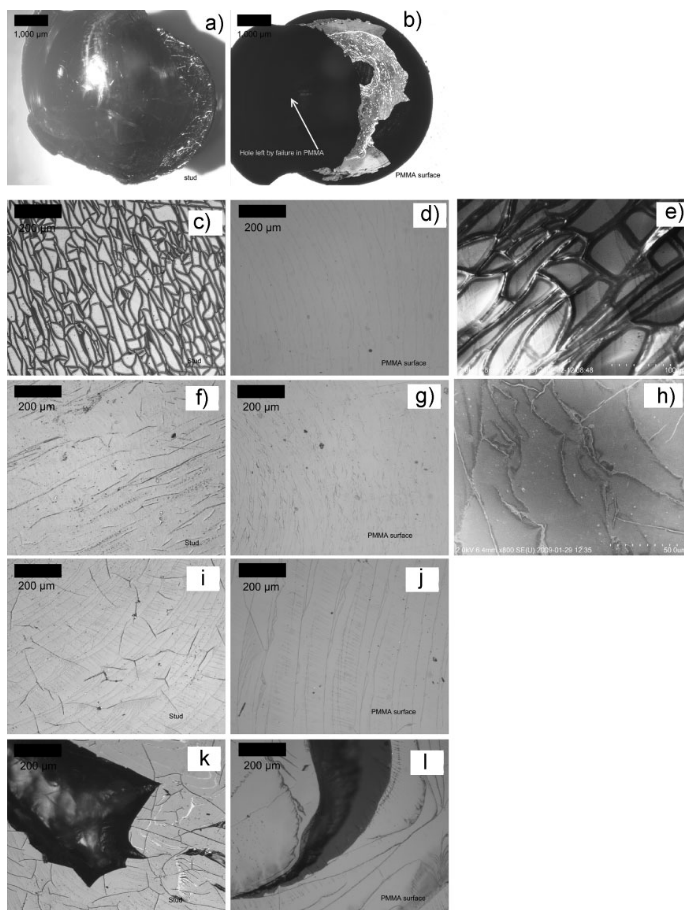

Figure 3. Fracture interface viewed from the metal stud surface after pull-off test: a, b) PMMA with 33 nm Al_2O_3 ALD and sputtered Ti (white arrow in Figure 3b points to the hole on the substrate surface left by failure in PMMA); c,d, e) PMMA with sputtered Ti; f, g, h) RF-plasma treated PMMA prior to 33 nm Al_2O_3 ALD and Ti sputtering; i, j) RF-plasma treated PMMA with 33 nm Al_2O_3 ALD prior to Ti sputtering; and k, l) behind quartz window RF-plasma treated PMMA prior to 33 nm Al_2O_3 ALD and Ti sputtering (darker area on the stud and on the PMMA surface are PMMA removed from the surface and the hole on the surface left by failure in PMMA respectively).

typical fracture interface of metal stud and PMMA surface respectively after the pull-off test of the combined ALD and sputtered film on PMMA. The removal of bulk PMMA material together with film from the sample is evident. The cohesive strength of bulk PMMA material has clearly been exceeded; an average fracture strength of 21 MPa was given by the pull-off test. Figure 3c–3e show the fracture interface of PMMA and sputtered Ti, where the substrate surface shows only PMMA and no ALD deposited material. The netlike structure on the fracture interface on the metal stud in Figure 3c indicates the removal of subsurface of PMMA as suggested by authors in previous studies.[9,15] The Scanning Electron Microscope (SEM) image from the metal stud surface in Figure 3e reveals that the point of fracture is deep within the PMMA as shown by the net-like structure standing proud of the ALD and metal films (light grey area). This sample failed the tape test and the average fracture strength measured by the pull-off test was less than 8 MPa. The fracture interfaces in Figure 3f–3j illustrate the adhesion failure mechanisms when the fracture strength is between the two extreme cases shown in Figure 3a–3e. Average fracture strength in the pull-off test for the samples in Figure 3f–3h and 3i-3j was higher than for sample in Figure 3c, 3d, and 3e, being 12.5 and 12.6 MPa, respectively. Figure 3f–3h illustrates the fracture interface of the sample which was RF-plasma treated for 10 min prior to 33 nm Al_2O_3 ALD and Ti sputtering. Figure 3i and 3j illustrate the fracture interface of the sample which was first deposited with 33 nm Al_2O_3 ALD film then RF-plasma treated for 10 min and finally coated with Ti by magnetron sputtering. Looking at the fracture interface in the cases in Figure 3f–3j, it can be seen that the features of polymer that exists on the fracture interface shown in Figure 3c and 3e have disappeared. The fracture surfaces adhering to the metal studs in Figure 3f and 3i have larger randomly oriented features coming from PMMA residues, but also smaller features which follow the stress distribution caused by tensile stress from the round shaped metal stud. This is attributed to the fact that the fracture interfaces in Figure 3f and 3i appear closer to the PMMA surface than in Figure 3c, since the height of the removed PMMA features is lower in Figure 3h than in Figure 3e. The PMMA sample surfaces in Figure 3d, 3g and 3j appear smoother compared to the opposite metal stud surfaces in Figure 3c, 3f and 3i due to the different contrast effect between transparent PMMA and more reflecting metal stud surface under microscopic examination. Similar type of structuring of PMMA surface, that can be seen in Figure 3c–3e has been reported earlier caused by plasma treatment.[14] Figure 3k and 3l present the fracture interface of the sample which was RF-plasma treated behind a quartz window prior to the deposition of the 33 nm

© 2009 WILEY-VCH Verlag GmbH & Co. KGaA, Weinheim

Al_2O_3 ALD and sputtered Ti layer. In this case, the fracture occurs in bulk PMMA, but the average fracture strength was reduced from 21 MPa to 16.4 MPa, indicating the degradation of PMMA subsurface due to the VUV radiation from RF-plasma above the wavelength of 170 nm (the absorbance edge of quartz window).

The effect of pulsed DC- and RF-plasma treatment on film adhesion is outlined in Table 1. As mentioned above, plasmas can affect the substrate surface by both ion bombardment and VUV radiation effects. It is important to try to distinguish between these in the effects of the ALD layer on adhesion. In the pulsed DC plasma situation, the substrate will be subjected to UV radiation and high energy ion bombardment since the self-bias voltage was −350 V (average), whereas in the RF plasma, only UV radiation is likely to be important. The first feature of note is that where

Table 1. Effect of different plasma treatments on film adhesion.

PMMA sample description in adhesion test (Ti – magnetron sputtered Titanium) (qw – sample behind the quartz window)				Adhesion		Fracture interface detected visually and by ATR-FTIR[b)]
Sample	Step 1	Step 2	Step 3 Metal	Tape test: % of film that adheres on the surface	Pull-off test[a)]: MPa	
1	10 min pulsed DC, 10 min DC Bias	Ti–	Ti	0		Subsurface of PMMA
2	10 min pulsed DC, 10 min DC Bias	ALD Al_2O_3 (33 nm)	Ti	0		Subsurface of PMMA
3	10 min pulsed DC, 10 min DC Bias	ALD TiO_2 (50 nm)	–	0		Subsurface of PMMA
4	10 min RF	Ti–	Ti	0		Subsurface of PMMA
5	10 min RF	ALD Al_2O_3 (33 nm)	Ti	5	12.5 ± 1.6	Subsurface of PMMA
6	10 min RF	ALD TiO_2 (50 nm)	–	0		Subsurface of PMMA
7	ALD Al_2O_3 (33 nm)	10 min RF	Ti	5	12.6 ± 2.8	Subsurface of PMMA
8	ALD Al_2O_3 (19 nm)	10 min pulsed DC, 10 min DC	–	0		Subsurface of PMMA
9	ALD Al_2O_3 (19 nm)	10 min pulsed DC, 10 min DC	Ti	0		Subsurface of PMMA
10	ALD Al_2O_3 (33 nm)	10 min pulsed DC, 10 min DC	–	100		[c)]
11	ALD Al_2O_3 (33 nm)	10 min pulsed DC, 10 min DC	Ti	100		[c)]
12	10 min RF with qw	ALD Al_2O_3 (33 nm)	Ti	50	16.4 ± 3.5	Subsurface/Bulk of PMMA
13	ALD TiO_2 (50 nm)	10 min RF	–	100		[c)]
14	ALD TiO_2 (20 nm)	10 min RF	–	0		Subsurface of PMMA
15	ALD TiO_2 (50 nm)	1 h pulsed DCDC	–	100		[c)]
16	ALD TiO_2 (20 nm)	1 h pulsed DCDC	–	0		Subsurface of PMMA
17	ALD TiO_2 (20 nm)	10 min pulsed DCDC	–	100		[c)]
18	ALD TiO_2 (20 nm)	10 min RF with qw	–	100		[c)]

[a)]Pull-off test carried out on the samples that have received indistinct result from the tape test. Fracture interface detection was done visually on the stud and by ATR-FTIR on the PMMA sample surface; [b)]Fracture interface detection was done visually on the tape and by ATR-FTIR on the PMMA sample surface; [c)]Fracture does not occur since the sample passed the tape test.

Plasma Process. Polym. **2009**, *6*, 631–641
© 2009 WILEY-VCH Verlag GmbH & Co. KGaA, Weinheim
DOI: 10.1002/ppap.200900038

there is no ALD layer between the plasma pretreatment and the Ti metallization, there is no adhesion (samples 1 and 4). When an intermediate ALD layer is included, both film thickness and material play a significant role. It is also clear that ion bombardment is not the major effect in giving poor adhesion in sputtered metallization. If that were the case, even 10 nm of an intermediate ALD layer would protect the surface since the penetration depth of the ions in pulsed DC magnetron sputtering will be at most a few nm. It can be seen from samples 2 and 3 that this did not happen. The major effect, therefore, must be UV radiation from the plasma.

The effects of the UV radiation on adhesion were investigated by depositing an ALD layer on the PMMA substrate and, in some cases, depositing a sputtered Ti layer on top. The sample was exposed to UV radiation from pulsed DC or RF plasmas either before or after the ALD layer was deposited to investigate its shielding effect against UV. In all cases, where the substrate was exposed to UV before ALD, the tape test showed very poor adhesion (samples 2, 3, 5, 6). When the ALD layer was deposited before plasma exposure, there was an improvement in adhesion, which depended on both the type of plasma to which the samples were exposed, and the thickness and composition of the ALD layer. With 10 min exposure to a pulsed DC plasma, 33 nm Al_2O_3 enabled the adhesion to successfully pass the tape test, whereas with TiO_2, only 20 nm was required (samples 10, 11, 17). 50 nm of TiO_2 provided good adhesion when the sample was exposed for 1 h pulsed DC plasma (sample 15). With an RF plasma, thicker layers were required; 33 nm of Al_2O_3 was not sufficient (sample 7) but 50 nm of TiO_2 was (sample 13). To try to evaluate the effects of the ALD layer against deep UV radiation, samples were exposed to the plasma, while shielded by a quartz window before and after ALD (samples 12, 18). It is clear that in sample 12, the quartz plate reduces the effect of plasma exposure compared to the unshielded sample 7, but the combination of the quartz plate and 20 nm TiO_2 allows the sample to pass the tape test. The absorption edge of the quartz window was 170 nm, thus the RF plasma emissions both above and below this wavelength have damaged the PMMA structure.

From the results described above, it is clear that one of the main effects of the ALD layer in improving adhesion on PMMA is that it protects the substrate from the damaging effects of UV radiation which occurs during the subsequent magnetron sputtering of the metal layer. It is also clear that TiO_2 is more effective than Al_2O_3 for this purpose. This can be ascribed to the different bandgaps of Al_2O_3 and TiO_2. The bandgap of TiO_2 measured by UV-VIS transmission on soda lime glass substrates was 3.58 eV (347 nm). The bandgap for 33 nm Al2O3 could not be measured due to the substrate, which had $E_g = 3.75$ eV (absorption edge at 331 nm). The real bandgap of the deposited Al_2O_3 is much higher; values

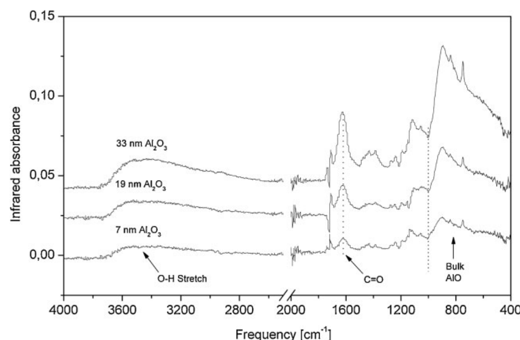

Figure 4. ATR-FTIR difference spectra of Al_2O_3 films on PMMA substrate after 70, 170 and 420 ALD cycles of TMA and ozone. The signal from the substrate has been subtracted from the spectra. Subtraction has been done by using equation (A - B*factor = C) in each measurement point of the spectra, where A represents a spectrum of mixture of Al_2O_3 and PMMA, B represents a spectrum of PMMA, and C is a result spectrum presented in Figure 4. Factor used in subtraction was 1.

of 5.4–8.8 eV have been reported.[29–31] Thus, a thin layer of TiO_2 will have a much higher absorption coefficient and be a more effective shield against UV radiation.

Film Structure and Structural Changes in Subsurface Region of PMMA

The infrared absorption spectra of ALD grown Al_2O_3 and TiO_2 films are shown in Figure 4 and Figure 5, respectively. Due to the linear growth, the linear increase with film thickness of the intensity of typical features in absorbance

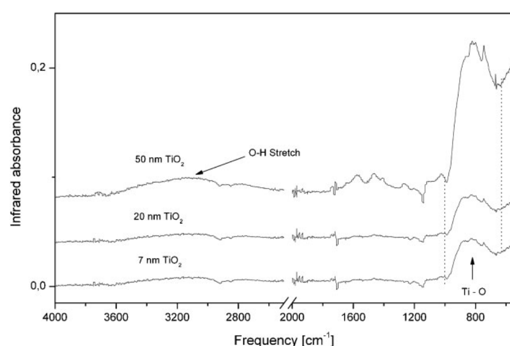

Figure 5. ATR-FTIR difference spectra of TiO_2 films on PMMA substrate after 120, 320 and 820 ALD cycles of TDMAT and ozone. The signal from the substrate has been subtracted from the spectra. Subtraction has been done by using equation (A - B*factor = C) in each measurement point of the spectra, where A represents a spectrum of mixture of TiO_2 and PMMA, B represents a spectrum of PMMA, and C is a result spectrum presented in Figure 5. Factor used in subtraction was 1.

© 2009 WILEY-VCH Verlag GmbH & Co. KGaA, Weinheim

can be expected.[27] In the model of film growth on polymers, the metal precursor absorbs into the polymer and, after subsequent oxidant precursor exposure, the Al_2O_3 starts to nucleate as clusters in the near surface region of the polymer. As this nucleation continues, the clusters fill the space between the polymer chains.[23] Both of the film materials have a broad absorption band at 3 000–3 500 cm^{-1} attributed to O–H stretching vibrations, which is increasing with increasing the film thickness. A similar increase can be observed for the stretching vibration of the bulk Al–O bond with broad band of spectrum in Figure 4 at 400–1 000 cm^{-1}, and broad band of spectrum at 630–1 000 cm^{-1} in Figure 5 attributed to the Ti–O stretching vibration.[27,32–35] The nonexistence of any particular phonon bands of crystalline structures of TiO_2 in this region can be explained by the amorphous film structure.[35] Furthermore, it has been shown earlier that the Raman active vibrational modes $E_g(\upsilon 6)$ and $E_g(\upsilon 5)$ can be detected for this TiO_2 film deposited at 55 °C using TDMAT and O_3 as a precursors.[24] The feature at 1 630 cm^{-1} in Figure 4, which arises only with ALD film and increases with increasing the film thickness, is attributed to the C=O bond in Al_2O_3 film, which is believed to be due to the incomplete reaction between TMA and ozone.

The IR spectra of untreated and DC argon plasma treated PMMA and Al_2O_3 ALD coated PMMA are shown in Figure 6a and 6b. The assignments of absorption bands are based on literature values.[9,36–38] Significant reduction of the absorbance in the bands of C=O at 1 724 cm^{-1}, C–O at 1 190 cm^{-1} and 1 140 cm^{-1}, O–CH_3 at 1 483 cm^{-1} and 2 996 cm^{-1} and CH_3 at 2 956 cm^{-1} of PMMA after plasma treatment indicates degradation and restructuring of the PMMA. The higher absorbance of C=O, C–O and O–CH_3 for plasma treated ALD deposited PMMA compared to plasma treated PMMA without ALD film are attributed to reduced degradation due to the shielding effect of the ALD film against plasma VUV radiation and plasma ion bombardment. The absorbance level of PMMA functionalities shown in FTIR spectra in Figure 6 reduce with increasing the ALD film thickness, which is due to the ATR method where the intensity of the IR radiation decays exponentially into the substrate so that a thicker ALD layer naturally reduces the absorption signal from the PMMA. Concentrating on the functionality of C=O at 1 724 cm^{-1} in Figure 6c., it can be clearly seen that untreated ALD deposited PMMA has higher functionality than plasma treated one, but still lower than untreated PMMA. This indicates that the plasma treatment has an effect on the subsurface which lowers the absorbance of the ALD-coated samples; the changes are not due to the ALD layer alone. The features at 1 630 cm^{-1} and 3 500 cm^{-1} shown in Figure 6a and 6b are attributed to the C=O and O–H stretch of the ALD Al_2O_3 film. This information, characteristic to the film, has also been used for evaluating the fracture interface and adhesion

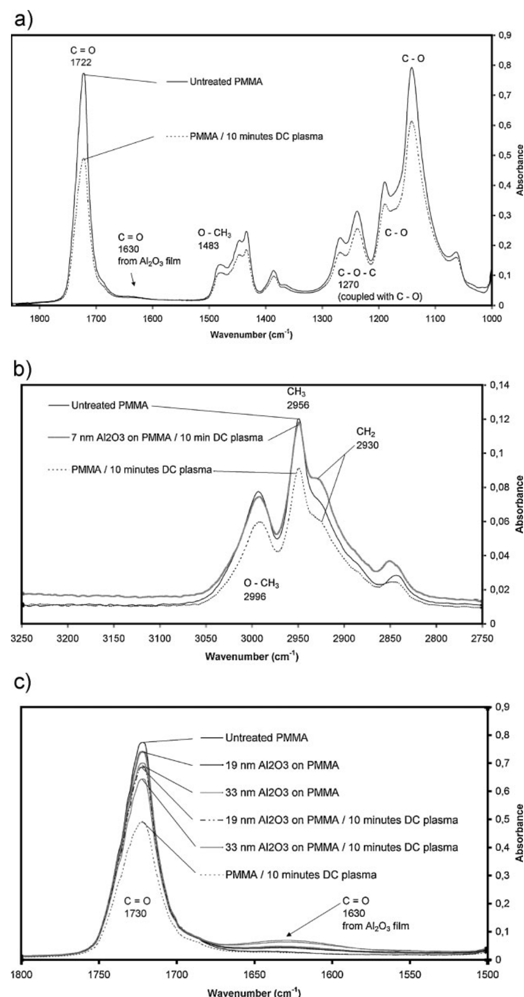

Figure 6. ATR-FTIR spectra of PMMA and Al_2O_3 ALD coated PMMA after DC plasma treatment: a) 1 000–1 850 cm^{-1} range; b) 2 750–3 250 cm^{-1} range; c) 1 500–1 800 cm^{-1} range.

mechanism of the ALD film. ATR-FTIR analysis of the ALD-deposited PMMA sample after the adhesion test shows the features belonging to the ALD film in case the film remains on the PMMA surface, whereas the features cannot be seen if the film has been removed. It is important to mention that when actual fracture interface occurs in the subsurface of PMMA, the removed subsurface cannot be detected by the ATR-FTIR method on the tape or stud which has been pulled off if the thickness of this layer is less than ~10 nm as reported earlier.[9] The IR spectra of the untreated and DC argon plasma treated PMMA and TiO_2 ALD deposited PMMA are shown in Figure 7. A similar kind of shielding

© 2009 WILEY-VCH Verlag GmbH & Co. KGaA, Weinheim
DOI: 10.1002/ppap.200900038

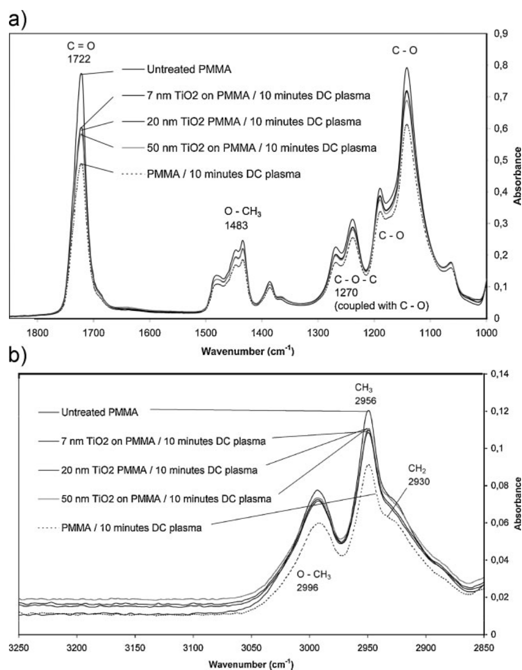

Figure 7. ATR-FTIR spectra of PMMA and TiO_2 ALD coated PMMA after DC plasma treatment: a) 1 000–1 850 cm^{-1} range; and b) 2 850–3 250 cm^{-1} range.

effect against ion bombardment and VUV radiation can be observed for TiO_2 ALD film than for Al_2O_3 film. This can be seen as higher functionalities of typical PMMA absorbance bands after plasma treatment for TiO_2 ALD-deposited PMMA compared with PMMA without ALD film. The results of ATR-FTIR analysis indicate that already 7 nm thick Al_2O_3 and TiO_2 can protect PMMA from plasma VUV radiation and ion bombardment to a certain degree, as shown in IR spectra in Figure 6 and Figure 7. The formation of the CH_2 band at 2 930 cm^{-1} for 7 nm Al_2O_3 coated PMMA, indicating PMMA side chain degradation, however, is a clear indication that the protection is limited. The formation of CH_2 cannot be seen for TiO_2 at any thickness range, which indicates its better shielding characteristics. As mentioned above, with the ATR-FTIR method, the smallest detectable layer thickness on PMMA is around 10 nm.[9] Thus, we can conclude that the PMMA subsurface region affected by DC plasma treatment used in our experiments was clearly thicker than 10 nm.

Changes in PMMA during the RF plasma treatment have been mainly attributed to plasma VUV radiation. The effects of UV radiation without ion bombardment were investigated by using 1 mm thick quartz plate (absorbance edge at 170 nm) during the RF-plasma treatment (sample 12 in Table 1). This protects the surface from ions, but still allows UV irradiation. After the RF-plasma treatment, the PMMA sample was deposited with 33 nm Al_2O_3 ALD film prior to sputtered Ti. Both the pull-off adhesion test (16.4 MPa), and the tape test results presented in Table 1, show reduced adhesion for this sample, indicating that UV radiation with wavelength above 170 nm also has a damaging effect on the PMMA subsurface. Visual inspection revealed that the fracture occurred in bulk PMMA, but the amount of PMMA removed was smaller than for the sample with highest fracture strength value.

As mentioned in Film Adhesion section, lower adhesion for the combined Al_2O_3 ALD and sputtered Ti film was also observed when a PMMA sample with 33 nm Al_2O_3 ALD film was RF-plasma treated prior to Ti sputtering (sample 7 in Table 1). This indicates that 33 nm Al_2O_3 ALD layer does not protect the PMMA against VUV radiation from the RF plasma at these particular plasma conditions. Looking at the ATR-FTIR spectra of RF-plasma treated PMMA, PMMA with 33 nm Al_2O_3 film and PMMA blocked with quartz plate in Figure 8a and 8b, no change in absorbance of typical functional groups of PMMA can be observed for these samples. This is attributed to the fact that the subsurface

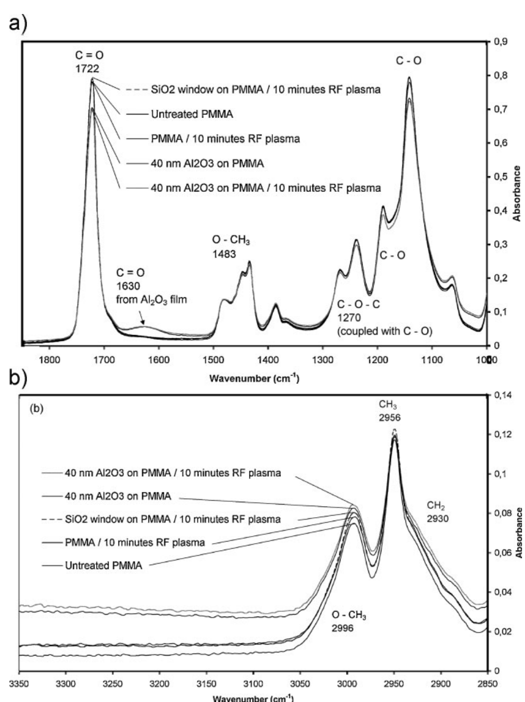

Figure 8. ATR-FTIR spectra of PMMA, Al_2O_3 ALD coated PMMA, and PMMA treated behind quartz window after RF plasma treatment: a) 1 000–1 850 cm^{-1} range; and b) 2 850–3 350 cm^{-1} range.

© 2009 WILEY-VCH Verlag GmbH & Co. KGaA, Weinheim

region affected by VUV from RF-plasma in these cases is less than 10 nm. This can be contrasted with the DC plasma experiments where the effect of the plasma in reducing this absorbance is much greater, as shown in Figure 6 and 7. Earlier studies have shown that both relatively long exposures of plasma VUV radiation (10–30 min) and strong emission in the VUV region (direct He plasma or H_2 plasma-generated VUV radiation) could be used to stabilize the subsurface region of PMMA for attaining improved coating adhesion of PE-CVD optical coatings.[14] It has been reported that argon plasma has relatively weak UV emission compared to e.g. hydrogen and nitrogen in the wavelength range of 100 to 400 nm.[12] Thus, we can expect that in the particular RF-plasma conditions used in our investigation, the VUV radiation emission that affected the PMMA subsurface within thickness of 10 nm was not intense enough to stabilize it.

The effect of the RF-plasma on the polymer substrate has particular interest in the case of plasma assisted ALD (PA-ALD). One of the advantages of PA-ALD is a low deposition temperature, allowing the deposition on temperature sensitive materials such as polymers. Typically, the gases used in PA-ALD include Ar, N_2, O_2, H_2 and NH_3. Moreover, the precursors like TMA and TDMAT for oxides provide natural source for hydrogen. These gases can form a complex plasma situation and provide an intense source of VUV radiation.[12] Our study has shown that, with the type of plasma conditions used in PA-ALD, it is possible to form a weakly bonded subsurface region on PMMA leading to reduced coating adhesion. This should be taken under consideration when plasma is used as a part of the ALD process.

Both DC- and RF-plasma treatment used in our study prior to film deposition have been shown to have an unfavorable effect on the PMMA subsurface causing insufficient adhesion of the ALD oxide layer, the magnetron sputtered Ti layer and combination of these. Nevertheless, the mechanism that affects PMMA differs significantly between these two plasma conditions. The modification depth is greater for DC plasma than for the RF-plasma, as shown in ATR-FTIR measurements, and also the RF plasma proved to be more aggressive than the DC-plasma in reducing the coating adhesion. This could be because, either the intensity of UV/VUV radiation is higher in the DC plasma, or because of the particular wavelengths of UV/VUV radiation present in each of the plasmas. The operating pressure for the RF-plasma was $\approx$1 mbar, while for the DC-plasma it was 3×10^{-2} mbar. Higher pressure allows higher concentration of nitrogen (from small air leaks) and hydrogen (from absorbed water) to be present in plasma. These gases produce higher emissions in the VUV region ($\lambda < 200$ nm), thus it may be that this is the reason for the more damaging effects of the RF plasma. Under RF plasma exposure, the radiation at these wavelengths causes greater degradation of the side chains of PMMA, consequently forming a weakly bonded surface layer with thickness less than 10 nm. This explanation remains only speculative at this stage. ATR-FTIR analysis revealed the reduction of the typical functional groups of PMMA after DC plasma treatment, even for the samples that were evaluated to possess good adhesion, namely the PMMA samples with 33 nm Al_2O_3 and 50 nm TiO_2 ALD layer. This means that some PMMA side chain degradation in subsurface region occurs, but it is not enough to affect film adhesion. Improvement of adhesion through the modification of the PMMA subsurface by plasma treatment alone, as reported by Schulz et al.[9] was not observed in our study. Only the addition of an intermediate ALD layer was effective in improving adhesion.

Conclusion

Amorphous Al_2O_3 and TiO_2 ALD films have been shown to be very effective intermediate layers in improving the adhesion of magnetron sputtered titanium and titanium carbide films on PMMA substrates. A 33 nm ALD Al_2O_3 film thickness was achieved adhesion strength higher than cohesive strength of PMMA itself. A 50 nm of ALD film of TiO_2 had the same effect, although it is clear that TiO_2 layers were better at protecting the substrate from UV radiation due to the lower bandgap of this material. The excellent adhesion of combined ALD oxide and sputtered Ti and TiC films on PMMA is attributed the characteristics of ALD film growth on PMMA, where a degree of interpenetration occurs, the ALD film structure compatible with sputtered layer, and the shielding effect of the ALD films against damaging VUV and ion bombardment. This shielding effect has been shown by ATR-FTIR analysis, where the application of an ALD layer causes a reduction in polymer degradation after exposure to plasmas, more effectively in the case of TiO_2 films. This technique could have wide application where a decorative or wear resistant coating has to be applied to PMMA substrates.

Received: March 15, 2009; Revised: June 8, 2009; Accepted: June 18, 2009; DOI: 10.1002/ppap.200900038

Keywords: adhesion; atomic layer deposition; oxides; PMMA; physical vapor deposition

[1] P. Munzert, U. Schulz, N. Kaiser, *Surf. Coat. Technol.* **2003**, *174–175*, 1048.
[2] T. Koerner, L. Brown, R. Xie, R. D. Oleschuk, *Sens. Actuators B* **2005**, *107*, 632.

© 2009 WILEY-VCH Verlag GmbH & Co. KGaA, Weinheim
DOI: 10.1002/ppap.200900038

[3] J.-Y. Cheng, C.-W. Wei, K.-H. Hsu, T.-H. Young, *Sens. Actuators B* **2004**, *99*, 186.
[4] C. Henry, T. J. Tutt, M. Galloway, Y. Y. Davidson, C. S. McWhorter, S. A. Soper, R. L. McCarley, *Anal. Chem.* **2000**, *72*, 5331.
[5] H. K. Varma, K. Sreenivasan, Y. Yokogawa, A. Hosumi, *Biomaterials* **2003**, *24*, 297.
[6] W. D. Dominic, B. T. Berhane, J. S. Mecomber, P. A. Limbach, *Anal. Bioanal. Chem.* **2003**, *376*, 349.
[7] J. Wang, T. Cui, *Microsyst. Technol.* **2005**, *11*, 452.
[8] J. M. Goddard, J. H. Hotchkiss, *Prog. Polym. Sci.* **2007**, *32*, 698.
[9] U. Schulz, P. Munzert, N. Kaiser, *Surf. Coat. Technol.* **2001**, *142–144*, 507.
[10] P. Gröning, O. M. Kuttel, M. Collaud-Coen, G. Dietler, L. Schlapbach, *Appl. Surf. Sci.* **1995**, *89*, 83.
[11] Y.-B. Guo, F. C.-N. Hong, *Diamond Relat. Mater.* **2003**, *12*, 946.
[12] M. R. Wertheimer, A. C. Fozza, A. Holländer, *Nucl. Instrum. Methods Phys. Res. B* **1999**, *151*, 65.
[13] H. Kaczmarek, H. Chaberska, *Appl. Surf. Sci.* **2006**, *252*, 8185.
[14] M. C. Coen, R. Lehmann, P. Groening, L. Schlapbach, *Appl. Surf. Sci.* **2003**, *207*, 276.
[15] C. Fozza, J. E. Klemberg-Sapieha, M. R. Wertheimer, *Plasmas Polym.* **1999**, *4*, 186.
[16] J. E. Klemberg-Sapieha, L. Martinu, N. L. S. Yamasaki, C. W. Lantman, *Thin Solid Films* **2005**, *476*, 101.
[17] C. Fozza, J. Roch, J. E. Klemberg-Sapieha, A. Kruse, A. Holländer, M. R. Wertheimer, *Nucl. Instrum. Methods Phys. Res. B* **1997**, *131*, 205.
[18] A. Holländer, R. Wilken, J. Behnisch, *Surf. Coat. Technol.* **1999**, *116–119*, 788.
[19] M. Ritala, M. Leskelä, in *Handbook of Thin Film Materials*, Vol. 1, H. S. Nalwa, Ed., Academic Press, San Diego, CA 2002, p. 103.
[20] T. Miyamae, H. Nozoye, *Surf. Sci.* **2003**, *532–535*, 1045.
[21] A. Wilson, R. K. Grubbs, S. M. George, *Chem. Mater.* **2005**, *17*, 5625.
[22] G. T. Lim, D.-H. Kim, *Thin Solid Films* **2006**, *498*, 254.
[23] R. Katamreddy, V. Omarjee, B. Feist, C. Dussarrat, *ECS Trans.* **2008**, *16*, 113.
[24] T. O. Kääriäinen, M.-L. Kääriäinen, R. P. Gandhiraman, D. C. Cameron, ALD 2007, *7th Int. Conf. At. Layer Deposition*, San Diego, California, USA, 24–27 June 2007.
[25] R. Pheamhom, C. Sunwoo, D.-H. Kim, *J. Vac. Sci. Technol. A* **2006**, *24*, 1535.
[26] J.-J. Park, W.-J. Lee, G.-H. Lee, I.-S. Kim, B.-C. Shin, S.-G. Yoon, *Integr. Ferroelectr.* **2004**, *68*, 129.
[27] R. Puurunen, *J. Appl. Phys.* **2005**, *97*, 121301.
[28] S. D. Elliott, G. Scarel, C. Wiemer, M. Fanciulli, G. Pavia, *Chem. Mater.* **2006**, *18*, 3764.
[29] K. S. Shamala, L. C. S. Murthy, K. Narasimha Rao, *Mater. Sci. Eng. B* **2004**, *106*, 269.
[30] R. H. French, *J. Am. Ceram. Soc.* **1990**, *73*, 477.
[31] H. Nohira, W. Tsai, W. Besling, E. Young, J. Petry, T. Conard, W. Vandervorst, S. De Gendt, M. Heyns, J. Maes, M. Tuominen, *J. Non-Cryst. Solids* **2002**, *303*, 83.
[32] N. C. da Cruz, E. C. Rangel, J. Wang, B. C. Trasferetti, C. U. Davanzo, S. G. C. Castro, M. A. B. De Moraes, *Surf. Coat. Technol.* **2000**, *126*, 123.
[33] *An Infrared Spectroscopy Atlas for the Coating Industry*, 4th Ed., *Vol. I*, D. R. Brezinski, Ed., Federation of Societies for Coatings Tecnology, Blue Bell, Pennsylvania 1991.
[34] M. J. Velasco, F. Rubio, J. Rubio, J. L. Oteo, *Thermochim. Acta* **1999**, *326*, 91.
[35] M. Kanna, S. Wongnawa, *Mater. Chem. Phys.* **2008**, *110*, 166.
[36] S. Rajendran, T. Uma, *Mater. Lett.* **2000**, *44*, 242.
[37] S. Rajendran, R. Kannan, O. Mahendran, *Mater. Lett.* **2001**, *49*, 172.
[38] S. Rajendran, T. Uma, *J. Power Sources* **2000**, *88*, 282.

© 2009 WILEY-VCH Verlag GmbH & Co. KGaA, Weinheim

Paper III

Atomic Layer Deposition on Polymer Based Flexible Packaging Materials: Growth Characteristics and Diffusion Barrier Properties.

Tommi O. Kääriäinen, Philipp Maydannik, David C. Cameron, Kimmo Lahtinen, Petri Johansson, Jurkka Kuusipalo

Thin Solid Films 519 (2011) 3146-3154

Reprinted with permission from Elsevier.

Thin Solid Films 519 (2011) 3146–3154

Contents lists available at ScienceDirect

Thin Solid Films

journal homepage: www.elsevier.com/locate/tsf

Atomic layer deposition on polymer based flexible packaging materials: Growth characteristics and diffusion barrier properties

Tommi O. Kääriäinen [a,*], Philipp Maydannik [a], David C. Cameron [a], Kimmo Lahtinen [b], Petri Johansson [b], Jurkka Kuusipalo [b]

[a] ASTRaL, Lappeenranta University of Technology, Prikaatinkatu 3 E, 50100 Mikkeli, Finland
[b] Tampere University of Technology, Paper Converting and Packaging Technology, P.O. Box 541, 33101 Tampere, Finland

ARTICLE INFO

Article history:
Received 22 March 2010
Received in revised form 17 December 2010
Accepted 18 December 2010

Keywords:
Atomic layer deposition
Thin films
Polymer extrusion
Flexible packaging materials
Atomic force microscopy
Attenuated Total Reflection Fourier-Transformed Infrared Spectroscopy (ATR-FTIR)
Gas diffusion barriers

ABSTRACT

One of the most promising areas for the industrial application of atomic layer deposition (ALD) is for gas barrier layers on polymers. In this work, a packaging material system with improved diffusion barrier properties has been developed and studied by applying ALD on flexible polymer based packaging materials. Nanometer scale metal oxide films have been applied to polymer-coated papers and their diffusion barrier properties have been studied by means of water vapor and oxygen transmission rates. The materials for the study were constructed in two stages: the paper was firstly extrusion coated with polymer film, which was then followed by the ALD deposition of oxide layer. The polymers used as extrusion coatings were polypropylene, low and high density polyethylene, polylactide and polyethylene terephthalate. Water vapor transmission rates (WVTRs) were measured according to method SCAN-P 22:68 and oxygen transmission rates (O_2TRs) according to a standard ASTM D 3985. According to the results a 10 nm oxide layer already decreased the oxygen transmission by a factor of 10 compared to uncoated material. WVTR with 40 nm ALD layer was better than the level currently required for most common dry flexible packaging applications. When the oxide layer thickness was increased to 100 nm and above, the measured WVTRs were limited by the measurement set up. Using an ALD layer allowed the polymer thickness on flexible packaging materials to be reduced. Once the ALD layer was 40 nm thick, WVTRs and O_2TRs were no longer dependent on polymer layer thickness. Thus, nanometer scale ALD oxide layers have shown their feasibility as high quality diffusion barriers on flexible packaging materials.

© 2011 Elsevier B.V. All rights reserved.

1. Introduction

In flexible packaging polymer extrusion coating has been the main technology for producing gas permeation barriers on fiber-based materials. The most commonly used polymers for such technology are high density polyethylene, low density polyethylene (LDPE) and polypropylene (PP). Depending on the requirements in the final application, other polymers may lead to better performance of the product. Polyethylene terephthalate (PET) has a very low absorption of the compounds causing odor whereas polymethylpentane possesses very high melting temperature providing good heat resistance [1,2]. In the group of copolymers, ethylene vinyl acetate, ethylene acrylic acid, ethylene methacrylic acid, ethylene butyl acrylate, ethylene methyl acrylate and ethylene ethyl acrylate are typically used for extrusion coating. Also a variety of so-called barrier polymers such as ethylene vinyl alcohol (EVOH) and polyamides like MXD-6 and PA-6 are used to provide high barrier performance. The tendency in the packaging material industry due to economical and environmental reasons is to replace the aluminum foil with other barrier structures and these barrier polymers are often used for that purpose. Economical and environmental drivers have also set a trend to explore new techniques and a variety of material combinations for manufacturing thinner structures enabling packaging material reduction at source with improved barrier properties. A very interesting and increasingly used group of polymers in extrusion coating is that of biodegradable polymers. They may have a great impact in sustainable development where the main challenges are the solid waste management and the reduction of usage of petrochemical sources [1]. In particular polylactides (PLA) have also been studied for their ability to meet the requirements of flexible packaging applications [3]. Polylactides and polyglycolic acids have also wide application in medicine and surgery due to their biocompatibility [1]. One drawback of the polymer-coated fiber-based materials still is that they do not meet all the demands of barrier performance in flexible packaging applications today. The demands are dependent on varying climatic

* Corresponding author. Lappeenranta University of Technology, Prikaatinkatu 3 E, FI-50100 Mikkeli, Finland. Tel.: +358 40 081 3473.
E-mail addresses: tommi.kaariainen@lut.fi (T.O. Kääriäinen), philipp.maydannik@lut.fi (P. Maydannik), david.cameron@lut.fi (D.C. Cameron), kimmo.lahtinen@tut.fi (K. Lahtinen), petri.johansson@tut.fi (P. Johansson), jurkka.kuusipalo@tut.fi (J. Kuusipalo).

0040-6090/$ – see front matter © 2011 Elsevier B.V. All rights reserved.
doi:10.1016/j.tsf.2010.12.171

and transportation conditions but also by the requirement to reduce the polymer coating weight to reduce technical and commercial disadvantages (curling, material costs etc.) [4]. Barrier requirements for sensitive food products have been reported to vary between 0.01 to 100 cm^3/m^2/day for oxygen transmission rate (O_2TR) and 0.01 to 100 g/m^2/day for water vapor transmission rate (WVTR) [5]. While requirements for barrier performance vary depending on packaging application the high barrier performance can be achieved with different barrier structures sufficient for each application. In flexible packaging the ultimate barrier performance has been traditionally achieved with aluminum laminate and increasingly with barrier polymers. The level of O_2TR for high barriers by using EVOH has been reported to be in the range of 0.2 to 2 cm^3/m^2/day (23 °C, 0% relative humidity (RH)) [1]. Biodegradability forbids the usage of conventional materials such as aluminum foil and barrier polymers in barrier structures and therefore the necessity to develop other structures for high performance barriers for biodegradable materials is validated.

Atomic layer deposition (ALD) is a thin film deposition method where sequential exposures of gas phase reactants are used for the deposition of thin films with atomic layer accuracy. Each atomic layer formed in the sequential process is a result of saturated surface controlled chemical reactions. Commonly, in the growth of binary compounds such as metal oxides, a reaction cycle consists of two reaction steps. In one step the metal compound precursor is allowed to react with the surface, and in the other step it reacts with the oxygen precursor. Between the steps a purge is applied to remove the excess of precursor and the reaction by-products. The self-controlled growth mode of atomic layer deposition contributes several advantages. The thickness of the films can be controlled in a straightforward manner by controlling the number of reaction cycles, therefore enabling the controlled growth of ultra thin layers. The precursors form stoichiometric films with large area uniformity and conformality even on complex surfaces with deformities [6–8].

ALD film growth characteristics on polymer substrates have been studied more fundamentally by George et al. [9–12]. While ALD is based on the chemical reactions at the substrate surface the initial growth mechanism of the film is strongly dependent on the surface chemical structure, namely the presence of functional surface groups. In previous studies, especially concerning oxides, the hydroxyl (-OH) groups are found to form on the native substrate surface and are the basis for the initial film growth and nucleation [5,8,13]. Polymers like polyethylene and polypropylene lack the favorable chemical functional groups for the ALD surface reactions [11]. According to Ferguson et al. ALD film growth follows the mechanism where initiation of ALD deposited Al_2O_3 on LDPE surface will take place through the adsorption of the aluminum precursor onto the LDPE surface or absorption into the porous LDPE. This will lead to Al_2O_3 cluster formation with subsequent water exposure and to the linear film growth after the nucleation period [10]. Wilson et al. demonstrated the same mechanism to be applicable for the other polymers as well, although the initiation of the first precursor doses may differ between the various polymers [9]. Nevertheless ALD films can be applied on a number of different polymers [9–12,14] and the potential of ALD on organic and biological substrates has been acknowledged [15]. It is also shown that ALD oxides adhere strongly to polymeric surface [16,17].

The gas permeation through a single inorganic layer is dominated by the defect size and density in the film [5,18,19]. The development of inorganic layer based ultrabarriers has concentrated e.g. on multilayer structures [18,20,21], modification of inorganic layer chemical structure [22] and single layer optimization by ALD [23–25]. The main advantages of ALD are the extreme degree of conformality and uniformity which can be obtained regardless of the orientation or shape of the substrate. Furthermore as a chemical vapor deposition method ALD is favorable over the physical methods such as sputtering that can be detrimental to the polymer surface. As a consequence, ALD layers provide excellent results when used as barrier layers where the diffusion of water vapor or oxygen must be minimized. For polyethylene naphthalate (PEN) and Kapton® substrates Groner et al. reported the 5 nm Al_2O_3 ALD film to possess O_2TR lower than 5×10^{-3} cm^3/m^2/day at 23 °C and 50% RH and 26 nm Al_2O_3 ALD film had WVTR of ~1×10^{-3} g/m^2/day [23]. Depending on the test method used even lower water vapor transmission rates (WVTRs) of ~6×10^{-6} g/m^2/day have been reported with 25 nm Al_2O_3 layers on PEN substrates suitable for organic light-emitting diode (OLED) devices [24].

For industrial applications, it is important to assess the usefulness of ALD as a technique compared to the more established processes. O_2TR and WVTR reported with related barrier structures produced with other thin film deposition methods such as magnetron sputtering [20] and plasma enhanced chemical vapor deposition [26] remain clearly at higher level compared to ALD barriers. It is also clear that, at present, conventional batch ALD processes suffers from slow throughput and the difficulty of applying a batch process to continuous webs. However, continuous and roll-to-roll processing of ALD is now being developed e.g. by Dickey and Barrow [27], and by the authors [28], which validates the study of the ALD film properties on flexible materials being processed in a roll-to-roll facility. Both the characteristics of ALD to produce the ultra thin and highly conformal films leading to extremely low gas diffusion rates on polymers and the efforts taken in the process development towards roll-to-roll ALD encourage exploring the possibilities for ALD films to be used as a barriers in other polymer based applications such as in flexible packaging.

In this paper we have studied the barrier system for flexible packaging applications combining inorganic nano-scale ALD layer and conventionally used polymer extrusion coated paper materials. We will demonstrate that the water and oxygen permeation through a variety of polymer extrusion coated paper can be significantly decreased by adding an Al_2O_3 ALD film. Furthermore, we show the effect of ALD film thickness on the barrier performance, behavior of polymer extrusion coated substrate materials during thermal ALD and its effect on overall barrier performance and permeation mechanism.

2. Experimental details

Al_2O_3 and TiO_2 were deposited on polymer extrusion coated paper materials at temperatures from 65 °C to 150 °C by ALD using a Beneq TFS-500 ALD tool. The polymer extrusion coated paper samples were prepared at the paper converting line of the Paper Converting and Packaging Technology of Tampere University of Technology. The coating polymers studied were LDPE (CA7230, Borealis), PP (WF420HMS, Borealis), PET (Lighter C98, Equipolymers) and PLA (test grade). The LDPE-coated paper was used to study the effect of the polymer layer thickness on diffusion barrier properties in the system combining the polymer and inorganic ALD layer. Three different polymer coating weights were used for this purpose; 18, 27, and 36 g/m^2. Other polymers were studied only by using 25 g/m^2 coating weight. The polymer coated paper samples were loaded to the ALD reactor as received from the paper converting line, only clean compressed air was used to remove the loose particles from the polymer surface prior to deposition. Two polymer extruded paper samples were pressed together polymer sides facing away from each other. This set up combining two samples was then pressed and sealed between polycarbonate frames laminated with aluminum foil, which leaves an area of 10×10 cm^2 inside the frame to be coated by ALD. Penetration of the ALD film inside the frame was ensured not to reach the effective coating area by having enough width in the frame boundary and pressing two frames against each other tightly by using metal clips. Al_2O_3 films were grown from trimethylaluminum (TMA) (STREM Chemicals, 98%) and O_3. TMA was vaporized from the source at a temperature of 20 °C. TiO_2 films were grown from tetrakis

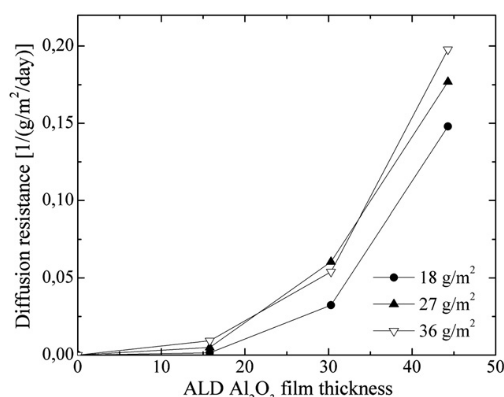

Fig. 1. Diffusion resistance against water vapor at 38 °C and 90% relative humidity (inverse of WVTR) of ALD Al_2O_3 deposited on LDPE extrusion coated paper material. The effect of the polymer substrate has been subtracted from the curves.

(dimethylamido)titanium (TDMAT) (Sigma-Aldrich, 99.999%) and O_3. TDMAT was vaporized from the source at a temperature of 41 °C. O_3 was chosen as it is a powerful oxidizing agent and has a faster desorption rate compared to water, which is known to be difficult to remove at low deposition temperatures leading to longer purge times and consequently decreased process efficiency [9]. O_3 was generated from O_2 (99.999%, AGA) in an ozone generator (Wedeco Ozomatic 4 HC) and injected into the reactor at a concentration of around 90 g/ Nm^3. One deposition cycle for Al_2O_3 consisted of a 0.5 s metal precursor pulse, 6 s N_2 purge, 3 s ozone pulse and 6 s N_2 purge. The timing sequence used for TiO_2 deposition was 1–10 s. For the both oxides the deposition started with 40 s ozone pulse and 90 s purge intended to increase the chemically reactive sites on the polymer surface. The ALD film thickness was varied by changing the number of ALD cycles. The number of cycles varied from 120 to 1660. Depositions were performed on the polymer coated side only.

ALD film thickness was measured from silicon (100) substrates by using spectroscopic ellipsometry (J.A.Woollam Co., Inc. M-2000FI). The ALD film and polymer structure was studied by attenuated total reflectance Fourier transform infrared spectroscopy (ATR-FTIR) using a Nicolet 4700 FT-IR spectrometer equipped with a Smart Orbit ATR accessory. The internal reflection element (IRE) used was a diamond crystal. The surface morphology of the polymer extrusion coated papers with and without the ALD film was examined by tapping-mode atomic force microscopy (AFM) (CP-II Scanning Probe Microscope, Veeco Instruments).

The diffusion barrier properties were tested by means of the WVTR and O_2TR. The test procedure for WVTR followed the SCAN P22:68 (cup method). In this method, a circular sample is positioned against an aluminum dish containing calcium chloride. The sample is then covered with a cylindrical weight with a base area of 50 cm^2. The sample is sealed tightly on the dish with hot wax. After the wax is cooled, the cylinder is removed and the dish is placed into the controlled atmosphere. After stabilization, the daily increase in weight of the dish is measured and the WVTR is expressed as g/m^2/24 h [2]. The WVTRs were measured in two atmospheric conditions: 23 °C, 50% RH and 38 °C, 90% RH. The O_2TR measurements were done with Mocon Ox-Tran Model 2/21 according to a standard ASTM D 3985 [29]. In this method, the coated side of the sample with active test area of 50 cm^2 is sealed against a test cell using vacuum grease, thus the paper side is facing oxygen/nitrogen gas mixture during the measurement [2]. 10% oxygen was used for the test. The result from O_2TR is expressed as cm^3/m^2/24 h. The conditions used for O_2TRs were 23 °C, 0% RH. Each WVTR and O_2TR result shown in this paper is a mean value of two parallel measurements.

3. Results and discussion

3.1. Barrier properties

LDPE coated paper was used as a substrate to study the diffusion barrier properties as a function of polymer coating thickness and ALD film thickness. In Fig. 1 the inverse of WVTRs (named as diffusion resistance) measured at 38 °C and 90% RH with three different polymer coating thicknesses as a function of ALD film thickness are plotted to demonstrate the dependency of barrier performance on ALD film thickness. The diffusion resistance was chosen for the y axis because it more clearly shows the effect of film thickness on performance. If the WVTR were to reduce in inverse proportion to the film thickness, this would give a straight line with a zero intercept on the diffusion resistance graph whereas it would give a hyperbolic curve on the WVTR graph. Fig. 1 clearly shows that when the ALD film thickness is less than around 15 nm the diffusion resistance is only slightly increased suggesting that the ALD film is not properly sealed. In this region the gas diffusion is dominated by the polymer coating. When the ALD film thickness is doubled to around 30 nm a clear rise in the rate of increase of diffusion resistance can be observed. If the slopes of the graphs for higher thicknesses are extrapolated back they intersect the x axis at between 20 and 30 nm film thickness. This indicates a change of behavior in this region after which the additional diffusion resistance is almost proportional to the additional ALD film thickness for all polymer coating weights, thus the ALD film dominates the diffusion through the material above this point. This is attributed to a more defect free and uniform ALD film structure leading to a more efficient barrier. Similar behavior where the diffusion barrier properties improve significantly after a certain ALD film thickness have been reported in earlier studies [23,25]. In both of these studies the polymer substrate was PET film and the clear improvement in WVTR appeared at Al_2O_3 ALD film thickness of around 10 nm. Langereis et al. attributed this to be due to a not completely pinhole-free structure of the film or not conformally sealed ALD film due to the defects on the polymer surface [25]. This behavior suggests that the ALD film dominates the diffusion through the material above the ALD film thickness located between 15 and 30 nm. The polymer coating weight of 27 g/m^2 was chosen for the further studies. After the ALD film thickness of around 45 nm, the diffusion resistance is still increasing with increasing ALD film thickness but with slower rate than in the region between 15 and 45 nm. After the film thickness of around 100 nm no change in WVTR can be observed as shown in Table 1. This behavior suggests that

Table 1
Summary of WVTR and O_2TR measurements of A_2O_3 ALD films deposited at 65 °C on LDPE, PP, PET and PLA extrusion coated paper materials (ref. in first column of each polymer refers to reference substrate material without Al_2O_3 ALD layer).

Polymer	LDPE			PP			PET			PLA		
ALD film thickness [nm]	Ref.	105	177	Ref.	122	143	Ref.	128	195	Ref.	108	208
WVTR, g/m^2*24 h, 23 °C, 50% RH	4.6	0.4	0.5	4.3	0.3	0.2	19.0	0.1	0.6	72.0	4.1	14.7
WVTR, g/m^2*24 h, 38 °C, 90% RH	21.1	2.6	3.5	10.5	1.9	2.7	69.0	0.8	5.6	290.0	53.0	279.5
O_2TR, cm^3/m^2*24 h, 23 °C, 0% (dry O_2)	9177	590		4000	230		150	2	0.9	660	53	12

above this certain film thickness, the ALD film on this type of flexible material is more susceptible to exterior effects, such as bending and tension caused by thermal misfit between the polymer and inorganic ALD film, resulting in irregularities or defects in to the film structure and consequently providing pathway for gases to diffuse through the film.

Concerning oxygen permeation the barrier system behaves differently than in the case of water vapor. The existence of a threshold at low ALD film thickness is not so obvious as it is in the case of diffusion resistance against water shown in Fig. 1, and increases in the diffusion resistance to oxygen can already be observed at low ALD film thickness region as shown in Fig. 2. This is attributed to the fact that the initial O_2TR of LDPE is quite high compared to the initial WVTR which is low and the effect of ALD film on to the barrier is more apparent in the case of oxygen permeation. Comparison between three different polymer coating weights in Fig. 2 suggests that the polymer coating weight does not have a major effect on barrier performance after the initial growth of ALD film, thus the barrier performance is ALD film dominated. Since it has been suggested earlier that the oxygen diffusion through the inorganic film is mainly dominated by defects and micron-scale pinholes [22], the increase in diffusion resistance already at low ALD film thickness region shown in Fig. 2 is taken to indicate the conformal film structure. When ALD film thickness is increased to around 100 nm no improvement in barrier against oxygen can be observed as O_2TR value shows in Table 1. It is suggested that one possible reason for this may be the defects generated to the ALD film similarly as suggested in the case of water vapor. The drop in diffusion resistance for 18 g/m^2 polymer coating with 25 nm ALD film is probably due to defect formation during the sample handling and is also good indication of sensitivity of nanometer-scale film to external effects.

The observations in water vapor and oxygen transmission measurements shown in Figs. 1 and 2 are of great importance when designing the barrier system combining micrometer scale polymer layer and nanometer scale inorganic layer. Based on the results in this study the effective barrier for Al_2O_3 ALD appears to be in the film thickness region between 15 nm and 180 nm. The results presented in Table 2 show higher WVTR for 180 nm Al_2O_3 than for 105 nm Al_2O_3 film suggesting that the actual upper level of effective and functional ALD film thickness lies somewhere between 105 and 180 nm. Since the barrier performance is not totally controlled by the ALD layer thickness, it suggests that the development of barrier performance of this type of flexible substrate shall concentrate on subjects such as polymer surface modification, polymer–inorganic layer interface modification and inorganic layer structure.

In addition to LDPE the Al_2O_3 ALD films were applied on PP, PET and PLA extrusion coated paper materials. The results in WVTR and

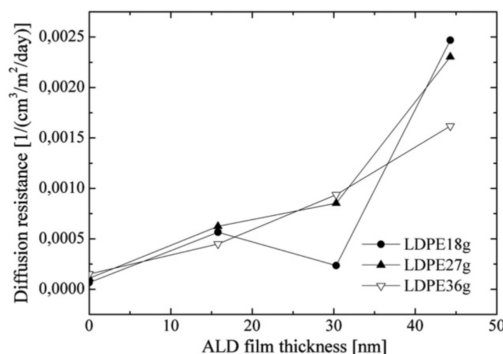

Fig. 2. Diffusion resistance against oxygen at 23 °C 0% relative humidity (inverse of O_2TR) of ALD Al_2O_3 deposited on LDPE extrusion coated paper material.

Table 2
Summary of WVTR and O_2TR measurements of TiO_2 ALD films deposited at 65 °C on LDPE extrusion coated paper materials (ref. in first column refers to reference substrate material without TiO_2 ALD layer).

Polymer	LDPE			
ALD film thickness [nm]	Ref.	10	23	40
WVTR, g/m^2*24 h, 38 °C, 90% RH	19.8	22.1	16.9	21.5
O_2TR, cm^3/m^2*24 h, 23 °C, 0% (dry O_2)	8745	10,026	1133	761

O_2TR measurements for the films over 100 nm thickness deposited at 65 °C are summarized in Table 1. Obviously the measurement conditions have major effect on transmission rates. For the LDPE, PP and PET with ALD film thickness of around 100 nm and above, the WVTRs at 23 °C and 50% RH show the level below 1 g/m^2/24 h. At 38 °C and 90% RH the WVTRs remain at higher levels for the film thickness around 100 nm and are increasing with increasing ALD film thickness. The effect of increasing ALD film thickness on barrier properties is more obvious when observing the transmission rates for PLA. A clear decrease in WVTR at 23 °C and 50% RH can be seen for the PLA with ALD film thickness of around 100 nm, but the barrier effect starts to deteriorate with 200 nm ALD film. This is more obvious at 38 °C and 90% RH where the WVTR has reverted to the level of bare PLA with ALD film thickness of around 200 nm.

In the case of O_2TR there are clear differences between the polymers both in O_2TR level achieved and in the barrier system behavior as a function of ALD film thickness. This difference between the polymers is demonstrated in Fig. 3 where the normalized WVTRs and O_2TRs of the samples with 1200 ALD cycles (105 nm for LDPE, 122 nm for PP, 128 nm for PET and 108 nm for PLA) are plotted with respect to transmission rate of bare polymer extrusion coated material. The bare polymer extrusion coated material in Fig. 3 has a transmission value of 1. It is clear that the films show divergent performance in gas permeation depending on both the polymer layer and measurement conditions used. With PET 100 times lower transmission rates can be obtained at any measuring conditions for both oxygen and water vapor permeation. The other three polymers behave differently within the measurement conditions. The relative permeation of water vapor measured at 38 °C and 90% RH remains remarkably higher compared to permeation measured at 23 °C and 50% RH for PP and PLA. The difference in LDPE is not so obvious. Oxygen permeation shows similar performance for LDPE, PP and PLA. Looking at the O_2TR of bare polymer coated samples in Table 1, it can be seen that the O_2TR of PET is more than four times lower than O_2TR

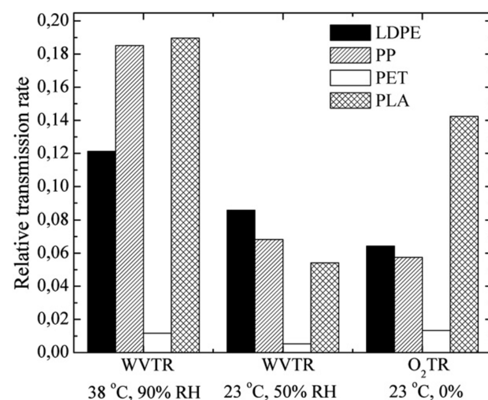

Fig. 3. Relative WVTR and O_2TR of 1200 ALD cycles deposited Al_2O_3 on polymer extrusion coated paper materials normalized by the transmission rate of bare polymer extrusion coated paper material.

Table 3
Summary of WVTR and O2TR measurements of Al_2O_3 ALD films deposited at 65 °C and 150 °C on PET extrusion coated paper materials (ref. in first column refers to reference substrate material without Al_2O_3 ALD layer).

Polymer	PET				
Growth temperature °C		65	65	150	150
ALD film thickness [nm]	Ref.	128	195	76	97
WVTR, g/m^2*24 h, 38 °C, 90% RH	69	0.8	5.6	21	17
WVTR, g/m^2*24 h, 23 °C, 50% RH	19	0.1	0.6	6	5.1
O_2TR, cm^3/m^2*24 h, 23 °C, 0% (dry O_2)	150	2	0.9	2000	2000

of PLA and almost two orders of magnitude lower than the O_2TR of LDPE and PP. This has been reported for PET also in the literature [1]. Evidently the PET structure itself is beneficial for the oxygen barrier but at the same time the highest decrease in WVTR for PET with ALD film gives reason to believe that PET is a favorable substrate for ALD film deposition for further development of the barrier performance. This can be explained e.g. through lower level and size of surface defects on PET that are able to be sealed by ALD film. The highest relative decrease in WVTR for PET supports this hypothesis as well. This makes also evident the fact that the low WVTR of bare polymer substrate is not the only factor in determining the performance of the barrier system where a micron-scale polymer layer and a nanometer scale inorganic layer are combined.

Relatively low WVTR can be achieved already with bare LDPE and PP whereas WVTR for bare PET remains several times higher. Looking back to the normalized transmission rates in Fig. 3 it can be concluded that LDPE, PP and PLA have a larger effect on permeation rates in the combined barrier system than PET. Therefore it is critical to concentrate on the structural characteristics of the polymer, particularly the reduction of irregularities on the polymer surface. Although the analysis of relative permeation provides a tool to develop the understanding of the barrier system, the actual permeation rates cannot be disregarded since they define the material usability in the final barrier application. For example the WVTR of all the polymers with around 100 nm ALD film, except PLA, meets the requirements for dry packaging solutions, but the ambient temperature in the final application may define the polymer chosen for the barrier structure. Another interesting observation from transmission rates of Al_2O_3 deposited PET and PLA is that for both materials the WVTR with around 200 nm ALD layer is increasing from the level with around 100 nm ALD layer while the O_2TR is decreasing with higher ALD layer thickness. This is attributed to the difference in permeation mechanism of water vapor and oxygen. One hypothesis can based on previous studies where it was suggested that the oxygen permeation is mainly happening through the nano-scale and micro-scale pinholes whereas the water vapor permeates through tortuous pathways and can also be affected by chemical interactions between water and the inorganic layer material [19,21]. If this model is applied in our study it suggests that the defect size or opening in 200 nm Al_2O_3 ALD film on PET and PLA is still at a low level but does occur and allows water to permeate into the film. The difference in permeation mechanism between water and oxygen is further proven with the results of WVTR and O_2TR of ALD TiO_2 shown in Table 2. There is no improvement seen in WVTR with 40 nm TiO_2 film but O_2TR decreases to over ten times lower level than that of bare LDPE substrate. As a conclusion by selecting carefully the polymer and ALD film combination in extrusion coated flexible packaging materials, it is possible to achieve the high barrier performance reported in literature. In respect of future development in recyclable flexible packaging materials the barrier results on PLA extrusion coated packaging material are very promising since the barrier results meet the requirements for sensitive food products today.

Graff et al. reported that to meet the requirements of barrier performance in OLEDs the single inorganic layer must have certain effective diffusivity that requires an equivalent defect size of 0.01 nm at a defect spacing of around 100 μm, or 10 nm defect size at 10 mm spacing [18]. ALD Al_2O_3 as an inorganic material is brittle and susceptible to cracking under primary mechanical stress and stress due to the thermal load when deposited on materials with higher coefficient of thermal expansion such as on polymers. It has been demonstrated by the recently developed fluorescent tag method [30] that 25 nm thick Al_2O_3 ALD using TMA and water on PEN substrates [9] is initially defect free. Particulate contamination on the substrate is suggested to be the reason for individual defects in the film [25,26] which consequently causes limited barrier performance [19,24]. The critical strain value for crack formation and their propagation in Al_2O_3 ALD film can be significantly improved by decreasing the ALD film thickness. This has been observed in a recent study where the critical strain improved from 0.88% to 5.08% when the Al_2O_3 ALD film thickness was decreased from 125 nm to 5 nm [17]. Furthermore in this same study, the critical strain value for 5 nm Al_2O_3 ALD film was found to be notably greater than for conventionally used micrometer scale thin film materials. Fine-scale morphology that means more densely packed coatings is suggested to be the reason for the lower WVTR values of sputtered coatings [22].

It is well documented that ALD film improves its properties such as film density and a lower level of impurities in the film with increasing deposition temperature [9,31]. With respect to barrier performance, denser film presumably provides smaller defect sizes in the film. Generally two properties of polymers, the coefficient of thermal expansion and the glass transition temperature, define their behavior under thermal cycling. Since inorganic materials used in barriers have significantly lower coefficient of thermal expansion than the underlying polymers, this elastic misfit will lead to an increase in strain and consequently cracking under thermal cycling [32]. In the case of Al_2O_3 ALD film on polymers this phenomenon has been explored more comprehensively by Miller et al. [17]. Here, we studied the effect of higher deposition temperature of ALD Al_2O_3 on the

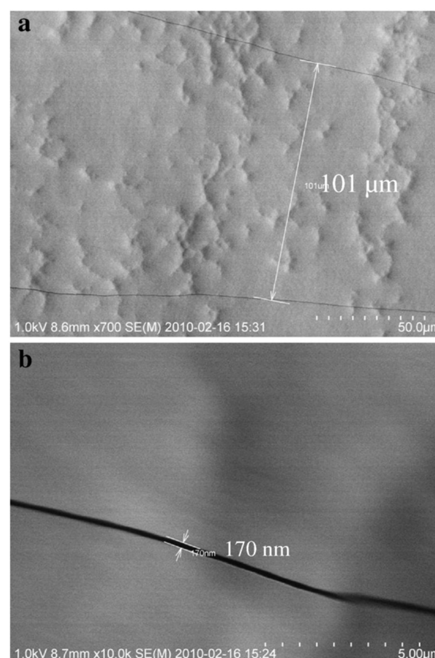

Fig. 4. The surface of PET with 80 nm Al_2O_3 ALD film deposited at 150 °C showing a) the crack spacing, and b) the crack opening.

barrier properties of PET. WVTR and O_2TR of Al_2O_3 film deposited at 150 °C on PET shown in Table 3 indicate the importance of an awareness of the thermal behavior of the substrate during the thermal cycling. Even allowing for the lower film thickness of the film deposited at 150 °C compared with the film deposited at 65 °C it is clear that the barrier performance of the Al_2O_3-PET combination has deteriorated. WVTR of the sample deposited at 150 °C shows four times lower value than bare PET substrate indicating that the ALD layer still has a role in the barrier system. However, the dramatic increase in O_2TR (over 2000 cm^3/m^2/day) for this sample suggests damage not only to the ALD film but to the polymer structure as well. This loss of barrier performance is attributed to be due to the both to cracking of Al_2O_3 layer and structural changes in the PET. Cracks appeared on the surface with spacing of around 100 µm and with openings of 170 nm as shown in Fig. 4. Cracks with smaller spacing and opening may not have been observed by SEM. Change in the PET structure was observed as a curling of the paper sample that exposed the ALD film to compressive stress. This is attributed to be due to the crystallization of PET when exposed to the deposition temperature of 150 °C. The curling effect of the PET sample leaves also the option for cracking of ALD film to happen during the sample handling when flattening it for further examination. The SEM sample was taken from the middle of the curled sample and it was not bent during the sample mounting. However at which point the cracks are formed cannot be confirmed in this study. Nevertheless the heavy curling effect of the polymer substrate is a disadvantage for the post-deposition handling of the sample since it is apparently detrimental to barrier performance. The difference in permeation mechanism between water vapor and oxygen was discussed earlier and can be observed here as well. The barrier performance against water vapor of PET with Al_2O_3 deposited at 150 °C still remains at a lower level than for bare PET while the barrier in this sample against oxygen is completely lost. These findings are similar to the results published earlier where the oxygen transmission through AlO_xN_y film was reported mainly happening through the micron scale defects whereas the mechanism of water vapor permeation was more complicated and the micron-scale defects in the coating had only minor role in total WVTR. Water permeation was also found to be affected by chemical interaction between water and film material [22]. This raises the idea that the ALD film structure and chemical composition can be controlled through doping the film e.g. by growing nanolaminates and so further develop the barrier properties.

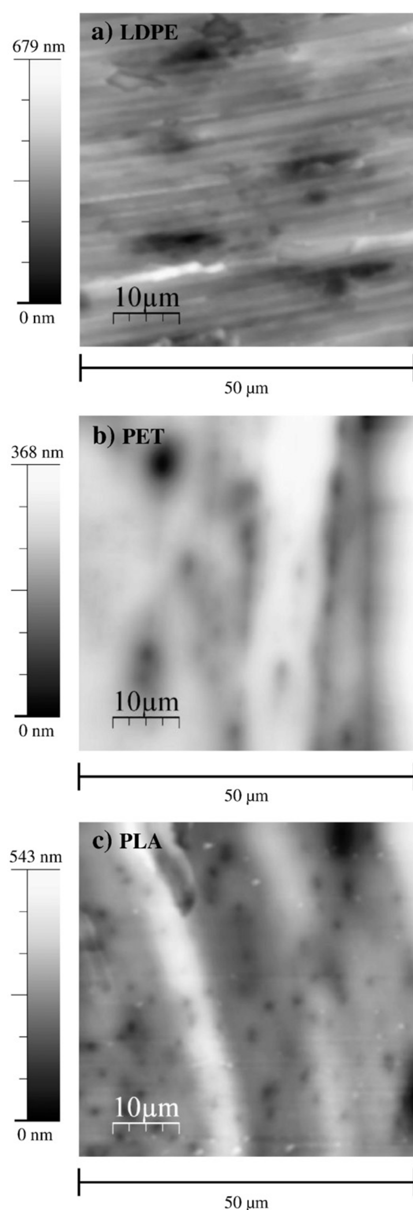

Fig. 5. 2500 μm^2 AFM images of bare a) LDPE, b) PET and c) PLA extrusion coated paper materials.

3.2. Nano-scale morphology by AFM

The surface morphologies of the materials used in this study are shown in Fig. 5. AFM images of 2500 μm^2 reveal that the surface is structured by the features such as longitudinal cavities and dents that have been formed during the polymer extrusion process. Using ALD on these type of surfaces is well justified since the ALD film grows conformally in deep trench structures [6]. Surface smoothness and defect density of the polymer are the key factors affecting the permeation performance of thin inorganic barrier layer [18,24]. Therefore it is more relevant to study the fine scale structure since the surface morphology and morphological changes during the ALD affecting the barrier performance are taking place in the nano-scale. For the deeper analysis of surface morphology the AFM images of 9 μm^2 are shown in Fig. 6. In general Al_2O_3 ALD film seems to overlay smoothly on all the polymers which is based on the observation in which the polymer surface features can be clearly seen underneath the ALD layer in Fig. 6b, d, f and h. Closer examination of each polymer surface shows the difference in their structure and structural change during the deposition. The surface structure of bare LDPE and Al_2O_3 deposited LPDE shown in Fig. 6a and b appear similar which indicates no change in surface structure during the deposition. Different behavior can be observed for the other polymer surfaces. The surface structure of PET and PP shown in Fig. 6d–i clearly changes during the deposition forming round shaped granules. Line profile analysis reveals that the maximum height of granules is in the range of around 40 nm for PET and 25 nm for PP. The surface of PP shown in Fig. 6g has also more general granularity with voids in the structure. These voids are suggested to be possible pathways for gas diffusion especially if they have appeared during the deposition or cooling period when there is a possibility for defect initialization in the ALD film due to the polymer contraction. The surface of bare PET shown in Fig. 6c is smoother than the surface of PP and it remains smooth during the

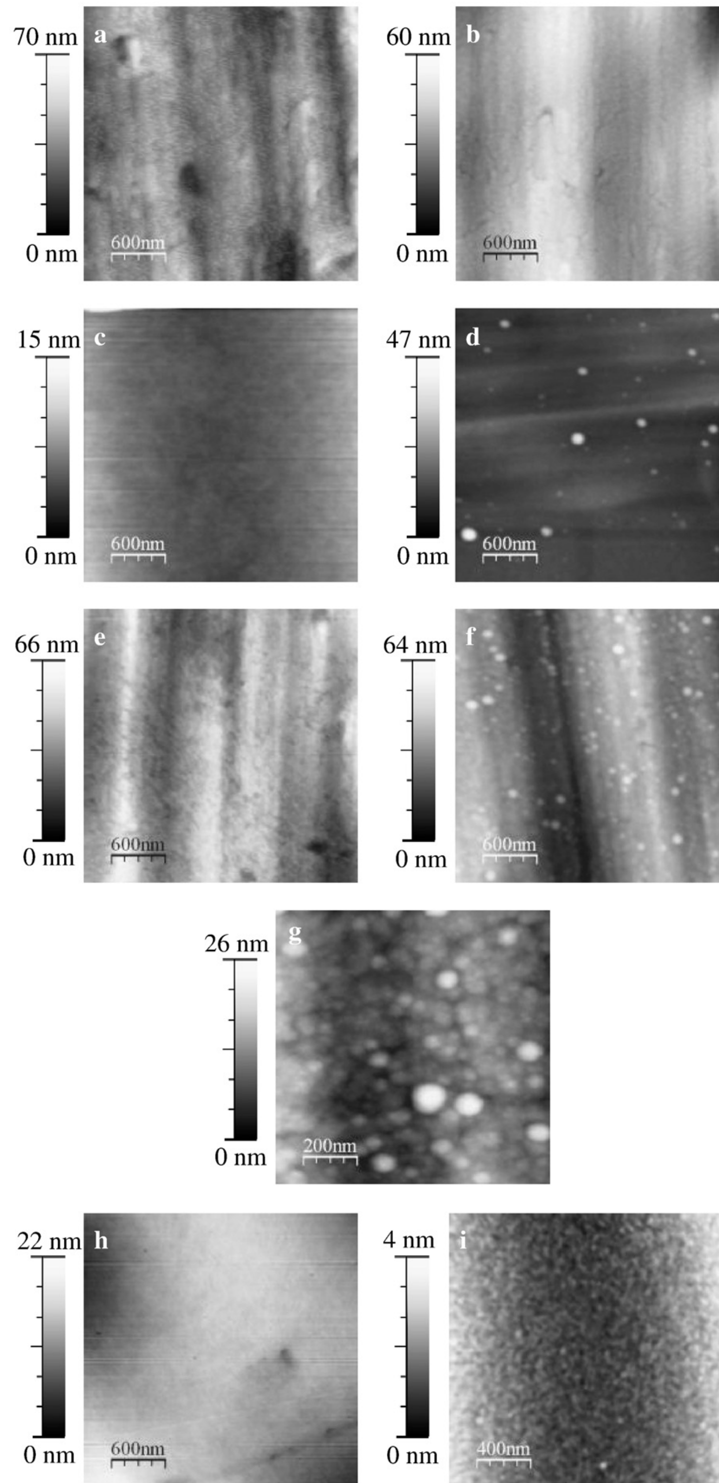
70 nm
0 nm
a
600nm
60 nm
0 nm
b
600nm
15 nm
0 nm
c
600nm
47 nm
0 nm
d
600nm
66 nm
0 nm
e
600nm
64 nm
0 nm
f
600nm
26 nm
0 nm
g
200nm
22 nm
0 nm
h
600nm
4 nm
0 nm
i
400nm

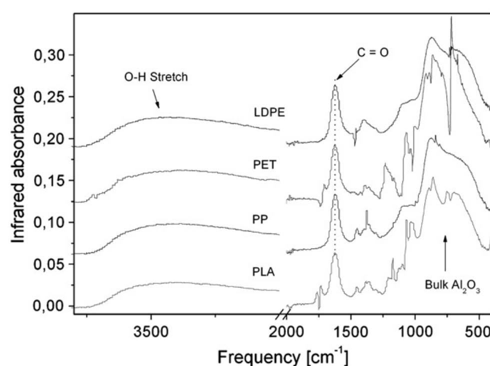

Fig. 7. ATR-FTIR difference spectra of Al_2O_3 films on polymer extrusion coated paper substrate after 1200 ALD cycles of TMA and ozone. The signal from the substrate has been subtracted from the spectra.

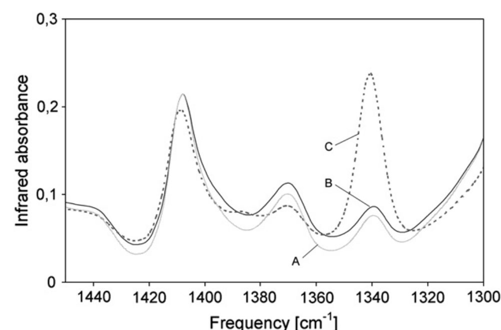

Fig. 8. ATR-FTIR spectra of bare PET extrusion coated substrate material (A), Al_2O_3 film deposited at 65 °C on PET substrate (B), and Al_2O_3 film deposited at 150 °C on PET substrate (C).

deposition with the exception of randomly spread granules. Combining this with the barrier performance presented in Fig. 3 and Table 2, where the ALD film on PET among the other polymers shows the deepest drop in WVTR and O_2TR, it can be stated that PET is favorable for ALD under these conditions.

A good indication of the capability of the ALD to seal the nanostructured surface is also the relatively low transmission rates achieved for PET, even when the round shape granules are formed at the surface during the deposition. The surface structure of bare PLA and PLA with ALD film shown in Fig. 6h and i suggests that the surface of PLA is smoothening during the deposition but at the same time small cavities with a size of 10 nm are formed. These cavities are suggested to provide a pathway for gases to permeate through the film. This is also shown as a moderate barrier performance in Fig. 3 and Table 2. The morphological change observed in the surface of PLA and PP during the deposition is a critical factor in the development of the barrier system combining polymer and inorganic thin film. It is also important to determine in which actual point of the process the morphological changes take place. If the cavities and larger voids in polymer are formed before the starting of the deposition the inorganic layer may still cover these irregularities resulting in good barrier performance. If the morphological changes take place during the cooling period after the deposition, the thermal misfit between the polymer and inorganic layer may cause cracking of the film resulting in reduced barrier performance. Further decrease in O_2TR for 200 nm Al_2O_3 deposited PLA compared to 100 nm Al_2O_3 sample though suggests that the number and size of voids leading to oxygen permeation has not increased during the longer ALD process.

3.3. Film structure and effect on barrier properties

The infrared absorption spectra of Al_2O_3 deposited at 65 °C on polymer extrusion coated paper materials are shown in Fig. 7. A typical broad absorption band is seen at 400–1000 cm^{-1} corresponding to the stretching vibration of bulk Al–O and a broad absorption band at 3000–3500 cm^{-1} attributed to O–H stretching vibration is shown on all the substrates. We have earlier reported similar film characteristics when Al_2O_3 was deposited on PMMA substrate [16]. The feature at 1630 cm^{-1} was attributed to the C=O bond in Al_2O_3 due to the incomplete reaction between TMA and ozone. The features arising from the absorbance spectra of all the substrates after Al_2O_3 deposition at 65 °C which are different from the bare polymer absorbance spectra are related to Al_2O_3. This suggests no change in chemical structure of polymer surface region during the Al_2O_3 deposition. PET extrusion coated paper material was also used for ALD at 150 °C. The degree of crystallinity of PET film can be examined by monitoring the changes in CH_2 wagging region of PET infrared absorbance spectrum. The decreases in absorbance band at 1370 cm^{-1} and increase at 1340 cm^{-1} indicate increased crystallinity based on a model described in previous studies [33,34]. Similar behavior can be seen in Fig. 8 where the absorbance spectra of bare PET, PET with Al_2O_3 deposited at 65 °C and PET with Al_2O_3 deposited at 150 °C are shown suggesting increased crystallinity for the PET that was deposited with Al_2O_3 at 150 °C. From this result together with the barrier results shown in Table 3 we conclude that the crystallization of PET structure taking place at 150 °C deposition temperature is detrimental to the barrier properties of this type of barrier system.

4. Conclusion

Atomic layer deposition was used to deposit oxide layers on various polymer extrusion coated paper materials. The results show enhanced barrier properties against water and oxygen permeation. The WVTR and O_2TR measurements indicated that for Al_2O_3 deposited on LDPE extrusion coated paper, the barrier performance of the structure improved with increasing ALD film thickness. Between 15 and 30 nm ALD film thickness the diffusion resistance starts rising rapidly. The water vapor barrier performance of the ALD film finds its optimum at approximately 100 nm thickness. For oxygen transmission the change in the rate of increase cannot be seen. That is believed to be due to the difference in permeation mechanism between water vapor and oxygen. Sample handling becomes more critical with increasing ALD film thickness since the film becomes less resistant to stress. Due to this the barrier performance especially with higher ALD film thickness may be influenced by irregularities produced in the film during the sample handling.

Differences in the diffusion barrier performance of the barrier system combining a polymer extrusion coating and inorganic ALD layer were observed for different polymers. These are attributed to the presence of irregularities both in the ALD layer and the polymer film as a consequence of different polymer chemical structure, surface morphology and behavior under thermal cycling. 128 nm Al_2O_3 film deposited on PET decreased WVTR measured at tropical conditions of 38 °C and 90% RH below the level of 1 g/m^2/day. On LDPE and PP with roughly the same ALD film thickness, WVTR around 2 g/m^2/day was achieved. The relative decrease in WVTR and O_2TR for PLA was in the same range with LDPE and PP, but the real WVTR of Al_2O_3 deposited

Fig. 6. 9 μm^2 AFM images of a) bare LDPE, b) LDPE with 100 nm Al_2O_3, c) bare PET, d) PET with 128 nm Al_2O_3, e) bare PP, f) PP with 122 nm Al_2O_3, g) PP with 122 nm Al_2O_3, 1 μm^2 image size, h) bare PLA, and i) PLA with 108 nm Al_2O_3, 4 μm^2 image size.

PLA remained still at moderate level, presumably because of a high defect level in the PLA. The results show that an ALD layer of Al_2O_3 on polymer extrusion coated paper can achieve sufficient levels of barrier performance suitable for tropical packaging use.

Acknowledgements

The authors thank ESF and the Center for Economic Development, Transport and the Environment of South Savo for supporting the project under S10148, and ERDF and the Finnish Technology Agency (TEKES) for supporting the project under 70018/08.

References

[1] J. Kuusipalo (Ed.), Papermaking Science and Technology, 2nd Ed, Paper and Paperboard Converting, Vol. 12, Helsinki, Finnish Paper Engineers' Association, Finland, 2008.
[2] K. Lahtinen, K. Nättinen, J. Vartiainen, Polym-Plast. Technol. 48 (2009) 561.
[3] K. Lahtinen, S. Kotkamo, T. Koskinen, S. Auvinen, J. Kuusipalo, Packag. Technol. Sci. 22 (2009) 451.
[4] J. Kuusipalo, K. Lahtinen, Int. J. Polym. Anal. Charact. 10 (2005) 71.
[5] C. Charton, N. Schiller, M. Fahland, A. Holländer, A. Wedel, K. Noller, Thin Solid Films 502 (2006) 99.
[6] T. Suntola, M. Simpson (Eds.), Atomic Layer Epitaxy, Chapman and Hall, New York, NY, 1990.
[7] M. Ritala, M. Leskelä, in: H.S. Nalwa (Ed.), Handbook of Thin Film Materials, Vol. 1, Academic Press, San Diego, CA, 2002, pp. 103–159.
[8] R. Puurunen, J. Appl. Phys. 97 (2005) 121301.
[9] M.D. Groner, F.H. Fabreguette, J.W. Elam, S.M. George, Chem. Mater. 16 (2004) 639.
[10] C.A. Wilson, R.K. Grubbs, S.M. George, Chem. Mater. 17 (2005) 5625.
[11] J.D. Ferguson, A.W. Weimer, S.M. George, Chem. Mater. 16 (2004) 5602.
[12] C.A. Wilson, J.A. McCormick, A.S. Cavanagh, D.N. Goldstein, A.W. Weimer, S.M. George, Thin Solid Films 516 (2008) 18.
[13] S.D. Elliott, G. Scarel, C. Wiemer, M. Fanciulli, G. Pavia, Chem. Mater. 18 (2006) 3764.
[14] M. Kemell, E. Färm, M. Ritala, M. Leskelä, Eur. Polym. J. 44 (2008) 3564.
[15] M. Knez, K. Nielsch, L. Niinistö, Adv. Mater. 19 (2007) 3425.
[16] T.O. Kääriäinen, D.C. Cameron, M. Tanttari, Plasma Processes Polym. 6 (10) (2009) 631.
[17] D.C. Miller, R.R. Foster, Y. Zhang, S.-H. Jen, J.A. Bertrand, Z. Lu, D. Seghete, J.L. O'Patchen, R. Yang, Y.-C. Lee, S.M. George, M.L. Dunn, J. Appl. Phys. 105 (2009) 093527.
[18] G.L. Graff, R.E. Williford, P.E. Burrows, J. Appl. Phys. 96 (2004) 4.
[19] A.S.D. Sobrinho, G. Czeremuszkin, M. Latreche, M.R. Wertheimer, J. Vac. Sci. Technol. A. 18 (2000) 149.
[20] J. Fahlteich, M. Fahland, W. Schönberger, N. Schiller, Thin Solid Films 517 (2009) 3075.
[21] J. Meyer, D. Schneidenbach, T. Winkler, S. Hamwi, T. Weimann, P. Hinze, S. Ammermann, H.H. Johannes, T. Riedl, W. Kowalsky, Appl. Phys. Lett. 94 (2009) 233305.
[22] A.G. Erlat, B.M. Henry, C.R.M. Grovenor, A.G.D. Briggs, R.J. Chater, Y. Tsukahara, J. Phys. Chem. B 108 (2004) 883.
[23] M.D. Groner, S.M. George, R.S. McLean, P.F. Carcia, Appl. Phys. Lett. 88 (2006) 051907.
[24] P.F. Carcia, R.S. McLean, M.H. Reilly, M.D. Groner, S.M. George, Appl. Phys. Lett. 89 (2006) 031915.
[25] E. Langereis, M. Creatore, S.B.S. Heil, M.C.M. Van de Sanden, W.M.M. Kessels, Appl. Phys. Lett. 89 (2006) 081915.
[26] A. Grüninger, A. Bieder, A. Sonnenfeld, Ph. Rudolf von Rohr, U. Müller, R. Hauert, Surf. Coat. Technol. 200 (2006) 4564.
[27] E.R. Dickey, W.A. Barrow, 52th Annual Technical Conference Proceedings of the Society of Vacuum Coaters, 0737-5921, 2009, p. 700.
[28] P.S. Maydannik, T.O. Kääriäinen, D.C. Cameron, 53rd Annual Technical Conference Proceedings of Society of Vacuum Coaters, 0737-5921, 2010, p. 138.
[29] ASTM standard D 3985-05, Standard Test Method for Oxygen Gas Transmission Rate Through Plastic Film and Sheeting Using a Coulombmetric Sensor, ASTM International, West Conshohocken, PA, 2005.
[30] Y. Zhang, Y.-Z. Zhang, D.C. Miller, J.A. Bertrand, S.-H. Jen, R. Yang, M.L. Dunn, S.M. George, Y.C. Lee, Thin Solid Films 517 (2009) 6794.
[31] A. Niskanen, K. Arstila, M. Ritala, M. Leskelä, J. Electrochem. Soc. 152 (2005) F90.
[32] M.-C. Choi, Y. Kim, C.-S. Ha, Prog. Polym. Sci. 33 (2008) 581.
[33] R. Belali, J.M. Vigoureux, Appl. Spectrosc. 48 (2004) 465.
[34] C. Sammon, J. Yarwood, N. Everall, Polym. Degrad. Stab. 67 (2000) 149.

Paper IV

Surface modification of Polymers by Plasma-assisted Atomic Layer Deposition

T. O. Kääriäinen, S. Lehti, M-L. Kääriäinen, D. C. Cameron.
Surface & Coating Technology 205 (2011) S475-S479

Reprinted with permission from Elsevier.

Surface & Coatings Technology 205 (2011) S475–S479

Contents lists available at ScienceDirect

Surface & Coatings Technology

journal homepage: www.elsevier.com/locate/surfcoat

Surface modification of polymers by plasma-assisted atomic layer deposition

T.O. Kääriäinen *, S. Lehti, M.-L. Kääriäinen, D.C. Cameron

Advanced Surface Technology Research Laboratory, Lappeenranta University of Technology, Prikaatinkatu 3 E, 50100 Mikkeli, Finland

ARTICLE INFO

Available online 3 April 2011

Keywords:
Plasma-assisted atomic layer deposition
PMMA
TiO_2
Polymers
Adhesion

ABSTRACT

The inhomogeneous and hydrophobic surface characteristics of many polymers can be incompatible with other substances which are required for their further functionalization. Various plasma methods have been used to overcome this problem and to enable functionalization to take place. Plasma modification can nevertheless lead to a nonuniform and chemically unstable surface which results in only a moderate performance in the final application. Deposition of ultrathin layers by atomic layer deposition (ALD) as a surface modification of the polymers is a useful way to bring the desired functionality to polymer surface. ALD at low temperature suffers from slow reaction rates, consequently giving low deposition rates. Among the different ALD methods, plasma assisted ALD (PA-ALD) is suitable for depositions at low temperatures with faster chemical reactions compared to thermal ALD. In this work tetrakis-dimethyl-amido titanium (TDMAT) and plasma excited O_2 precursors were used to deposit TiO_2 on Si(100) and polymethylmethacrylate (PMMA) substrates. Changes in the process conditions were studied by means of varying plasma power, oxygen pulse length and the point in time of plasma ignition during the ALD cycle. In the case where a mixture of nitrogen and argon was introduced into the reactor to act as a purge gas between precursor pulses and also to facilitate the generation of a plasma during the plasma cycle, the plasma did not show detrimental effects on film adhesion on PMMA substrate, whereas using only argon as a carrier and plasma gas was found to cause poor film adhesion to the PMMA. ATR-FTIR analysis showed lower levels of carbonaceous compounds for the film grown at lower plasma power. The films grown with lower plasma power also showed higher refractive index which suggests the low plasma power is more beneficial for this particular PA-ALD TiO_2 process.

© 2011 Elsevier B.V. All rights reserved.

1. Introduction

As an oxide semiconductor TiO_2 (titanium dioxide) has been extensively studied both in bulk and thin film forms because of its attractive properties such as photocatalytic activity [1–3], photo-induced hydrophilicity [4], electron transport properties in solar cell applications [5–7], gas sensing [8], biocompatibility [9] and optical properties [10]. In many of these applications, thermoplastics such as poly (methyl methacrylate) (PMMA) [11–14], polycarbonate (PC) [12,14], polyethylene terephtalate (PET) [14,15], polyethylene napthalate (PEN) [15] and polypropylene (PP) have been advantageous as substrates compared with the conventional materials because of the ease of processing, inexpensiveness, lightness, corrosion and chemical resistance, insulation property etc. [16].

Due to the inhomogeneous and hydrophobic characteristics of the polymer surface, further functionalization is often desired to improve the performance [17]. Deposition of ultrathin layers by atomic layer deposition (ALD) has been demonstrated to be useful way to bring the desired functionality to polymer surface. Thin ALD layers can be used e.g. as a barrier on polyimide against atomic-oxygen flux in spacecrafts in low Earth orbit [18], as an adhesion promoting layer for sputtered metal and ceramic coatings and barrier against damaging effect of plasma UV radiation on PMMA [19], to change the polymer surface hydrophilicity under UV radiation (PMMA, PC)[20], (PMMA, PEEK, ETFE, PTFE) [21], as a gas diffusion barrier on flexible PEN [22–25] and flexible PET, PP and PLA substrates [25], and to create polymer nanocomposite materials with polyamide (PA) [26] and poly(styre-divinylbenzene) (PS-DVB) [27].

Atomic layer deposition (ALD) is a CVD type thin film deposition method where sequential exposures of gas phase reactants are used for the deposition of thin films with atomic layer accuracy. Each atomic layer formed in the sequential process is a result of saturated surface controlled chemical reactions. In plasma-assisted atomic layer deposition (PA-ALD), plasmas are used to produce radicals by gas dissociation. These bring advantages through increased reaction rates giving increased process efficiency, increased fragmentation of the precursor molecules, enhancement of the removal of product molecules. Furthermore the addition of non-thermal energy to the process can result in lower substrate temperatures than for conventional ALD which extends the range of materials which can be used as substrates [28,29]. Recent PA-ALD studies have concentrated on low temperatures suitable for polymer substrates [23,30–33]. Here it is relevant to make a distinction between plasma-assisted (PA-ALD) or plasma enhanced (PE-ALD) (both meanings are the same) and radical enhanced ALD (REALD). In PA-ALD

* Corresponding author.
E-mail address: tommi.kaariainen@lut.fi (T.O. Kääriäinen).

0257-8972/$ – see front matter © 2011 Elsevier B.V. All rights reserved.
doi:10.1016/j.surfcoat.2011.03.094

and PEALD the substrate will be exposed to plasma discharge since it is located in the same space with the plasma source or very near at the substrate [28,32,34]. In REALD the plasma source is separated from the substrate so that only radicals generated by the plasma are allowed to reach the substrate [35]. In the plasma reactor used in our study [33] the plasma source and the substrate are located in the same space but separated by metal grid to block the ion bombardment but allow the flow of radicals to the substrate surface. However the metal grid does not shield the substrate from plasma UV exposure, which will also effect the substrate surface. The definition of PA-ALD is used in our study because the plasma will have this ambiguous function. The divergence between PA-ALD and REALD becomes relevant especially when depositing on polymers that are sensitive not only to the flux of plasma species but also to photoemission from the plasma. Such a polymer is PMMA, which is susceptible to radiation damage. Depending on the plasma conditions, the plasma UV radiation can be detrimental to the PMMA surface leading to poor film adhesion [19].

In this paper, we report the details of low temperature PA-ALD of amorphous TiO_2 on various polymer substrates. We show that the film adhesion on PMMA is dependent on the gas mixture and plasma power used. The effect of different plasma conditions on the film growth rate and properties has been measured.

2. Experimental

2.1. Film deposition

TiO_2 films were deposited on silicon (100), PMMA (PLEXIGLAS® XT, $M_w = 150000–160000$ g/mol), PC and PP substrates at temperatures between 50 and 70 °C by PA-ALD with a Beneq TFS-500 ALD plasma tool described elsewhere [33]. Both nitrogen (99.999%, AGA) and argon (99.999%, AGA) were studied as precursor carrier gas and purging gas between the precursor pulses, and consequently the plasma forming gas during the plasma pulse. In both cases argon was also introduced to the reactor through the plasma electrode to improve the plasma generation and also to ensure a pressure difference between the reactor and argon flow channel. Precursors used were tetrakis(dimethylamido)titanium (TDMAT) (Sigma-Aldrich) vaporized from the source at a temperature of 40 °C and O_2 (99.999%, AGA) mixed with carrier gas (N_2 or Ar) and argon through the showerhead electrode. One deposition cycle consisted of a 500 ms TDMAT pulse, 10 s purge, a plasma pulse which varied from 250 ms to 6 s and a 10 s purge. Plasma power was varied between 25 and 200 W. The overall number of cycles used was 500. The PMMA substrate material was pre-cleaned in 5% NaOH solution for ten minutes and in de-ionized water for 20 min in an ultrasonic bath at room temperature. PC and PP substrates were pre-cleaned similarly except the NaOH was replaced with isopropanol. Samples were then baked in an oven at 50 °C for several hours to remove the absorbed water.

2.2. Film analysis

The film thickness and consequently the film growth rate were measured from the films deposited on silicon by using a spectroscopic ellipsometer M-2000FI from J. A. Woollam Co. Inc. The structure of the deposited film was studied with ATR-FTIR spectroscopy using a Nicolet 4700 FT-IR spectrometer equipped with a Smart Orbit ATR accessory. The internal reflection element used was a diamond crystal. The absorption spectrum of PMMA was measured with UV–vis spectrophotometer Evolution 500 (Thermo Electron Corporation). The TiO_2 surface was analyzed using an XPS instrument (PHI 5400) with Mg K_α radiation (energy of 1253.6 eV) in pressure of $1 \cdot 10^{-9}$ Torr. The photo activity of the deposited film was verified with water contact angle measurement under UV exposure (302 nm). Plasma emission during the plasma pulse was observed with optical emission spectrometry (OES) by using two OES systems. An IFU AOS-4 was used for time-resolved monitoring of particular spectral lines and a Plasus Emicon system (version 2.33.9.9) was used to collect the full emission spectra between the wavelengths of 180 nm and 880 nm. The optical fiber was placed on the quartz window perpendicular to the plasma electrode. The distance between the substrate surface and plasma electrode was 28 mm.

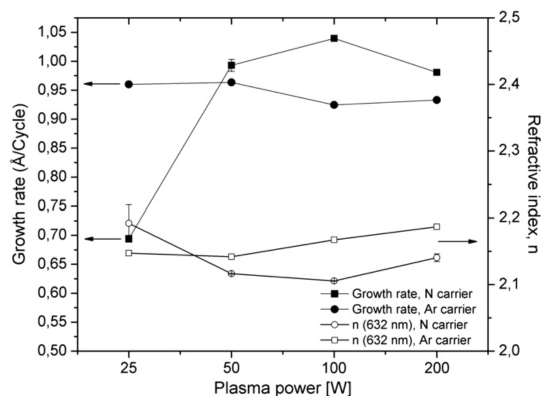

Fig. 1. Growth rate and refractive index of TiO_2 films as a function of plasma power.

3. Results and discussion

3.1. Film growth

The film growth rate increases slowly with increase of oxygen plasma pulse length and saturates with around 3 s O2 pulse for nitrogen carrier gas grown films. Based on this, 3 s plasma pulse length was chosen for plasma power variation study with nitrogen and argon carrier gasses. The film growth rate and refractive index at 632 nm as a function of the plasma power are shown in Fig. 1 for both nitrogen and argon carrier gasses. With nitrogen carrier gas the low plasma power (25 W) results in considerably lower growth rate than with plasma power of 50 W and above. This was not observed with argon carrier gas.

OES monitoring of the plasma during the plasma pulse step revealed that argon and nitrogen carrier gasses form considerably different plasma conditions and consequently different reaction mechanisms for the film growth. Fig. 2 shows the emission spectra for argon and nitrogen carrier

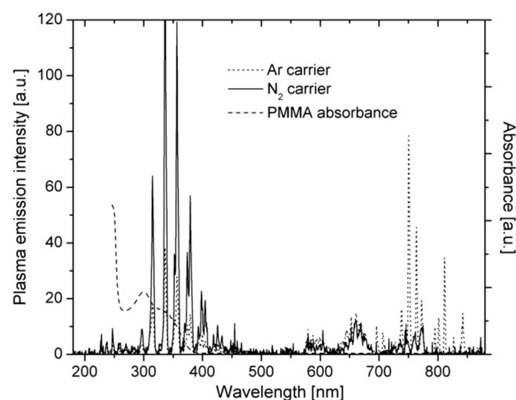

Fig. 2. Plasma emission spectra from argon and nitrogen carrier gas plasma with 50 W plasma power during the plasma exposure step of the PA-ALD cycle. Additionally, the graph shows the absorption of PMMA in the wavelength region from 190 nm to 880 nm.

gasses used during the plasma pulse step of ALD cycle. The spectra are the average from the emission intensity during the 3 s plasma pulse. Typical emission for nitrogen from the first positive system ($B^3\Pi_g$–$A^3\Sigma_u^+$) and from the second positive system ($C^3\Pi_u$–$B^3\Pi_g$) can be seen in the wavelength ranging from 503.08 nm to 880 nm (limited by OES detection range) and 218.43–497.64 nm respectively. Atomic argon emission can be seen in the wavelength ranging from 696.54 nm to 794.82 nm [36,37]. It is noticeable that the emission typical to nitrogen is also present when argon is used as a carrier gas but with lower intensity. This emission probably arises from the background gas, mainly air remaining in the chamber. Time-resolved OES measurement of atomic oxygen shown in Fig. 3a clearly indicates that with argon carrier gas the oxygen radical concentration increases during the plasma pulse and saturates at a high level after approximately two seconds showing that the surface reactions between oxygen radicals and surface species also saturate. With nitrogen carrier gas the atomic oxygen concentration shows a gradual decline from its initial level (although with some scatter in the data). Although the oxygen radical concentration is decreasing during the plasma pulse with nitrogen carrier gas it is reasonable to believe that surface reactions still saturate because the film growth rate and the film elemental composition for both nitrogen and argon carrier gas grown films are nearly the same. Decreasing oxygen radical concentration during the plasma pulse with nitrogen carrier gas suggests that after the surface reactions with oxygen radicals are saturated, oxygen radicals are further consumed in other chemical reactions in the plasma. From a process development perspective further chemical reactions of oxygen radicals in the nitrogen plasma may help to decrease the following purge step length. One example is the excess of H_2O contamination in argon plasma that does not appear in nitrogen plasma. A clear difference between the optical emissions from when the Ar and N_2 purge gasses are used is shown in Fig. 3b. Water is known as a substance difficult to remove in low temperature ALD processes. Argon carrier gas produces an excess of oxygen radicals (peaks at 777.194 nm, 777.417 nm and 777.516 nm). It also produces H_2O (peaks at 646.8 nm and 651.68 nm) and CH and CH_2 groups, which can not be detected when nitrogen is used as a carrier gas. Another difference in nitrogen carrier gas compared to argon is the intensive OH cation production during the plasma pulse (peaks between e.g. 356.85 nm and 357.35 nm), which may indicate the water molecule breakage [38]. More detailed OES monitoring of reaction products and other plasma species and their effect on ALD process will be a topic for future investigations. Oxygen radical emission monitoring and its saturation during the plasma pulse were also used for PA-ALD process studies for TMA and O2 by Heil et.al. [32,34].

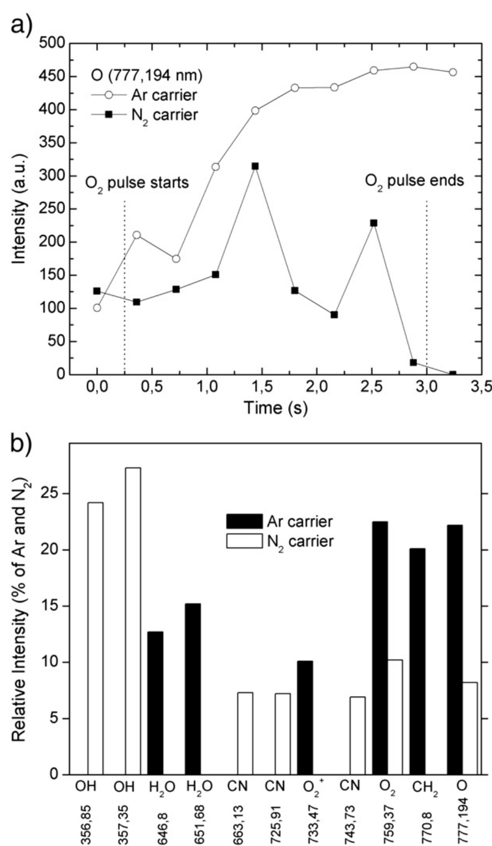

Fig. 3. Optical emission of O radical (777.194 nm) concentration in argon and nitrogen carrier gas plasmas as a function of time during the plasma pulse step (a), and average optical emission of plasma species in argon and nitrogen carrier gas plasmas during the plasma pulse step (b).

3.2. Film properties

The results of elemental analysis performed by XPS for the films deposited in different conditions are shown in Table 1. XPS measurement was performed both on as–deposited and argon ion-sputtered surfaces. Sputtering time prior to XPS measurements was 15 min with an acceleration voltage of 3 kV and ion current of 2 µA on 4×4 mm^2 rastered area. No significant difference in Ti, O, N, and C concentration between the films can be observed. An interesting observation is relatively high nitrogen incorporation in the film. Nitrogen is incorporated in the film with both nitrogen and argon carrier gas suggesting that nitrogen is coming from TDMAT. This was not observed earlier in a TDMAT and water process for thermal ALD TiO_2, where the possibility of nitrogen doping was considered [39]. The nitrogen content remains almost unchanged after argon sputtering compared to the untreated surface suggesting that most of the N is bonded in the film. By contrast a clear decrease in C content after argon sputtering reveals high surface contamination on the as-deposited surface.

Chemical bonding in the films was investigated from the Ti 2p, O 1 s, N 1 s and C 1 s peaks of the XPS spectra. The analysis was done on the as-deposited surfaces since the argon ion sputtering can greatly alter the chemical states of the film surface. Deconvoluted Ti 2p spectra of the film A (marked in Table 1) into two Lorentz–Gauss type peaks shown in Fig. 4a display peaks at binding energy (BE) of 458.6 eV corresponding

Table 1
Chemical composition of TiO2 films and plasma characteristics during the plasma pulse step of ALD cycle.

	Chemical composition (At.%)								Plasma pulse characteristics		
	As-deposited surface				Argon sputtered surface						
Sample	Ti	O	N	C	Ti	O	N	C	Plasma power [W]	Plasma gas	Oxygen pulse length [ms]
A	20.2	50.8	5	24	32.7	55.1	4.7	7.5	100	N	250
B	20.1	50.2	4.5	25.2	33.5	55	4.7	6.8	100	N	500
C	18.1	47.4	5	29.5	31.8	57.4	4.4	6.4	100	N	3000
D	20	50.9	4.1	25	33.2	57.9	4	4.9	100	N	6000
E	22.2	52.8	3	22	34.3	55.2	4.1	6.4	25	N	3000
F	20.5	52.4	5.3	21.8	32.4	56.2	4.5	6.9	50	N	3000
G	20.2	52	4.8	23	32.8	57.2	4.3	5.7	200	N	3000
H	20.8	53.5	5.2	20.5	32.5	57.5	4.3	5.7	25	Ar	3000
I	19.2	48.7	5	27.1	33.5	55.4	4.7	6.4	50	Ar	3000
J	21.6	55.1	4.6	18.7	33.5	56.8	4.2	5.5	200	Ar	3000

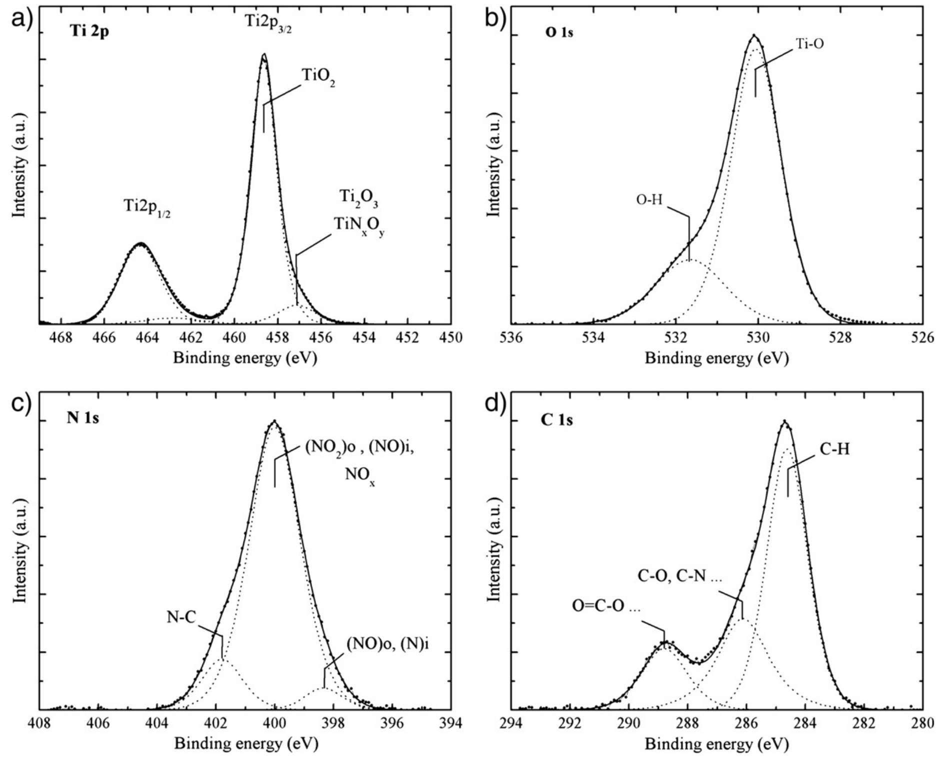

Fig. 4. Deconvoluted XPS spectra of TiO_2 film; (a) Ti 2p, (b) O 1 s, (c) N 1 s where $(NO_2)o$ denotes substitutional NO_2, (NO)i interstitial NO, (NO)o substitutional NO and (N) interstitial N, and (d) C 1 s.

to TiO_2 and at BE of 457.1 eV corresponding to Ti_2O_3 or TiN_xO_y type structures [40–43]. Analysis of the deconvoluted spectra of the films for which the overall elemental compositions and process descriptions are given in Table 1 are summarized in Table 2. Ti 2p spectral analysis suggests that the oxidation state is somewhat related to plasma power and carrier gas used. This can be seen as a higher composition of reduced oxidation state (Ti_2O_3, Ti^{3+}) for the film grown with nitrogen carrier gas and with plasma power of 25 W. With nitrogen carrier gas at higher plasma power and argon carrier gas at any plasma power studied here, the oxidation remains at higher state referring to the TiO_2 structure. Deconvoluted spectra of O 1 s, C 1 s and N 1 s are shown in Fig. 4b, c and d respectively. Lineshape analysis of O 1 s shows typical oxygen bonding both bulk TiO_2 (O-Ti at BE of 530.1 eV) and surface contamination (OH- at BE of 531.7 eV). N 1 s lineshape reveals that nitrogen is mainly incorporated as different NO-types (BE of 400 eV and 398.3 eV) with some N–C bonding (BE of 401.8 eV) [44,45]. Weakly physisorbed N at the surface has also been suggested to present the peak at around 402 eV [41]. Low plasma power (25 W) with nitrogen carrier (sample E) gas leads to a higher amount of N–C in the film as shown in Table 2. Higher concentration of C–N can also be observed from the C 1 s lineshape for this sample. One possible source for this excessive N–C in the film is from the Ti-N-CH_3 branch in TDMAT due to the incomplete breakage or substitution of the N-CH_3 during the oxidation step of PA-ALD cycle. By using argon carrier or higher plasma power with nitrogen carrier gas make this reaction more efficient leading to lower N–C concentration. Lineshape analysis of C 1 s indicates high concentration of C–H contamination (BE of 284.7 eV) for all of the samples (A–J) believed to originate mainly from atmospheric surface contamination

Table 2
Results of lineshape analysis of deconvoluted XPS Ti 2p, O 1s, C 1s and N 1s spectra.

Peak	State interpretation	Position BE [eV]	Reference	Sample/Component ratios (value multiplied by 100%)									
				A	B	C	D	E	F	G	H	I	J
Ti 2p	TiO_2	458.6	[38,43]	0.92	0.87	0.93	0.93	0.80	0.88	0.88	0.88	0.85	0.90
	TiN_xO_y, Ti_2O_3	457.1	[38,43]	0.08	0.13	0.07	0.07	0.20	0.12	0.12	0.12	0.15	0.10
O 1s	O–Ti	530.1	[38,43]	0.81	0.79	0.78	0.79	0.87	0.77	0.78	0.80	0.80	0.82
	OH	531.7	[38,41,43]	0.19	0.21	0.22	0.21	0.13	0.23	0.22	0.20	0.20	0.18
C 1s	C–H	284.7	[41,43]	0.61	0.67	0.68	0.68	0.65	0.57	0.60	0.52	0.68	0.59
	C–O, C–N, etc.	286.1	[38,41,43]	0.25	0.16	0.12	0.12	0.25	0.15	0.20	0.21	0.13	0.17
	O=C–O	288.8	[41,43]	0.14	0.16	0.19	0.19	0.10	0.27	0.20	0.27	0.19	0.24
N 1s	(NO)i, $(NO_2)o$, NO_x	400	[39,42,43]	0.81	0.84	0.85	0.85	0.67	0.84	0.86	0.83	0.87	0.86
	(NO)o, (N)i	398.3	[39,42]	0.08	0.06	0.06	0.06	0.04	0.09	0.07	0.10	0.07	0.08
	N–C	401.8	[40,43]	0.11	0.10	0.09	0.09	0.29	0.07	0.07	0.07	0.06	0.07

and carbon contamination in the film as a form of C–O and C–N types (BE of 286.1 eV) and O=C–O type (BE of 288.8 eV) [38,41,43]. The decrease of the component interpreted as O=C–O concentration of sample E agrees well with our earlier study where C=O bonding could not be found from this sample by ATR-FTIR analysis [46].

The detrimental effect of plasma UV radiation was observed as a poor film adhesion on PMMA. Satisfactory adhesion with tape peel off test (Scotch tape 810) was observed only for the films E and F showing the importance of selecting appropriate plasma conditions for depositions on PMMA. Films E and F were deposited with nitrogen in the plasma gas and with 25 W and 50 W plasma powers respectively. Plasma emission during the deposition of the film F and comparatively for deposition where argon was used with the same plasma power (film I in Table 1) were shown in Fig. 2. The spectra reveal that nitrogen used as a carrier gas produces photoemission with higher energy than argon in the wavelength region from 180 nm to 880 nm. Furthermore the photoemission with low plasma powers at this wavelength region was not the cause of film delamination when depositing on PMMA, as shown for films E and F. This suggests that in the case of photo emission the detrimental emission lies below the wavelength of 180 nm and is related to interaction between the argon and other plasma species, or that the detrimental effect of plasma to PMMA is related to interaction of energetic ions (ion bombardment). The characteristic of long-lived argon metastables is that they can transfer energy very efficiently e.g. to species such as H_2, H_2O, air, and hydrocarbons, and consequently lead to intense photoemission in the VUV region. This has been reported earlier by Wertheimer et al. [47]. The other possibility, that the chemical modification of the PMMA surface is due to low energy argon ion bombardment, has also been reported by Gröning et. al [48]. In our study relatively low plasma power with argon carrier gas (25 W) already resulted in detrimental film adhesion on PMMA. Considering this factor together with the PA-ALD reactor design, where the plasma and deposition area are separated with metal mesh, it is concluded that the detrimental effect is most probably caused by photoemission from plasma at wavelength below 180 nm. The source of this photoemission is most probably created by the interaction between argon and other plasma species, mainly reaction products and residuals during the ALD cycle. The films deposited under these conditions on polymer substrates showed photo-induced hydrophilicity behavior under UV (302 nm) light illumination.

4. Conclusions

We have shown that the gas mixture forming the plasma and plasma power during the plasma pulse in PA-ALD process play a significant role in radical formation and chemical reactions at the substrate surface and in the plasma. Argon and nitrogen carrier gasses formed different plasma conditions and consequently different reaction mechanisms for the film growth. The effect of different reaction mechanism on the film chemical structure was relatively small. Different plasma conditions, however, showed different film adhesion behavior on PMMA. Argon carrier gas used at any plasma power between 25 and 200 W caused plasma conditions detrimental to adhesion on PMMA as shown by TiO_2 film delamination. Satisfactory film adhesion was achieved with nitrogen carrier gas below 50 W plasma power. Relatively high nitrogen concentration found in the film supports the usage of TDMAT as a precursor when nitrogen doping of TiO_2 is desired.

Acknowledgments

The authors thank ESF and the Center for Economic Development, Transport and the Environment of South Savo for supporting the project under S10148, and the Finnish Technology Agency (TEKES) for supporting the project under 40155/08.

The authors thank also laboratory engineer Markku Heinonen from University of Turku, Department of Physics and Astronomy for performing XPS characterization.

References

[1] A. Fujishima, K. Honda, Nature 238 (1972) 38.
[2] M. Kemell, V. Pore, J. Tupala, M. Ritala, M. Leskelä, Chem. Mater. 19 (2007) 1816.
[3] M.-L. Kääriäinen, T.O. Kääriäinen, D.C. Cameron, Thin Solid Films 517 (2009) 6666.
[4] R. Wang, K. Hashimoto, A. Fujishima, M. Chikuni, E. Kojima, A. Kitamura, M. Shimohigoshi, T. Watanabe, Nature 388 (1997) 431.
[5] B.O. Aduda, P. Rairajan, K.L. Choy, J. Nelson, Int J Photoenergy 6 (2004).
[6] S.K. Dhungel, J.G. Park, Renewable Energy 35 (2010) 2776.
[7] S. Günes, N.S. Sariciftci, Inorg. Chim. Acta 361 (2008) 581.
[8] O.K. Varghese, D. Gong, M. Paulose, K.G. Ong, C.A. Grimes, Sens. Actuators B 93 (2003) 338.
[9] K. Uetsuki, H. Kaneba, Y. Shirosaki, S. Hayakawa, A. Osaka, Mater. Sci. Eng. B 173 (2010) 213.
[10] A. Convertino, G. Leo, M. Tamborra, C. Sciancalepore, M. Striccoli, M.L. Curri, A. Agostiano, Sens. Actuators B 126 (1) (2007) 138.
[11] H.I. Elim, W. Ji, A.H. Yuwono, J.M. Xue, J. Wang, Appl. Phys. Lett. 82 (2003) 16.
[12] U. Schulz, Appl. Opt. 45 (2006) 7.
[13] S.R. Nugen, P.J. Asiello, J.T. Connelly, A.J. Baeumner, Biosens. Bioelectron. 24 (2009) 2428.
[14] Y.H. Tennico, M.T. Koesdjojo, S. Kondo, D.T. Mandrell, V.T. Remcho, Sens. Actuators B 143 (2010) 2.
[15] J. Fahlteich, M. Fahland, W. Schönberger, N. Schiller, Thin Solid Films 517 (2009) 3075.
[16] R.J. Crawford, Plastics Engineering, third ed. Butterworth-Heinemann, Burlington, 1998.
[17] J.M. Goddard, J.H. Hotchkiss, Prog. Polym. Sci. 32 (2007) 698.
[18] R. Cooper, H.P. Upadhyaya, T.K. Minton, M.R. Berman, X. Du, S.M. George, Thin Solid Films 516 (2008) 4036–4039.
[19] T.O. Kääriäinen, D.C. Cameron, M. Tanttari, Plasma Process. Polym. 6 (2009) 631.
[20] T.O. Kääriäinen, M.-L. Kääriäinen, R.P. Gandhiraman, D.C. Cameron, ALD, 7th Int. Conf. Atomic Layer Deposition, San Diego, California, USA, 24–27 June 2007, 2007.
[21] M. Kemell, E. Färm, M. Ritala, M. Leskelä, Euro. Polymer J. 44 (2008) 3564.
[22] M.D. Groner, S.M. George, R.S. McLean, P.F. Carcia, Appl. Phys. Lett. 88 (2006) 051907.
[23] E. Langereis, M. Creatore, S.B.S. Heil, M.C.M. Van de Sanden, W.M.M. Kessels, Appl. Phys. Lett. 89 (2006) 081915.
[24] A.A. Dameron, S.D. Davidson, B.B. Burton, P.F. Carcia, R.S. Mclean, S.M. George, J. Phys. Chem. C 112 (2008) 4573.
[25] T. Hirvikorpi, M. Vähä-Nissi, T. Mustonen, E. Iiskola, M. Karppinen, Thin Solid Films 518 (2010) 2654.
[26] K. Nevalainen, R. Suihkonen, P. Eteläaho, J. Vuorinen, P. Järvelä, N. Isomäki, C. Hintze, M. Leskelä, J. Vac. Sci. Technol. A 27 (4) (Jul/Aug 2009).
[27] X. Liang, S.M. George, A.W. Weimer, Chem. Mater. 19 (2007) 5388.
[28] S.M. Rossnagel, A. Sherman, F. Turner, J. Vac. Sci. Technol. B 18 (4) (2000) 2016.
[29] M. Ritala, M. Leskelä, in: H.S. Nalwa (Ed.), Handbook of Thin Film Materials, vol. 1, Academic Press, San Diego, CA, 2002, p. 103.
[30] A. Niskanen, K. Arstila, M. Leskelä, M. Ritala, Chem Vap. Deposition 13 (2007) 152.
[31] S.B.S. Heil, J.L. van Hemmen, M.C.M. van de Sanden, W.M.M. Kessels, J. Appl. Phys. 103 (2008) 103302.
[32] S.B.S. Heil, P. Kudlacek, E. Langereis, R. Engeln, M.C.M. van de Sanden, W.M.M. Kessels, Appl. Phys. Lett. 89 (2006) 131505.
[33] T.O. Kääriäinen, D.C. Cameron, Plasma Process Polym. 6 (2009) S237.
[34] S.B.S. Heil, J.L. van Hemmen, M.C.M. van de Sanden, W.M.M. Kessels, J. Appl. Phys. 103 (2008) 103302.
[35] A. Niskanen. Radical Enhanced Atomic Layer Deposition of Metals and Oxides. Academic dissertation. University of Helsinki, Helsinki, 2006.
[36] R.W.B. Pearse, A.G. Gaydon, The Identification of Molecular Spectra, fourth ed, Chapman and Hall, London, 1976.
[37] J.R. Fuhr, W.L. Wiese, L.I. Podobedova, D.E. Kelleher, in: W.M. Haynes (Ed.), Handbook of Chemistry and Physics 91st ed, 2011, Internet Version 2011.
[38] V.N. Fishman, J.J. Grabowski, J. Phys. Chem. A 103 (1999) 4879.
[39] G. K. Hyde. Functional Textiles via Self-Assembled Nanolayers and Atomic Layer Deposition. Academic dissertation. Ch. 9. North Carolina State University, Raleigh, NC, 2007.
[40] I. Bertoti, M. Mohai, J.L. Sullivan, S.O. Saied, Applied Surface Science 84 (1995) 357.
[41] S.-H. Lee, E. Yamasue, K.N. Ishihara, H. Okumura, Applied Catalysis B: Environmental 93 (2010) 217.
[42] A. Vesel, M. Mozetic, J. Kovac, A. Zalar, Appl. Surf. Sci. 253 (2006) 2941.
[43] N. Ohtsu, N. Masahashi, Y. Mizukoshi, K. Wagatsuma, Langmuir 25 (19) (2009) 11586.
[44] R. Asahi, T. Morikawa, Chemical Physics 339 (2007) 57.
[45] C. Ni, Z. Zhang, M. Wells, T.P. Beebe Jr., L. Pirolli, L.P. Mendez De Leo, A.V. Teplyakov, Thin Solid Films 515 (2007) 3030.
[46] T.O. Kääriäinen, P. Maydannik, M.-L. Kääriäinen, D.C. cameron, ALD, 9th Int. Conf. Atomic Layer Deposition, Monterey, California, USA, 19–22 July 2009, , 2009.
[47] M.R. Wertheimer, A.C. Fozza, A. Holländer, Nucl. Instr. Meth. In Phys. Res. B 151 (1999) 65.
[48] P. Gröning, O.M. Kuttel, M. Collaud-Coen, G. Dietler, L. Schlapbach, Appl. Surf. Sci. 89 (1995) 83.

ACTA UNIVERSITATIS LAPPEENRANTAENSIS

419. TOURUNEN, ANTTI. A study of combustion phenomena in circulating fluidized beds by developing and applying experimental and modeling methods for laboratory-scale reactors. 2010. Diss.

420. CHIPOFYA, VICTOR. Training system for conceptual design and evaluation for wastewater treatment. 2010. Diss.

421. KORTELAINEN, SAMULI. Analysis of the sources of sustained competitive advantage: System dynamic approach. 2011. Diss.

422. KALJUNEN, LEENA. Johtamisopit kuntaorganisaatiossa – diskursiivinen tutkimus sosiaali- ja terveystoimesta 1980-luvulta 2000-luvulle. 2011. Diss.

423. PEKKARINEN, SATU. Innovations of ageing and societal transition. Dynamics of change of the socio-technical regime of ageing. 2011. Diss.

424. JUNTTILA, VIRPI. Automated, adapted methods for forest inventory. 2011. Diss.

425. VIRTA, MAARIT. Knowledge sharing between generations in an organization – Retention of the old or building the new 2011. Diss.

426. KUITTINEN, HANNA. Analysis on firm innovation boundaries. 2011. Diss.

427. AHONEN, TERO. Monitoring of centrifugal pump operation by a frequency converter. 2011. Diss.

428. MARKELOV, DENIS. Dynamical and structural properties of dendrimer macromolecules. 2011. Diss.

429. HÄMÄLÄINEN, SANNA. The effect of institutional settings on accounting conservatism – empirical evidence from the Nordic countries and the transitional economies of Europe. 2011. Diss.

430. ALAOUTINEN, SATU. Enabling constructive alignment in programming instruction. 2011. Diss.

431. ÅMAN, RAFAEL. Methods and models for accelerating dynamic simulation of fluid power circuits. 2011. Diss.

432. IMMONEN, MIKA. Public-private partnerships: managing organizational change for acquiring value creative capabilities. 2011. Diss.

433. EDELMANN, JAN. Experiences in using a structured method in finding and defining new innovations: the strategic options approach. 2011. Diss.

434. KAH, PAUL. Usability of laser - arc hybrid welding processes in industrial applications. 2011. Diss.

435. OLANDER, HEIDI. Formal and informal mechanisms for knowledge protection and sharing. 2011. Diss.

436. MINAV, TATIANA. Electric drive based control and electric energy regeneration in a hydraulic system. 2011. Diss.

437. REPO, EVELIINA. EDTA- and DTPA-functionalized silica gel and chitosan adsorbents for the removal of heavy metals from aqueous solutions. 2011. Diss.

438. PODMETINA, DARIA. Innovation and internationalization in Russian companies: challenges and opportunities of open innovation and cooperation. 2011. Diss.

439. SAVITSKAYA, IRINA. Environmental influences on the adoption of open innovation: analysis of structural, institutional and cultural impacts. 2011. Diss.

440. BALANDIN, SERGEY, KOUCHERYAVY, YEVGENI, JÄPPINEN, PEKKA, eds. Selected Papers from FRUCT 8 .2011.

441. LAHTI, MATTI. Atomic level phenomena on transition metal surfaces. 2011. Diss.

442. PAKARINEN, JOUNI. Recovery and refining of manganese as by-product from hydrometallurgical processes. 2011. Diss.

443. KASURINEN, JUSSI. Software test process development. 2011. Diss.

444. PEKKANEN, PETRA. Delay reduction in courts of justice – possibilities and challenges of process improvement in professional public organizations. 2011. Diss.

445. VANHALA, MIKA. Impersonal trust within the organization: what, how, and why? 2011. Diss.

446. HYNYNEN, KATJA. Broadband excitation in the system identification of active magnetic bearing rotor systems. 2011. Diss.

447. SOLONEN, ANTTI. Bayesian methods for estimation, optimization and experimental design. 2011. Diss.

448. JABLONSKA, MATYLDA. From fluid dynamics to human psychology. What drives financial markets towards extreme events. 2011. Diss.

449. MYÖHÄNEN, KARI. Modelling of combustion and sorbent reactions in three-dimensional flow environment of a circulating fluidized bed furnace. 2011. Diss.

450. LAATIKAINEN, MARKKU. Modeling of electrolyte sorption – from phase equilibria to dynamic separation systems. 2011. Diss.

451. MIELONEN, JUHA. Making Sense of Shared Leadership. A case study of leadership processes and practices without formal leadership structure in the team context. 2011. Diss.

452. PHAM, ANH TUAN. Sewage sludge electro-dewatering. 2011. Diss.

453. HENNALA, LEA. Kuulla vai kuunnella – käyttäjää osallistavan palveluinnovoinnin lähestymistavan haasteet julkisella sektorilla. 2011. Diss.

454. HEINIMÖ, JUSSI. Developing markets of energy biomass – local and global perspectives. 2011. Diss.

455. HUJALA, MAIJA. Structural dynamics in global pulp and paper industry. 2011. Diss.

456. KARVONEN, MATTI. Convergence in industry evolution. 2011. Diss.

457. KINNUNEN, TEEMU .Bag-of-features approach to unsupervised visual object categorisation. 2011. Diss.

458. RUUSKANEN, VESA. Design aspects of megawatt-range direct-driven permanent magnet wind generators. 2011. Diss.

459. WINTER, SUSANNA. Network effects: scale development and implications for new product performance. 2011. Diss.

460. JÄÄSKELÄINEN, ANSSI. Integrating user experience into early phases of software development. 2011. Diss.